School of Medicine
Oregon Health Sciences University

CERTIFICATE OF APPROVAL

This is certify that the Ph.D. thesis of

Wendy Knosp

has been approved

[redacted]
Mentor/Advisor

[redacted]
Member

[redacted]
Member

[redacted]
Member

[redacted]
Member

QUANTITATIVE ANALYSIS OF HOXA13 FUNCTION IN THE DEVELOPING LIMB

By

Wendy M. Knosp

A DISSERTATION

Presented to the Department of Molecular and Medical Genetics

and the Oregon Health & Science University

School of Medicine

in partial fulfillment of

the requirements for the degree of

Doctor of Philosophy

August 2006

TABLE OF CONTENTS

LIST OF FIGURES

CHAPTER 1

CHAPTER 2

CHAPTER 3

LIST OF ABBREVIATIONS

aa	amino acid
A13-DBD	HOXA13 DNA binding domain peptide
AER	apical ectodermal ridge
bHLH	basic helix-loop-helix
bp	base pairs
BMP	bone morphogenetic protein
BMPR	BMP receptor
CD	circular dichroism
ChIP	chromatin immunoprecipitation
DAPI	4'-6-Diamidino-2-phenylindole
D. melanogaster	*Drosophila melanogaster*
DNA	deoxyribonucleic acid
E	embryonic day
EDTA	ethylene diamine tetra-acetic acid
EM	electron micrograph
EMSA	electrophoretic mobility shift assay
enoLOGOS	energy normalized sequence LOGOS
Fgf	Fibroblast growth factor protein
FP	footpad
g	acceleration of gravity
G. gallus	*Gallus gallus*

GFP	green fluorescent protein
GSH	glutathione, reduced
GSSH	glutathione, oxidized
HPLC	high performance liquid chromatography
H. sapiens	*Homo sapiens*
IDT	interdigital tissues
IPCD	interdigital programmed cell death
IPTG	isopropyl β-D-1-thiogalactopyranoside
K_a	association constant
Kb	kilobase pairs
K_d	dissociation constant
LPM	lateral plate mesoderm
MES	2-(N-morpholino) ethanesulfonic acid
M. musculus	*Mus musculus*
NG108-15	mouse neuroblastoma/rat glioma hybrid cell line
PCR	polymerase chain reaction
PEG	polyethylene glycol
PIC	protease inhibitor cocktail
PZ	progress zone
QRT-PCR	quantitative reverse transcriptase PCR
rh	recombinant human protein
RLU	relative luciferase units

RNA	ribonucleic acid
rpm	rotations per minute
RSTK	receptor serine/threonine kinase
SELEX	systematic evolution of ligands by exponential enrichment
SHH	sonic hedgehog protein
TALE	three amino acid loop extension protein
TUNEL	terminal deoxynucleotidyl transferase biotin-dUTP nick end labeling
VISTA	visualization tool for alignment
ZPA	zone of polarizing activity
Δ	change or deletion

ACKNOWLEDGEMENTS

The writing of one's thesis dissertation is a once in a lifetime experience. In reviewing all of my experiments and results of the past six years I am reminded of all the people who have contributed so much to my scientific career and successes, and I am grateful for the opportunity to thank them.

First, I would like to sincerely thank my graduate school mentor, Dr. H. Scott Stadler, without whom I would not have been able to write the many words of this dissertation. When I first came to Scott's lab the extent of my research skills included performing PCR and running gels; but Scott took the time to patiently teach me many of the skills I have today, from confocal microscopy to microdissections and embryo genotyping. In addition to the research training I learned from Scott, he has always been a supportive mentor and advisor. I truly appreciate the many hours he has spent thinking critically about my work, lending insight, troubleshooting experiments, reading my abstracts, papers and posters, and investing in preparing me for a successful scientific career. I also appreciate the freedom that Scott has given me to pursue different scientific questions, it has been an amazing experience to learn such a variety of skills and apply them to the scientific questions I desired to answer. For all these things and more, Thank You Scott!

In addition I would like to thank all the past and present Stadler Lab members. My fellow graduate student, Carley Shaut, your friendship and support both in and out of the lab have been a critical part of the past six years; I really

appreciate all the conversations we have had about science and life. Thanks to Gin Scott (co-first author of my 2004 paper, thanks for all the hard work!), Susan Nguyen, and Emily Morgan who were the original Stadler Lab girls; all those *in situ* washes you changed for me when I had to run to seminar or journal club have paid off! Thanks also to Chie Saneyoshi, the Queen of chromatin, who has been a great friend and collaborator in science. Thanks to Diane Sexton and Crystal Weller for their technical support; and thanks to Siming Shou for kindly sharing his microarray data which has added greatly to my thesis work.

My family and friends have provided amazing support to me as I embarked upon the adventure of graduate school. First and foremost, I am very thankful for the love and support of my husband Jon, he has taken wonderful care of me throughout the adventure of graduate school and I am forever grateful. Many thanks also to my parents, Bill and Diane Mueller, who have supported and encouraged my goals and aspirations throughout my life. And thanks to my many friends at OHSU, in Portland, and across the country; the fun times and laughter we have shared have truly enriched my life.

And finally, thanks to all the professors, students and staff at OHSU and Shriner's Hospital for Children who have been a part of my graduate school experience. Thanks to Hans Peter Bächinger and the members of his lab who gave invaluable assistance in teaching me how to do protein biochemistry. And thanks to the members of my thesis advisory committee, Dr. Jan Christian, Dr. Melissa Wong, and Dr. Mike Liskay who have provided great scientific insight and support.

ABSTRACT

The *Hox* family of transcription factors are key regulators of embryonic development. First identified in the fruit fly *Drosophila melanogaster*, *Hox* gene mutations cause homeotic transformations of one body segment into another. A striking example of this is mutations affecting the expression of the *Hox* gene *Antennapedia* which transform the developing antennae into legs in *D. melanogaster*. In humans and mice there are 39 *Hox* genes located in four clusters on four different chromosomes. To date, mutations in three of these *Hox* genes have been found to be the basis for human syndromes.

The loss of HOXA13 function causes severe malformations of the appendicular skeleton including pre-axial digit loss, soft tissue syndactyly, and carpal/tarsal bone brachydactyly in both humans and mice. Analysis of *Hoxa13* expression reveals a pattern of localization overlapping with sites of reduced *Bmp2* and *Bmp7* expression in *Hoxa13* mutant limbs. Biochemical analyses identified a novel series of *Bmp2* and *Bmp7* enhancer regions that directly interact with the HOXA13 DNA-binding domain and activate gene expression in the presence of HOXA13. Immunoprecipitation of HOXA13-*Bmp2* and –*Bmp7* enhancer complexes from the developing autopod confirm that endogenous HOXA13 associates with these regions. Exogenous applications of BMP2 or BMP7 partially rescues the *Hoxa13* mutant limb phenotype, suggesting that decreased BMP-signaling contributes to the malformations present in these tissues.

In addition, to accurately correlate HOXA13's transcriptional function with its mutant phenotypes, a quantitative assay was used to identify the DNA sequences bound by HOXA13 with high affinity. Comparing the presence of high affinity HOXA13 binding sites with genes exhibiting altered expression in *Hoxa13* homozygous mutant limbs revealed elevated expression of *Sostdc1*, a BMP antagonist, previously demonstrated to function in tooth and kidney development. In the absence of HOXA13 function, *Sostdc1* is ectopically expressed in the pre-axial autopod, causing the reduced expression of BMP-activated genes, as well as a decrease in Smad 1, 5, and 8 phosphorylation in the digit I anlagen. Limb chromatin immunoprecipitation confirmed HOXA13 binding at two conserved *Sostdc1* regulatory sites *in vivo. In vitro,* HOXA13 represses gene expression through the *Sostdc1* gene regulatory elements.

Together, these results provide conclusive evidence that HOXA13 regulates *Bmp2*, *Bmp7*, and *Sostdc1* expression in the developing limb, providing a mechanistic link between HOXA13, BMP signaling, and the specific developmental processes affected by loss of HOXA13 function. In addition, these findings provide new insights into mechanisms regulating BMP signaling and autopod development and patterning.

CHAPTER 1

Introduction

I. *Hox* genes

A. Discovery of Hox genes in Drosophila melanogaster

Hox genes were first discovered in the early 1900's, at the dawn of the study of genetics. In 1909, the embryologist Thomas Hunt Morgan (Fig 1.1) began work using the fruit fly *Drosophila melanogaster* as a model organism for scientific study. Chosen for its small size, short life span (about two weeks), and its inexpensive maintenance, *D. melanogaster* has proved a useful tool in the study of developmental biology and genetics. With the introduction of *D. melanogaster* as a model system also came the identification of the first *Hox* gene mutations.

Figure 1.1 Thomas Hunt Morgan in his office at Columbia (ca. 1917).

Courtesy of the Archives, California Institute of Technology.

As we now know, *Hox* genes function to pattern segments of the developing embryo, and when *Hox* gene expression is perturbed the result is profound changes in the developmental fate of specific embryonic tissues. One of the first fly *Hox* mutants identified was the *bithorax* mutant (*bx*), discovered by C.B. Bridges in 1915. The *bx* mutant is an example of the famous "four-winged" fly, where the mutation causes a transformation of the third thoracic segment (T3) toward the second (T2), and the halteres (balance organs) develop as a second set of wings (Bridges, 1921; Bridges, 1935; Bridges and Morgan, 1923). This fly mutant was further characterized and additional alleles were identified by Edward B. Lewis, a pioneer in the study of *Hox* genes. A picture of one of the *bithorax* mutant flies graced the cover of the July 1, 1983 edition of Science (Fig 1.2).

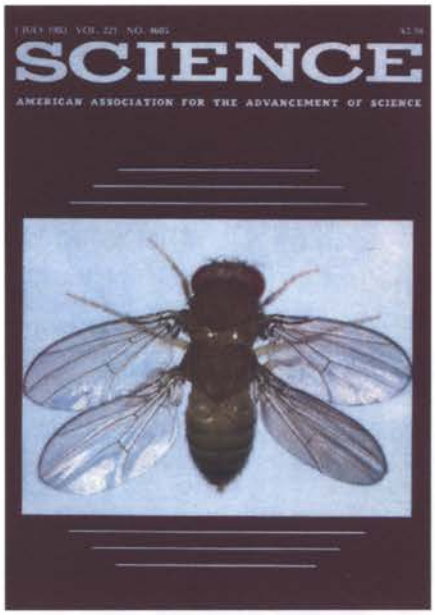

Figure 1.2 1983 cover of Science. Picture of the "four-winged fly" caused by mutations affecting Ultrabithorax expression. Reprinted with permission from *Science* Vol. 221, no. 4605, 1 July 1983. E.B. Lewis, California Institute of Technology, Pasadena, CA 91125. Copyright 1983 AAAS.

A defining feature of *Hox* genes is this phenomenon of "homeosis" that occurs when *Hox* genes are mutated or misexpressed in the developing embryo. The term was first coined by William Bateson in 1894 in his text: *Materials for the Study of Variation, Treated with Especial Regard to Discontinuity in the Origin of the Species*; where "homeosis" is defined as a type of variation in which "something has been changed into the likeness of something else" (Lewis, 1994). In addition to the original *bx* mutation, mutations in other *Hox* genes also result in homeotic transformations. Misexpression of the gene *Antennapedia* results in

the transformation of antennae to legs (Fig 1.3) (Postlethwait and Schneiderman, 1971). And ectopic expression of *Ultrabithorax* transforms the wings into a second set of halteres (resulting in a "wingless" fly) (Roch and Akam, 2000). These striking phenotypes emphasize the importance of *Hox* gene function in embryonic development and patterning.

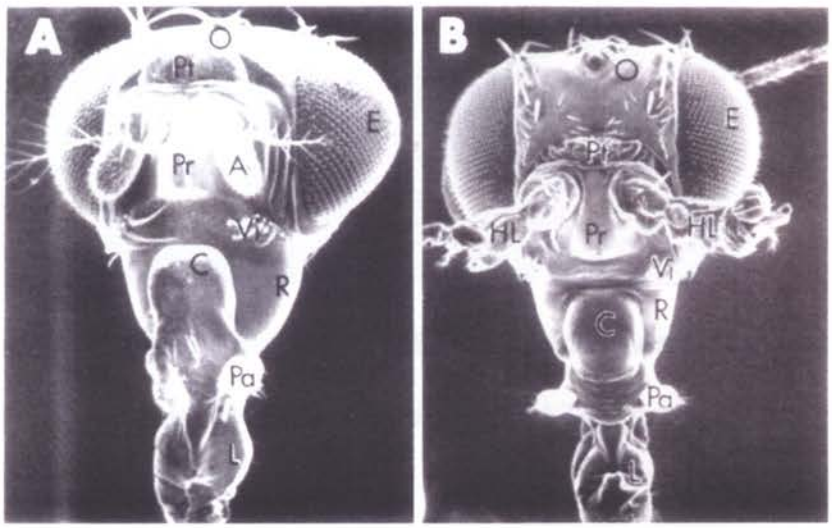

Figure 1.3 Antennapedia and wild-type *D. melanogaster* heads. A. Scanning electron micrograph of a wild-type fly with normal antennae. B. Scanning electron micrograph of an $Antp^{R}$ head. A, antenna; C, clypeus; E, eye; L, labellum; O, ocelli; Pa, maxillary palpus; Pr, prefrons; HL, homeotic leg; Pt, ptilinum; R, "Rostralhaut"; Vi, vibrissae. Reproduced with the permission of John Postlethwait (Postlethwait and Schneiderman, 1971).

The pioneering work defining the function and genetic organization of the Bithorax complex (BX-C) was carried out by Edward B. Lewis (Fig 1.4) in the mid-1950's (Duncan and Montgomery, 2002). Lewis studied under Alfred H.

Sturtevant, who was a student of T.H. Morgan and one of the first scientists to study *D. melanogaster* genetics.

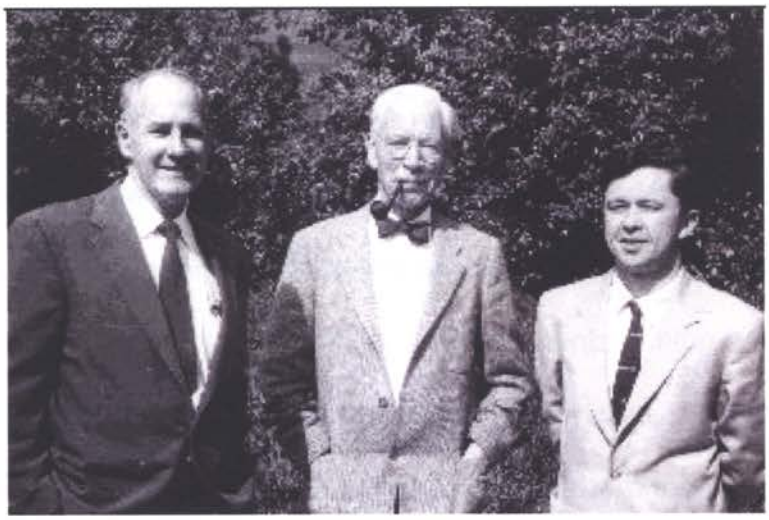

Figure 1.4 George Beadle, Alfred H. Sturtevant, and Edward B. Lewis (ca 1952). Courtesy of the Archives, California Institute of Technology.

The hypothesis that the *bithorax* family of mutants control the development of particular segments in the embryo was put forth in a 1951 paper published by Lewis. The discovery that the function of the *bithorax Hox* genes in *D. melanogaster* is to convert developing body segments from a "ground state" to their differentiated segmental identity has been fundamental in our thinking about how *Hox* genes function (Lewis, 1951; Lipshitz, 2005).

The BX-C, found on chromosome 3 in *D. melanogaster*, was eventually found to be part of a larger complex containing a total of 8 *Hox* genes and numerous non-coding regulatory domains. For his important "discoveries concerning the genetic control of early embryonic development" Lewis was

awarded the Nobel prize in 1995 along with Christiane Nusslein-Volhard and Eric F. Wieschaus.

B. Hox cluster colinearity and conservation

One interesting characteristic of *Hox* genes is their spatial and temporal colinearity within the developing embryo, a phenomenon identified by Lewis's extensive studies. Colinearity is when the physical position of the *Hox* gene along the chromosome correlates with the developmental timing and location of its expression along the antero-posterior axis of the embryo. In general, the 5' *Hox* genes are expressed later in development and pattern the posterior end of the embryo, while the 3' *Hox* genes are expressed earlier in development and function at the anterior end of the embryo (Lewis, 1951).

Moving from *D. melanogaster* to mouse (*M. musculus*) and man (*H. sapiens*) these same general principles of spatial and temporal colinearity also hold true. The situation in *M. musculus* and *H. sapiens* is also more complex, as there are four *Hox* gene clusters containing 39 *Hox* genes in these species (Fig 1.5). This expansion in the number of *Hox* genes in higher organisms has further complicated the study of *Hox* genes. However, our understanding of *Hox* gene function has been greatly advanced by both the discovery of human *Hox* gene mutations as well as the ability to perturb *Hox* gene expression *in vivo* in the mouse.

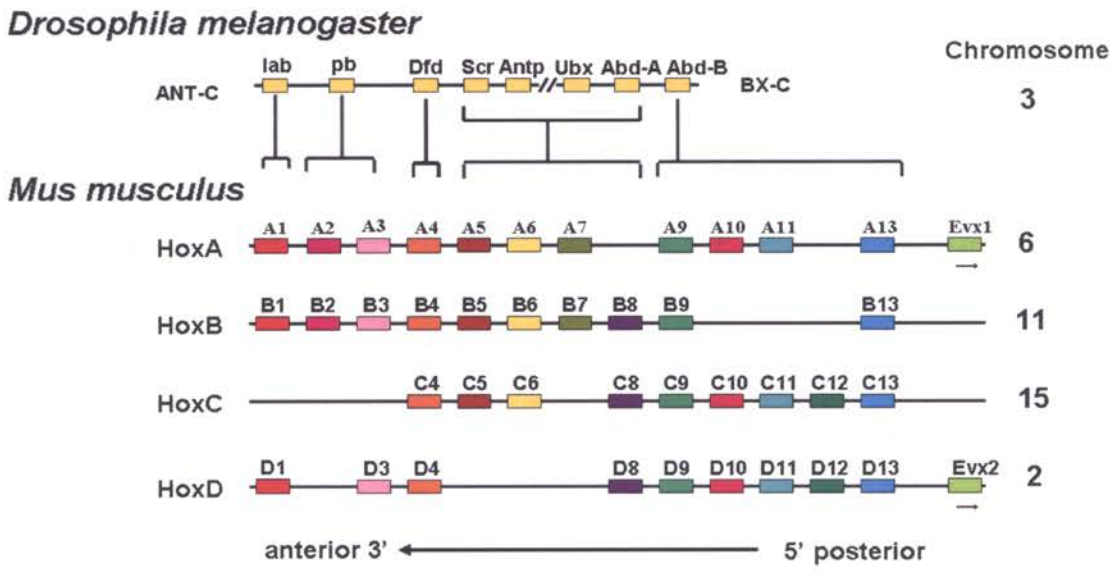

Figure 1.5 *Hox* gene organization. Arrangement of *Hox* genes along the chromosome in *Drosophila melanogaster* and *Mus musculus*. Chromosomal location of *Hox* clusters is indicated on the right side; organism and *Hox* cluster designation are labeled on the left side. Paralogs are represented as the same color.

We now know that *Hox* genes function as transcription factors within the nucleus of the cell. The phenotypic effects of perturbing *Hox* gene expression are then predicted to be the result of misregulation of *Hox* target gene expression within *Hox* expression domains. One of the key challenges in *Hox* gene research, as outlined by Lewis in his 1998 review, is the identification of target genes turned on or off by HOX proteins (Lewis, 1998).

C. Human Hox mutations

Due to the severity of the phenotypes seen in *D. melanogaster Hox* mutants, it was somewhat surprising when viable *Hox* gene mutations were implicated in human disease as well. To date, there are only three *Hox* genes that have been found to have a role in human diseases: *Hoxd13*, *Hoxa1*, and *Hoxa13*. Mutations in these *Hox* genes results in developmental abnormalities which include malformations of the limbs, eyes, ears, face, vasculature, lungs, and genitourinary tissues.

Mutations in *Hoxd13* cause autosomal dominant synpolydactly, characterized by polydactyly (extra digits), syndactyly (fused digits) and brachydactyly (shortened digits) of the hand and foot. Disease causing mutations include polyalanine tract expansions, intragenic deletions resulting in frameshift and nonsense mutations, as well as missense mutations (Akarsu et al., 1996; Debeer et al., 2002; Goodman et al., 1998; Johnson et al., 2003; Muragaki et al., 1996).

Most recently, in 2005, homozygous truncating mutations in *Hoxa1* were identified in patients with autosomal recessive Bosley-Salih-Alorainy syndrome. Associated phenotypes include horizontal gaze abnormalities, deafness, facial weakness, hypoventilation, vascular malformations of the internal carotid arteries and cardiac outflow tract, mental retardation and autism spectrum disorder (Tischfield et al., 2005). This finding was unique in that it is the first discovery of a viable homozygous truncating mutation in any human *Hox* gene.

D. Hoxa13: HFGS and Guttmacher syndromes

Hoxa13 mutations have been identified in patients with Hand-Foot-Genital syndrome (HFGS) and Guttmacher syndrome. HFGS is characterized by hypodactyly (loss of digits), shortened first metacarpal and metatarsal, syndactyly, hypospadias and genitourinary defects. This syndrome is typically inherited as an autosomal dominant condition, where mutation in one copy of *Hoxa13* results in the manifestation of the phenotypes associated with this syndrome. The mutations identified to date include deletions, nonsense and missense mutations, and polyalanine tract expansions (Fig 1.6) (Goodman et al., 2000; Mortlock and Innis, 1997; Utsch et al., 2002).

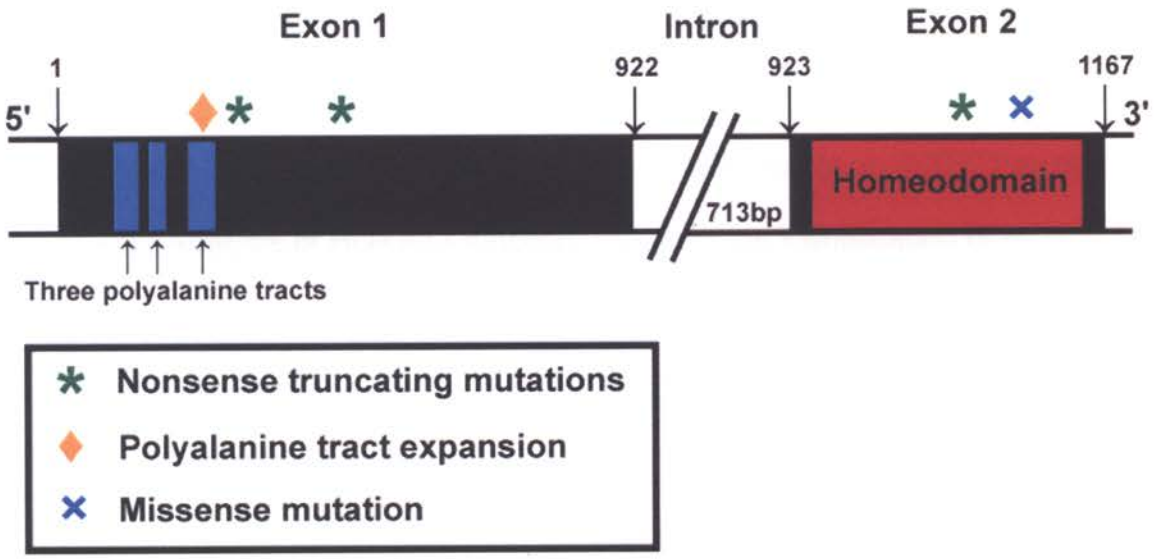

Figure 1.6 Mutations in *Hoxa13*. *Hoxa13* is comprised of two exons and one intron; exon 1 encodes three polyalanine tracts (blue boxes), exon 2 encodes the homeodomain (red box). Locations of disease causing mutations are indicated with symbols; the types of mutations are defined below the figure. Adapted from Goodman et al. (2000).

Guttmacher syndrome is an autosomal dominant inherited disorder characterized by distal limb and genital tract abnormalities. Patients with Guttmacher syndrome have been found to have an allele of *Hoxa13* with a dinucleotide deletion in the promoter and a missense mutation in the HOXA13 homeobox (Innis et al., 2002).

In addition to these defined syndromes, *Hoxa13* has a potential role in the common genitourinary malformation of hypospadias, which involves the arrested growth, formation and closure of the urethra in the external genitalia (Allera et al., 1995; Sutherland et al., 1996). To date, the cellular and molecular mechanisms underlying this malformation are unknown, however loss of functional HOXA13 leads to hypospadias in HFGS and in mice. This malformation has biomedical relevance as the incidence of hypospadias has been increasing dramatically, from 1 in 500 male births in 1970 to as many as 1 in 125 live male births in recent years (Baskin et al., 2001; Baskin et al., 1998; Gallentine et al., 2001; Paulozzi et al., 1997). Analysis of HOXA13 function, including the identification of HOXA13 DNA binding sites and target genes will have important implications in understanding and preventing birth defects such as hypospadias and limb malformations (Morgan et al., 2003).

II. The Homeodomain

A. Homeodomain structure

One of the defining features of *Hox* genes is a highly conserved 180 bp DNA sequence called the homeobox. The homeobox was discovered as a region of DNA sequence homology within the 3' exon of the *Hox* genes *Antennapedia*, *fushi tarazu*, and *Ultrabithorax* in *D. melanogaster*. This cross-homology facilitated its use as a probe to identify additional homeobox-containing genes in *D. melanogaster* and other species, including mouse, human, chicken, and frog (McGinnis et al., 1984a; McGinnis et al., 1984b; McGinnis et al., 1984c).

The homeobox DNA sequence encodes a 60 amino acid (aa) homeodomain found in all HOX proteins. The homeodomain forms a helix-turn-helix DNA binding motif critical for HOX protein regulation of target gene expression. The crystal structure for the *D. melanogaster* homeodomain-containing proteins Ultrabithorax and Extradenticle bound to DNA, as well as the structure of the human HoxB1-Pbx1-DNA complex were resolved in 1999 (Fig 1.7) (Passner et al., 1999; Piper et al., 1999). Structural studies of these different homeodomain containing proteins have given us some insight into the physical interactions that take place at the interface of a homeodomain-DNA interaction.

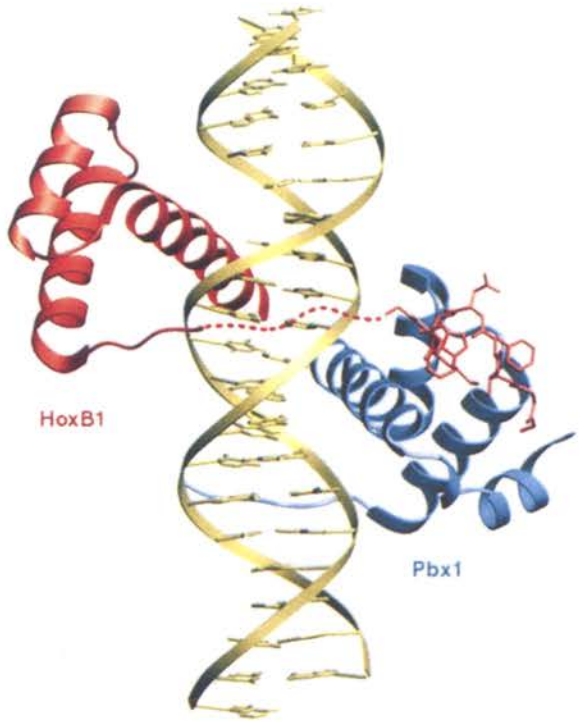

Figure 1.7 The HoxB1-Pbx1-DNA Complex. Ribbon diagram of the HoxB1 protein (red) and its cofactor protein Pbx1 (blue) bound to DNA. Reprinted from Cell, Vol. 96, Derek E. Piper, Adrian H. Batchelor, Ching-Pin Chang, Michael L. Cleary, and Cynthia Wolberger. Structure of a HoxB1-Pbx1 Heterodimer Bound to DNA: Role of the Hexapeptide and a Fourth Homeodomain Helix in Complex Formation, 587-597, Copyright 1999, with permission from Elsevier.

Both HoxB1 and Ultrabithorax bind DNA as heterodimers with cofactor DNA-binding proteins. For HoxB1, Ubx and many other HOX proteins, a conserved pentapeptide motif, F/Y-P-W-M-R/K, within the homeodomain has been demonstrated to be essential for cooperative DNA binding (Knoepfler and Kamps, 1995). However, the *Hox* paralog groups 11-13 do not contain this motif

and the protein-protein interaction domains are currently unknown for a majority of these HOX proteins, including HOXA13 (Phelan et al., 1995).

B. DNA binding

An important component to understanding how HOX proteins function is the identification of HOX DNA binding sites. Elucidation of these DNA sequences is a critical step in identifying the genes regulated by HOX proteins and understanding how HOX proteins are functioning within the cell. Biochemical studies using purified homeodomain peptides in DNA binding assays have facilitated the identification of a number of HOX protein DNA binding sites. For the group 13 HOX proteins, HOXC13 and HOXD13 have been demonstrated to bind distinct DNA sequences, suggesting variations in the amino acid sequences of their homeodomains confer differences in DNA binding (Fig 1.8).

Hoxc13, expressed in the developing hair follicle, binds a TT(T/A)AT sequence within promoters of the early human hair keratin genes *hHa5* and *hHa2* (Jave-Suárez et al., 2002). Surprisingly, members of the TALE class of proteins, which have been demonstrated to interact with some HOX proteins to enhance DNA binding specificity, were found to be differentially expressed within the hair follicle and did not colocalize with HOXC13 (Jave-Suárez et al., 2002; Moens and Selleri, 2006). This finding suggests that HOXC13 DNA binding and activation of these target genes does not require the TALE proteins as co-factors.

A screen for HOXD13 DNA binding sites identified "TTAT" and "TTAC" as sequences bound by HOXD13. In contrast, a point mutation in the HOXD13

homeodomain (I47L), which causes a novel form of brachydactyly and polydactyly, was found to bind different DNA sequences than the wild-type HOXD13 protein. The core "TTAC" sequence was preferred by the HOXD13 (I47L) homeodomain, but the DNA bases flanking this core sequence varied from the flanking bases bound by wild-type HOXD13. In addition, a novel "TAAC" sequence was also bound by the HOXD13(I47L) homeodomain, suggesting that the substitution of a single amino acid confers novel DNA binding capabilities (Caronia et al., 2003).

In 1993, Cory Abate's group identified a consensus site (C/G)TAATTG that is bound by the homeodomain proteins HOXA3, MSX1 and En-1 *in vitro* (Catron et al., 1993). Interestingly, the TAAT core sequence was found to be required for DNA binding activity, but changes in the nucleotides flanking this core sequence altered the binding specificity of each HOX protein. These *in vitro* findings suggest that differences in DNA binding specificity could contribute to the *in vivo* interactions of HOX proteins with binding sites in the control regions of target genes.

		% Identity to A13
A13:	RRGRKKRVPYTKVQLKELEREYATNKFITKDKRRRISATTNLSERQVTIWFQNRRVKEKK	100%
B13:	RRGRKKRIPYSKGQLRELEREYAANKFITKDKRRKISAATSLSERQITIWFQNRRVKEKK	85%
C13:	RRGRKKRVPYTKVQLKELEKEYAASKFITKEKRRRISATTNLSERQVTIWFQNRRVKEKK	93%
D13:	RRGRKKRVPYTKLQLKELENEYAINKFINKDKRRRISAATNLSERQVTIWFQNRRVKDKK	90%

Figure 1.8 Group 13 homeodomain alignment. Conserved amino acids are black, divergent amino acids are red. Percent identity to the HOXA13 homeodomain sequence is indicated on the right.

III. Limb development

A. Patterning of the limb axes

One of the critical domains for HOXA13 function is within the developing limb (Figs 1.10 and 1.13). To form a mature limb containing interconnected bones, muscles, tendon, joint and skin, the cellular processes of cell fate specification, proliferation, apoptosis and migration must all be tightly controlled. Perturbations in any of these cellular processes can affect proper tissue patterning and result in structural malformations within the developing limb.

The limbs are derived from the lateral plate mesoderm (LPM), located along the flank of the main body axis lateral to the somites. Initiation of limb bud outgrowth is stimulated by cues from the tissues medial to the prospective limb-forming regions (reviewed by Capdevila and Izpisua Belmonte, 2001). The early limb bud is composed of loosely organized mesenchymal cells surrounded by a layer of ectoderm, and these cells subsequently develop into the different structural elements of the limb, including: the stylopod (humerus or femur), zeugopod (radius and ulna; tibia and fibula), and the autopod (hand or foot).

The developing limb is organized along three primary axes: antero-posterior (thumb to little finger), proximo-distal (shoulder to finger tips), and dorso-ventral (back of the hand to the palm). Patterning of each of these limb axes is controlled by different signaling centers within the developing limb bud (Fig 1.9). The zone of polarizing activity (ZPA) is located in a posterior domain of the limb bud and expresses the secreted protein SHH to pattern the antero-

posterior axis (reviewed by (Tickle, 2003). A specialized ectodermal structure which runs along the length of the distal tip of the limb bud, called the apical ectodermal ridge (AER), expresses Fgf secreted proteins to pattern the proximo-distal axis (Martin, 1998). Dorso-ventral patterning is controlled by expression of *En1* in the ventral ectoderm and *Wnt7a* in the dorsal ectoderm (Dealy et al., 1993; Logan et al., 1997; Loomis et al., 1996; Parr and McMahon, 1994).

One of the fundamental questions of developmental biology is how the body plan is established during embryonic development and how the precise arrangement and patterning of specialized cells and tissues arise. The processes that regulate limb development are tightly coordinated, as each digit forms in a specific place at a specific time within the developing autopod. However, the molecular mechanisms and genetic pathways coordinating these processes are still largely unknown (Karsenty, 2003).

Figure 1.9 Anatomy of the developing limb bud. (A) Scanning EM of a mouse embryo at E10 (lateral view) shows the protrusion from the lateral body wall of the nascent hindlimb bud (HLB) and forelimb bud (FLB). The somites (so) and tail bud (TB) are readily visible. (B) Scanning EM of a chick hindlimb bud (ventro-lateral, posterior view) at stage 24, showing the distinctive morphology of the AER. (C) A ventro-lateral, posterior view of an established chick limb bud at stage 23, showing the locations of the three major signaling centers that control outgrowth and patterning of the limb: dorsal ectoderm (DE); apical ectodermal ridge (AER); and zone of polarizing activity (ZPA). The dashed oval indicates the location of the progress zone (PZ) in the mesenchyme sub-adjacent to the AER, which contains the stem cell population that gives rise to limb skeletal elements in response to signals from the DE, AER, and ZPA. Reprinted with permission from G.R. Martin and Cold Spring Harbor Laboratory Press (copyright 1998).

Figure 1.9

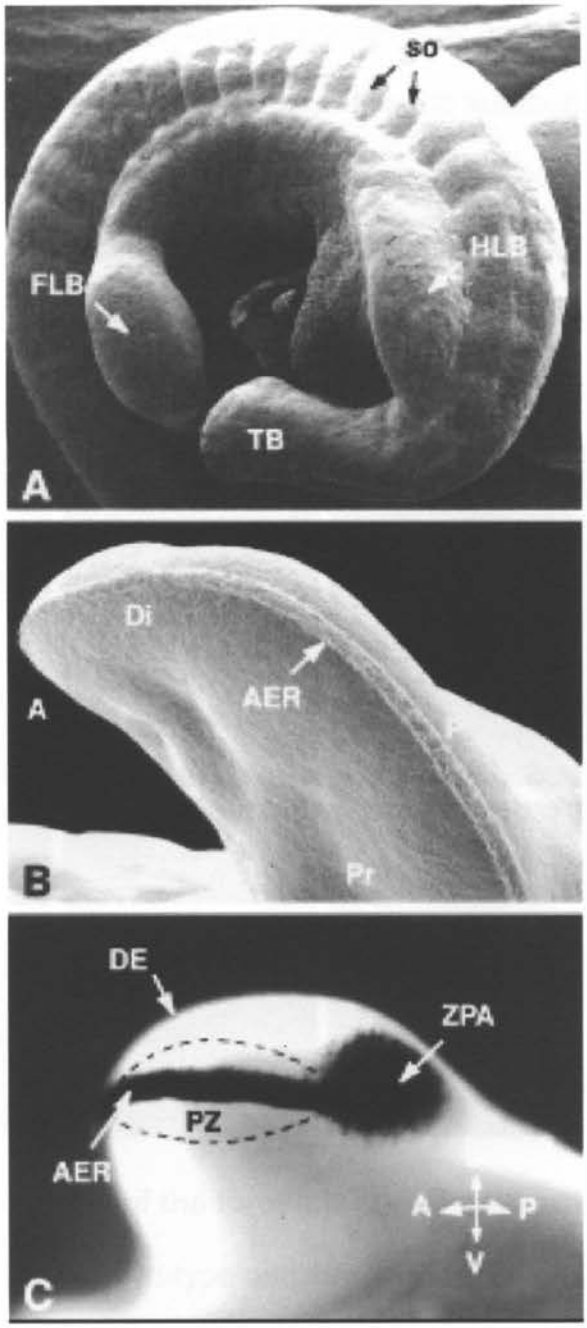

B. Digit formation

Within the developing autopod, digit formation begins as prechondrogenic condensations, which are morphologically detectable as local regions of increased cell density at specific locations within the autopod (Fig 1.10 A and C). In the absence of functional HOXA13, the mesenchyme does not condense correctly and the digits fail to form properly. The most severe defects are seen in the loss of digit I and reduction of digit V in *Hoxa13*$^{-/-}$ embryos (Fig 1.10 B,D,F,H).

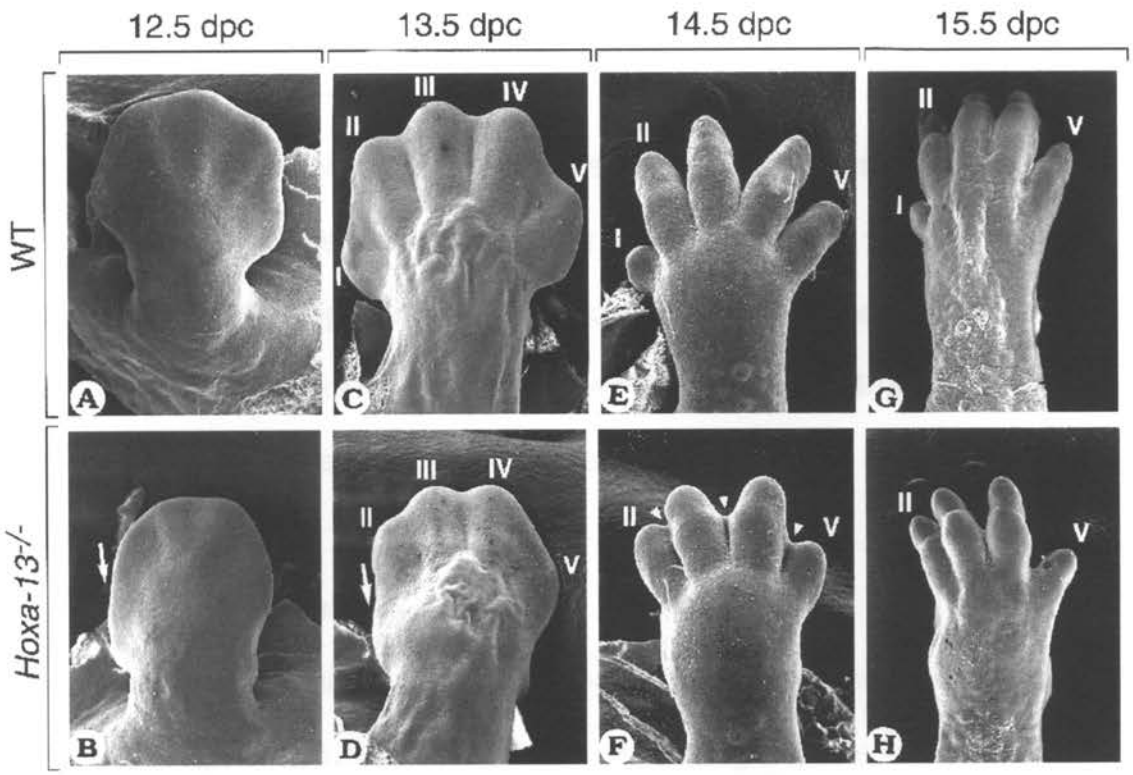

Figure 1.10 Scanning EM of the forelimb in wild-type and *Hoxa13*$^{-/-}$ embryos. Dorsal views of wild-type and *Hoxa13*$^{-/-}$ embryos at E12.5-E15.5. Arrows indicate a loss of digit I, arrowheads indicate poor digit separation. Reproduced from (Fromental-Ramain et al., 1996b) with the permission of The Company of Biologists Ltd.

The bone morphogenetic proteins (BMPs) belong to the transforming growth factor β superfamily of secreted proteins that have been implicated in cartilage and bone formation. BMPs were initially discovered because of their ability to promote ectopic cartilage and bone formation when implanted under the skin or into the muscle of adult rats (Sampath and Reddi, 1981; Urist et al., 1979). Several BMPs, including BMP2, BMP4, BMP6 and BMP7 are expressed in the developing limb and induce cartilage and bone growth by ectopic application or overexpression in the limb bud (Duprez et al., 1996; Iwasaki et al., 1997; Macias et al., 1997). In addition, ectopic expression of the BMP antagonist Noggin in embryonic chick (*G. gallus*) limbs inhibits BMP signaling and blocks cartilage formation (Pizette and Niswander, 2000). Based on these findings, perturbations in BMP signaling may be involved in the reduced chondrogenesis phenotype found in *Hoxa13*$^{-/-}$ limbs, however the status of BMPs and BMP signaling in these tissues had not been previously tested.

C. Interdigital programmed cell death

In addition to digit condensation, another key process in digit formation is interdigital programmed cell death (IPCD). As the digits develop they are separated by interdigital tissue composed of undifferentiated mesenchymal cells. In species with separated digits, such as mouse and human, IPCD functions to remove the interdigital tissues and separate the digits. In *Hoxa13*$^{-/-}$ embryos, IPCD is reduced and interdigital webbing persists between the digits (Fig 1.10, white arrowheads in F,H).

BMPs, which have a role in bone formation, have also been implicated in triggering programmed cell death in the interdigital regions of the limb (Zuzarte-Luis and Hurlé, 2005). Application of BMP proteins to chick limb buds results in growth and differentiation of the prechondrogenic mesenchyme as well as massive apoptosis in the undifferentiated mesoderm (Macias et al., 1997). These data suggest that one modulator of the response to a BMP signal within the limb is the developmental state of the cells that are receiving the BMP signal. Based on our current knowledge of BMP function, compromised BMP signaling is a candidate for both the chondrogenic and IPCD defects manifested in *Hoxa13*$^{-/-}$ autopods, suggesting HOXA13 may directly regulate BMP signaling in these tissues.

IV. BMPs and limb development

A. BMP signaling in the limb

BMPs function as secreted growth factors that signal through serine/threonine receptor kinases (RSTKs) composed of type I and type II receptors. Type IA and IB receptors have been shown to mediate the chondrogenic effect of BMPs, but the receptor involved in the control of apoptosis has not yet been definitively characterized (Yi et al., 2000; Zuzarte-Luis and Hurlé, 2005).

The intracellular signaling pathways triggered by BMP-RSTK binding are not completely known. One pathway involves the phosphorylation of the intracellular Smad proteins: Smads 1, 5, and 8, triggered by binding of the BMP ligand to an RSTK. Phosphorylated Smads 1, 5, and 8 then bind to a cofactor, Smad 4, and translocate to the nucleus where they activate BMP target gene transcription (Fig 1.11) (Zuzarte-Luis et al., 2004).

One way in which BMP signaling is mediated, is through the action of BMP antagonists. To date, a number of BMP antagonists have been identified, including: Noggin, Gremlin, Chordin, Follistatin, and Sostdc1 (Capdevila and Johnson, 1998; Francis-West et al., 1999a; Laurikkala et al., 2003; Merino et al., 1999b; Merino et al., 1999c). One conserved feature of these proteins is that they all contain a cysteine knot, a protein motif typically found in secreted proteins involved in extracellular signaling (Avsian-Kretchmer and Hsueh, 2004). The BMP antagonists function as secreted molecules that bind to BMPs and

prevent BMP binding to RSTKs and transduction of the BMP signal (Hsu et al., 1998; Piccolo et al., 1996).

The BMP antagonist SOSTDC1 (also referred to in the literature as USAG1 and ECTODIN) is a secreted protein that binds to BMP2, BMP4, BMP6, and BMP7 with high affinity and blocks BMP signaling in a dose-dependant manner (Laurikkala et al., 2003; Yanagita et al., 2004). *Sostdc1* is abundantly expressed in the developing kidney and tooth bud where it is predicted to regulate the availability of "active" BMPs within these tissues. Indeed, in the developing tooth bud *Sostdc1* is critical for the development and patterning of the enamel knot and cusps by restricting functional BMP (Kassai et al., 2005). Interestingly, *Sostdc1* expression is also induced by BMPs, suggesting a regulatory feedback system for regulating both BMP activation and inhibition (Laurikkala et al., 2003).

An additional level of complexity within BMP signaling is mediated by the use of different types of BMP receptors (BMPRs) to receive and transduce the BMP signal. BMPs bind to type I and II RSTK receptors for signal transduction. There are three known type I receptors bound by BMPs: ALK-2, BMPR-IA, and BMPR-IB. In addition, there are three type II receptors: BMPR-II, ActR-II, and ActR-IIB which are bound by BMPs (Miyazono et al., 2005). The type I BMPRs, BMPR-IA and BMPR-IB, have been found to regulate distinct processes during chick limb development. BMPR-IB is expressed in the cartilage primordium, and its activity is necessary for the initial steps of chondrogenesis. BMPR-IA is expressed at later stages of chondrogenesis and regulates chondrocyte

differentiation. In addition, BMPR-IB also mediates the process of apoptosis. Constitutive activation of BMPR-IB causes increased cell death in the limb, and expression of a dominant negative BMPR-IB inhibits apoptosis in this same domain (Zou et al., 1997b). These findings provide a framework for understanding the complexity of how the expression of specific BMPRs within tissues can mediate the different outcomes of chondrocyte formation and maturation or programmed cell death.

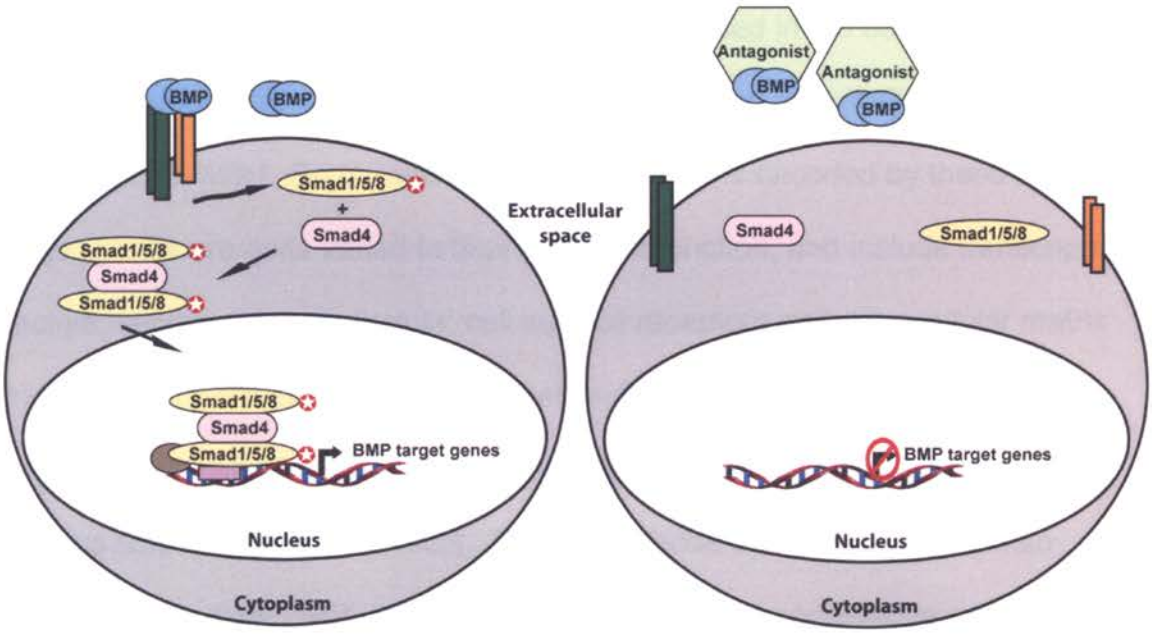

Figure 1.11 BMP signaling in the developing limb. In a cell receiving an "active BMP signal" (left side), BMP-induced heteromeric receptor complex formation leads to the phosphorylation of Smads 1, 5, and 8. Activated Smad1/5/8 form complexes with Smad4 and translocate to the nucleus where they interact with transcription factors and co-regulators in a transcription complex to regulate the expression of target genes. In a cell with "inactive BMP signaling" (right side), a BMP antagonist interacts with BMPs in the extracellular space. This interaction prevents receptor binding, Smad phosphorylation, and BMP-induced target genes are not expressed.

B. BMP target genes

A number of BMP-responsive genes expressed in the developing limb have been identified, including: *Msx1*, *Msx2*, *Collagen type II*, *Collagen type X*, *Sox9*, *Ihh*, *Id*, *Mfh1*, *Bambi* and *Runx2*. The proteins encoded by these BMP target genes are quite varied in their form and function, and include transcription factors, secreted growth factors, cell surface receptors and extracellular matrix molecules. However, one common feature is that these genes are important regulators of limb development and perturbations in their expression cause various limb and skeletal defects. Several of these BMP target genes also function to mediate BMP signaling by direct or indirect cooperative or inhibitory functions.

Msx1 and *Msx2* are homeodomain transcription factors expressed in multiple regions of the developing embryo, including the limb and tooth buds (Hill et al., 1989; Robert et al., 1989). Mice that are homozygous mutant for both *Msx1* and *Msx2* have severe limb defects including loss of digit I and persistence of interdigital tissues (Lallemand et al., 2005). *Sox9* is a high-mobility-group (HMG) domain transcription factor involved in chondrocyte differentiation in the limb, and its expression can be induced in chick somite explants treated with ectopic BMP (Zeng et al., 2002). In humans, mutations in *Sox9* result in campomelic dysplasia, a lethal skeletal malformation, and XY sex reversal (Bi et al., 1999). Homozygous deletion of *Sox9* in the mouse results in embryonic lethality at E11.5 due to cardiovascular defects, and removal of *Sox9* specifically

in the limb mesenchyme results in the complete absence of both cartilage and bone (Akiyama et al., 2002; Bi et al., 2001).

Mfh1 is a member of the forkhead/winged helix transcription factor family. Mice null for *Mfh1* have defects in both axial and cranial skeletogenesis. *Mfh1* is expressed in the same limb domains as BMPs and can be induced in *M. musculus* E11.5 limb buds with ectopic BMP treatment (Nifuji et al., 2001). *Runx2* is also a transcription factor that is induced by BMP signaling and physically interacts with Smads to regulate the transcription of target genes involved in osteoblast differentiation (Zhang et al., 2000).

Collagen type II and *Collagen type X* are extracellular matrix molecules involved in chondrocyte maturation that have been shown to be induced by BMPs in cultured mesenchymal stem cells (Bosnakovski et al., 2006; Lengner et al., 2004; Park et al., 2005). Mutations in *Collagen type II* result in several skeletal dysplasias, including: Langer-Saldino achondrogenesis and spondyloepiphyseal dysplasia congenita (Lee et al., 1989; Vissing et al., 1989). *Collagen type X* is also implicated in skeletal dysplasias, including: Schmid-type metaphyseal chondrodysplasia and spondylometaphyseal dysplasia (Hasegawa et al., 1994; Warman et al., 1993).

Ihh is a secreted growth factor expressed in chondrocytes and has a role in the development of the endochondral skeleton (Long et al., 2004). *Ihh* colocalizes with the BMP type I receptor ALK2 in chick limb buds and is induced by BMP signaling (Zhang et al., 2003). *Bambi* is a BMP antagonist that is induced by BMP signaling (Karaulanov et al., 2004). The *Bambi* gene encodes a

transmembrane pseudoreceptor for BMPs that lacks the intracellular kinase domain required for intracellular signaling (Balemans and Van Hul, 2002).

Id family members encode negative regulators of the basic helix-loop-helix (bHLH) transcription factors that are involved in the control of cell growth, differentiation and tumorigenesis (Norton et al., 1998). The Id proteins lack the basic region but contain the HLH motif, allowing them to form heterodimers with bHLH proteins and render them inactive for DNA binding and target gene activation. In ES cells and osteoblast-like cells *Id1*, *Id2*, and *Id3* have been identified as BMP-induced early target genes (Hollnagel et al., 1999; Ogata et al., 1993). In differentiating tissues, regulation of *Id* expression has been found to be involved in several processes including: myogenesis, bone morphogenesis, and trophoblast development (Janatpour et al., 2000; Jen et al., 1992; Kurabayashi et al., 1994).

Perturbations in BMP signaling affect the expression and function of a variety of downstream target genes. In order to determine the status of BMP signaling in *Hoxa13*$^{-/-}$ autopods, it will be necessary to ascertain the expression status of genes downstream from the BMP signal.

V. *Hoxa13* and embryonic development

A. The Hoxa13-GFP mouse model

To study the function of HOXA13 during embryonic development a *Hoxa13-GFP* knockout mouse model was engineered by my mentor Dr. H. Scott Stadler while in the laboratory of Dr. Mario Capecchi (Stadler et al., 2001). This system utilizes a protein produced by the jellyfish *Aequorea victoria* called green fluorescent protein (GFP), which absorbs blue light and emits green light. The introduction of the DNA coding sequence for this protein into specific genes provides a useful molecular marker for expression, which is detected as green fluorescence in the presence of oxygen and excitatory light (Godwin et al., 1998). A *Hoxa13* loss-of-function allele, $Hoxa13^{GFP}$, was generated by replacing the homeobox sequence with the coding sequence for GFP. This construct was targeted to the *Hoxa13* locus of mouse ES cells by homologous recombination (Fig 1.12) (Stadler et al., 2001).

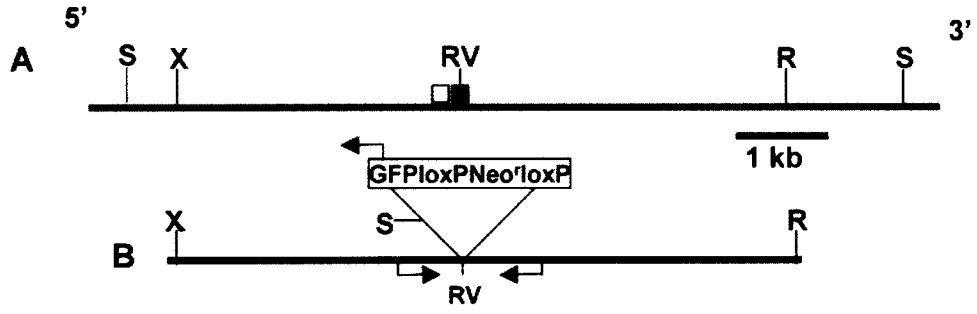

Figure 1.12 *Hoxa13*^{GFP} targeting vector. (A) Partial restriction map of the *Hoxa13* locus. White and black boxes represent exons 1 and 2 respectively. S, SphI; X, XhoI; RV, EcoRV; R, EcoRI. (B) The 10 kb *Hoxa13*^{GFP} targeting vector; forward and reverse PCR primer sites are denoted by the black arrows. Reproduced with permission from H. Scott Stadler (Stadler et al., 2001).

Analysis of *Hoxa13*^{GFP} expression in the developing mouse embryo correlates with the previously published *Hoxa13* mRNA expression patterns in the developing limb, genitourinary tissues and umbilical arteries (Fig 1.13).

Figure 1.13 *Hoxa13*^{GFP} expression in the developing mouse embryo. (A) Expression in the distal forelimb at E10.5. Arrowhead denotes no expression in the AER. (B) *Hoxa13*^{GFP} expression expands within the progress zone at E11.5. Localization of *Hoxa13*^{GFP}-expressing cells to the condensing digit regions in E13.5 forelimbs (C) and hindlimbs (D). (E) Condensing vascular mesenchyme in the umbilical arteries (UA) also expresses *Hoxa13*. (F) Expression of *Hoxa13*^{GFP} is also readily detected in the genital ridge (GR) and tissues surrounding the urogenital sinus (US). Reproduced with permission from H. Scott Stadler (Stadler et al., 2001).

Figure 1.13

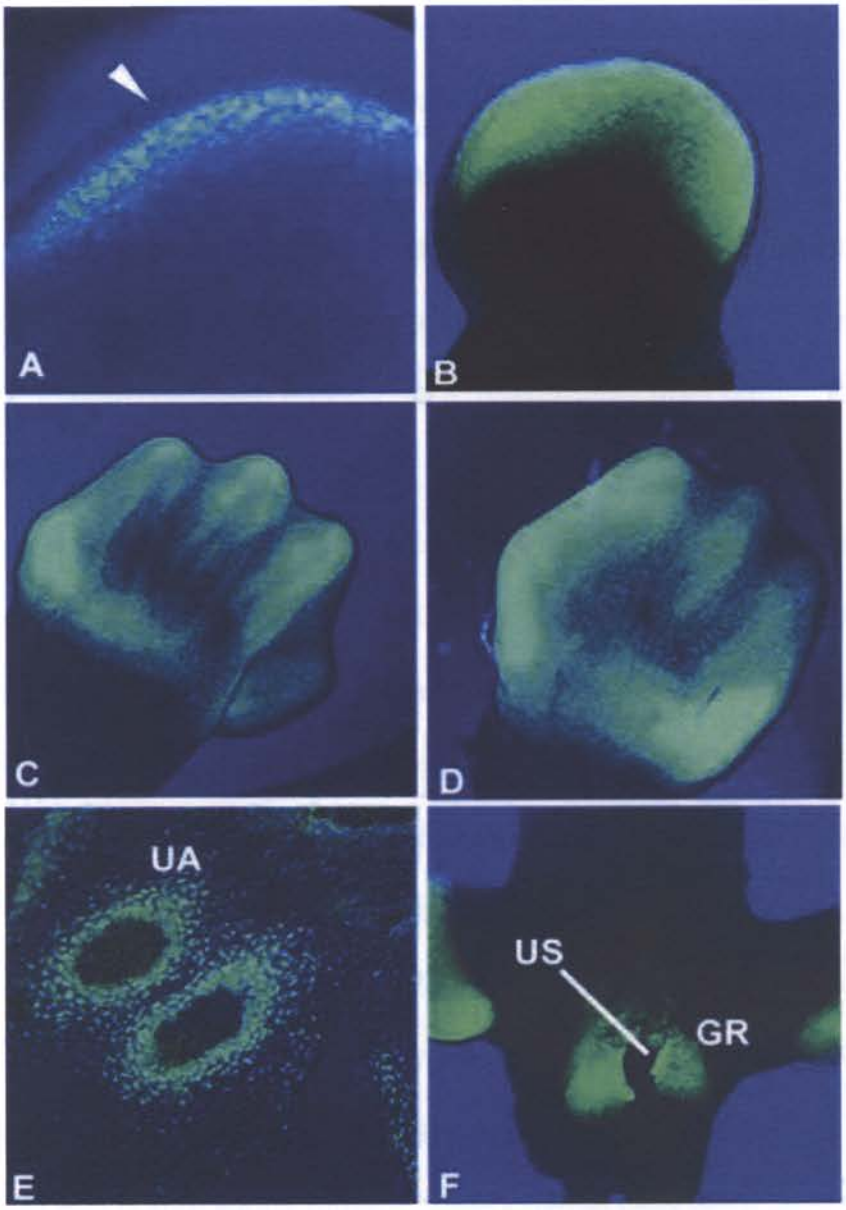

B. Hoxa13 mutant phenotypes

One key difference between the mouse and human phenotypes is the dosage requirements for *Hoxa13 in utero*. In HFGS and Guttmacher syndrome, defects in one allele of *Hoxa13* are sufficient to cause developmental malformations. However, in the mouse a single $Hoxa13^{GFP}$ allele does not cause a significant phenotype other than soft tissue fusions between hindlimb digits II and III in 37% of adult $Hoxa13^{GFP}$ heterozygotes. The $Hoxa13^{GFP/GFP}$ mutant embryos die *in utero* between E11.5-E14.5, presumably from cardiovascular defects (Stadler et al., 2001).

Analysis of $Hoxa13^{GFP/GFP}$ mutant embryos reveals a recapitulation of the phenotypes associated with Hand-Foot-Genital syndrome. Loss of functional HOXA13 results in reduced chondrogenesis, syndactyly, hypodactyly, umbilical artery defects, and hypospadias. These phenotypes correlate exactly with the sites of *Hoxa13* expression, suggesting that the loss of functional HOXA13 has effects within its wild-type expression domain (Figs 1.10 and 1.13).

One aspect of limb development that is severely compromised in $Hoxa13^{GFP/GFP}$ mutant embryos is the formation of mesenchymal condensations in the autopod. To characterize this defect, FACS sorted $Hoxa13^{GFP}$ heterozygous and homozygous mutant mesenchymal cells were isolated. $Hoxa13^{GFP/GFP}$ mutant mesenchymal cells were found to be defective in forming chondrogenic condensations *in vivo*. Analysis of adhesion molecules present in wild-type and $Hoxa13^{GFP/GFP}$ mutant limbs and mesenchymal cells revealed a reduction in *Epha7* expression $Hoxa13^{GFP/GFP}$ mutant tissues, suggesting a role

for Epha proteins in mediating cell adhesion in these tissues. Indeed, when an Epha7 blocking antibody was used to treat micromass cell cultures, the capacity of *Hoxa13*^{GFP} heterozygous cells to condense and form chondrogenic condensations was inhibited (Stadler et al., 2001).

These finding implicate Epha7 as a critical component of chondrogenesis in limb mesenchyme, suggesting a role for Epha7 in the *Hoxa13*$^{GFP/GFP}$ mutant phenotype. The identification of additional perturbations in gene expression in *Hoxa13* homozygous mutant tissues are integral to the analysis of HOXA13 function in the developing limb, which will be addressed in Chapters 2 and 3 of this dissertation.

C. HOXA13 homeodomain

A critical component of HOXA13 function in developing tissues is the HOXA13 homeodomain. Despite conservation of the homeodomain motif across species and HOX homologs, there is evidence that variation in homeodomain amino acid sequences conveys specificity and functional divergence.

An example of the inherent specificity of the HOXA13 homeodomain comes from a homeodomain swap experiment where the HOXA11 homeodomain was replaced by the HOXA13 homeodomain in a mouse model. The homeodomain swap allele was inserted in frame within the *Hoxa11* locus and is expressed in the same spatio-temporal pattern as endogenous *Hoxa11*. Wild-type *Hoxa11* is expressed within discrete regions of the limb and reproductive tract, and its expression does not overlap with *Hoxa13*. Despite the

conservation of amino acid identity between the HOXA11 and HOXA13 homeodomains, they were not functionally interchangeable in the mouse (Fig 1.14). Regions of the limb and female reproductive tract patterned by HOXA11 took on a phenotype resembling tissues normally patterned by HOXA13 (Zhao and Potter, 2001).

		% Identity to A13
A11:	QRTRKKRCPYTKYQIRELEREFFFSVYINKEKRLQLSRMLNLTDRQVKIWFQNRRMKEKK	60%
A13:	RRGRKKRVPYTKVQLKELEREYATNKFITKDKRRRISATTNLSERQVTIWFQNRRVKEKK	100%

Figure 1.14 HOXA11 and HOXA13 homeodomain alignment. Conserved amino acids are black, divergent amino acids are red. Percent identity to the HOXA13 homeodomain sequence is indicated on the right.

The DNA sequences bound by the HOXA13 homeodomain have not been previously identified. Studies to identify and quantitate HOXA13 DNA-binding interactions are an important step in understanding how HOXA13 functions within the cell. Identification of HOXA13 binding sites will also provide a useful tool for identifying target genes whose transcriptional regulation requires HOXA13 DNA-binding function.

D. HOXA13 protein-protein interactions

Several recent studies have focused on identifying proteins that interact with HOXA13. A yeast two-hybrid screen using a truncated HOXA13 protein identified SMAD5 as a candidate interactor. SMAD5 is a receptor activated

Smad that is involved in transcriptional regulation of BMP target genes. However, this interaction was not confirmed by co-immunoprecipitation studies and the amino acid residues required for the interaction have not been characterized (Williams et al., 2005a). An analysis of co-localization domains of HOXA13 and SMAD5, as well as the identification of target genes and DNA binding sites should provide more insight into any potential function of this interaction *in vivo*.

Another potential HOXA13 interactor is MEIS1B, which interacts with HOXA13 in yeast and transfected NIH 3T3 cells. This interaction may have a role in HOXA13 function in the developing genitourinary system where HOXA13 and MEIS proteins are co-expressed. However, MEIS proteins are not expressed in the developing limb, precluding a role for this interaction in limb development (Williams et al., 2005b). Currently, there is not a clear understanding of how HOXA13 protein-protein interactions may affect HOXA13 function during embryonic development. Additional research is still required to identify proteins that interact with HOXA13 and are expressed in tissues relevant to HOXA13 function.

E. HOXA13 target genes

The identification of HOXA13 target genes is a new area of research that will provide insight into how HOXA13 functions to pattern the developing embryo. In a recently published study to identify HOXA13 target genes, a *Hoxa13*-FLAG-IRES-EGFP expression construct was retrovirally transfected into NIH 3T3 cells

and selected for stably transfected cells (McCabe and Innis, 2005). These *Hoxa13*-FLAG-IRES-EGFP cells were then used for a chromatin immunoprecipitation (ChIP) assay, where chromatin from *Hoxa13*-FLAG-IRES-EGFP expressing cells and untransfected cells were immunoprecipitated with a FLAG antibody, cloned and sequenced. From this assay HOXA13 binding to a genomic region within intron 2 of the gene *Enpp2* was identified. *Enpp2* was originally identified as a protein secreted by cultured melanoma cells and has been implicated in cell motility (Chen and O'Connor, 2005; Koike et al., 2006). A role for *Enpp2* in embryonic development has not yet been identified or characterized.

One critique of this experimental design is the use of a system in which HOXA13 is overexpressed in a cultured cell line. From our quantitative analysis of HOXA13-DNA binding we have found that HOXA13 binds specific DNA sequences with high affinity (3 nM), and increasing HOXA13 protein levels facilitates DNA binding at low affinity sequences that may not be physiologically relevant (Chapter 3). Exceeding the *in vivo* levels of HOXA13 protein within a cell would potentially saturate the *bona fide*, *in vivo* binding sites and result in the detection of DNA binding events that are merely an artifact of overexpression. Additional studies, such as those described here, to identify HOXA13 target genes within relevant HOXA13-expressing embryonic tissues are critical for understanding HOXA13 function in patterning the developing embryo.

VI. Hypothesis and Rationale

The goal of my thesis research is to characterize how HOXA13 functions to pattern the developing limb. Although the limb defects associated with a loss of HOXA13 function have been well documented, the underlying cause of these phenotypes is not well understood. A thorough analysis of HOXA13 DNA binding function, and the identification of HOXA13 target genes is critical for understanding how this transcription factor mediates normal limb development.

Hypothesis:

HOXA13 function is mediated by specific homeodomain-DNA interactions that regulate the expression of downstream target genes in the developing autopod.

To test this hypothesis I have addressed three specific aims:

1. **Assess the status of BMP expression and function in *Hoxa13*$^{GFP/GFP}$ mutant autopods.**
2. **Identify DNA sequences bound by the HOXA13 homeodomain and quantitate these interactions.**
3. **Identify novel HOXA13 target genes misexpressed in *Hoxa13*$^{GFP/GFP}$ mutant autopods.**

CHAPTER 2

HOXA13 regulates *Bmp2* and *Bmp7*

HOXA13 regulates the expression of bone morphogenetic proteins 2 and 7 to control distal limb morphogenesis

Wendy M. Knosp[2,4], Virginia Scott[1,4], Hans Peter Bächinger[1,3] and H. Scott Stadler[1,2*]

1. Shriners Hospital for Children Research Division Portland, Oregon 97239
2. Department of Molecular and Medical Genetics Oregon Health and Science University Portland, Oregon 97239
3. Department of Biochemistry and Molecular Biology Oregon Health and Science University Portland, Oregon 97239
4. These authors contributed equally to this work

***Development*, 131(18), 4581-4592 (2004).**

I. Abstract

In humans and mice, loss of HOXA13 function causes defects in the growth and patterning of the digits and interdigital tissues. Analysis of *Hoxa13* expression reveals a pattern of localization overlapping with sites of reduced *Bmp2* and *Bmp7* expression in *Hoxa13* mutant limbs. Biochemical analyses identified a novel series of *Bmp2* and *Bmp7* enhancer regions that directly interact with the HOXA13 DNA-binding domain and activate gene expression in the presence of HOXA13. Immunoprecipitation of HOXA13-*Bmp2* and –*Bmp7* enhancer complexes from the developing autopod confirm that endogenous HOXA13 associates with these regions. Exogenous applications of BMP2 or BMP7 partially rescues the *Hoxa13* mutant limb phenotype, suggesting that decreased BMP-signaling contributes to the malformations present in these tissues. Together, these results provide conclusive evidence that HOXA13 regulates *Bmp2* and *Bmp7* expression, providing a mechanistic link between HOXA13, its target genes, and the specific developmental processes affected by loss of HOXA13 function.

II. Introduction

The analysis of limb development has yielded remarkable insights into the molecular and genetic mechanisms required to form a functional three-dimensional structure. In mice, initiation of the forelimb buds occurs at embryonic day (E) 9.0 as a small outgrowth of the lateral plate mesoderm at the junction of the caudal and thoracic somites (Kaufman and Bard, 1999; Solursh et al., 1990; Tickle et al., 1976). Following induction, limb bud growth and expansion continues under the influence of signals emanating from the three primary limb axes: including FGFs to maintain proliferation in the proximal-distal axis, sonic hedgehog which establishes the zone of polarizing activity in the anterior-posterior axis, and *Wnt7a* and *En1* which specify the dorsal-ventral polarity of the developing limb (Chiang et al., 1996; Crossley et al., 1996; Lewandoski et al., 2000; Loomis et al., 1998; Min et al., 1998; Moon and Capecchi, 2000; Ohuchi et al., 1997; Parr and McMahon, 1994; Riddle et al., 1993; Sekine et al., 1999).

While many of the genes required for normal limb development have been identified (see reviews by Gurrieri et al., 2002; Logan, 2003; Mariani and Martin, 2003; Niswander, 2003; Tickle, 2003), surprisingly little is known about how these genes are transcriptionally regulated. Among the factors likely to regulate the expression of limb patterning genes are the 5' HOX transcription factors, whose loss of function phenotypes demonstrate their capacity to regulate key developmental processes such as cell adhesion, apoptosis, proliferation and

migration (Boulet and Capecchi, 2004; Davis and Capecchi, 1994; Davis et al., 1995; Dollé et al., 1989; Fromental-Ramain et al., 1996a; Fromental-Ramain et al., 1996b; Kmita et al., 2002; Spitz et al., 2003; Stadler et al., 2001; Wellik and Capecchi, 2003). While it is clear that HOX proteins mediate many of the cellular events during limb morphogenesis, the mechanistic links between these transcription factors, their target genes, and their effects on specific cellular processes are still largely unknown (Boulet and Capecchi, 2004; Morgan et al., 2003; Stadler et al., 2001; Wellik and Capecchi, 2003). One reason for this is that HOX proteins may not regulate the global expression of any particular target gene, but instead control the development of specific tissues through direct interactions with tissue-specific gene regulatory elements (Grenier and Carroll, 2000; Hombria and Lovegrove, 2003; Weatherbee et al., 1998).

In the developing limb, HOXA13 localizes to discrete domains within the interdigital and interarticular regions where its function is required for interdigital programmed cell death (IPCD), digit outgrowth, and chondrogenesis (Fromental-Ramain et al., 1996b; Stadler et al., 2001). This observation lead us to hypothesize that HOXA13 directly regulates genes whose products are necessary for IPCD and joint formation. Testing this hypothesis, we detected changes in the expression of bone morphogenetic proteins 2 and 7 (*Bmp2*, *Bmp7*) in the interdigital and distal joint tissues, suggesting that HOXA13 may directly regulate their expression in these discrete regions. Scanning the DNA sequences upstream of *Bmp2* and *Bmp7* we identified a series of nucleotide sequences preferentially bound by the HOXA13 DNA-binding domain (A13-

DBD). *In vivo* characterization of these DNA sequences revealed they function as enhancer elements which, in the presence of HOXA13, activate the expression of reporter constructs independent of sequence orientation. Furthermore, in the developing autopod, endogenous HOXA13 binds these same enhancer elements, which can be immunoprecipitated with a HOXA13-specific antibody. In *Hoxa13* mutant limbs, both IPCD and *Msx2* expression are partially restored with exogenous BMP2 or BMP7 treatment, suggesting that HOXA13 is required for sufficient levels of BMP2 and BMP7 to be expressed in the interdigital tissues as well as the competency of these tissues to fully respond to BMP signaling. Together, these results provide the first molecular evidence that HOXA13 controls distal limb morphogenesis through direct regulation of *Bmp2* and *Bmp7* expression, whose combined functions are necessary for normal digit morphogenesis and IPCD.

III. Results

Hoxa13 is expressed in discrete regions of the developing autopod

Examination of *Hoxa13* expression in the developing autopods revealed a dynamic spatio-temporal pattern of expression in tissues critical for IPCD and digit chondrogenesis. At E12.5 *Hoxa13* expression is localized to the distal autopod mesenchyme in both the digit condensations and interdigital tissues (data not shown, Haack and Gruss, 1993). By E13.5 *Hoxa13* expression transitions to the peridigital tissues and interarticular condensations (Fig 2.1 A) whereas in E14.5 forelimbs, *Hoxa13* expression becomes restricted to the distal interarticular joint fields and nail beds (Fig 2.1 C). In homozygous mutants, the localization of *Hoxa13* transcripts is consistently elevated at all gestational ages when compared to wild-type controls, suggesting that HOXA13 may negatively regulate its own expression or that mutant *Hoxa13-GFP* transcripts turn over at a slower rate than wild-type *Hoxa13* mRNA (Fig 2.1 B and D).

To correlate the sites of *Hoxa13* localization with malformations present in *Hoxa13* mutant limbs, we examined digit separation and development in E15.5 limbs. In these tissues the loss of *Hoxa13* function resulted in severe malformations of the distal joints as well as a persistence of the interdigital tissues (Fig 2.1 E and F) (Fromental-Ramain et al., 1996b; Stadler et al., 2001). Interestingly, the separation of digits II-V is affected in a highly reproducible pattern in *Hoxa13* mutant forelimbs, where digits II-III and IV-V exhibit the

greatest degree of soft-tissue fusion, whereas digits III-IV exhibit modest removal of the distal interdigital tissue (Fig 2.1 C-F).

Reduced *Bmp2* and *Bmp7* expression in *Hoxa13* mutant autopods

Recognizing that limbs lacking *Hoxa13* exhibit severe defects in the initiation of IPCD and joint formation (Stadler et al., 2001) (Fig 2.1) and that BMP2 and BMP7 function as key regulators of IPCD and digit chondrogenesis (Macias et al., 1997; Merino et al., 1998; Yokouchi et al., 1996; Zou et al., 1997a; Zou and Niswander, 1996; Zuzarte-Luis and Hurlé, 2002), we examined their expression in *Hoxa13* wild-type and mutant forelimbs. Analysis of *Bmp7* expression in E12.5 -13.5 wild-type embryos revealed high levels of expression in the interdigital tissues (Fig 2.1 G,I). In contrast, age-matched homozygous mutants exhibited a marked reduction in *Bmp7* expression in the interdigital and peridigital regions, specifically in domains that co-express *Hoxa13* (Fig 2.1 H,J and S-V).

Bmp2 expression was also reduced in the interdigital tissues, developing nail beds, and distal joints of E 12.5 and 14.5 homozygous mutants, which exhibited a diffuse distribution of *Bmp2* transcripts as compared to wild-type controls (Fig 2.1 A,C and K-N). Next, to determine whether the loss of BMP signaling in *Hoxa13* mutant limbs affects the expression of BMP-regulated genes, we examined *Msx2* expression in the distal interdigital tissues. In *Hoxa13* mutant limbs, *Msx2* expression was noticeably reduced in the interdigital tissues when compared to wild-type controls at E12.5 and 13.5 (Fig 2.1 O-R).

Figure 2.1 Spatio-temporal expression of *Hoxa13* correlates with sites of malformation and decreased Bmp expression. (**A-D**) Analysis of *Hoxa13* expression by *in situ* hybridization. *Hoxa13* is expressed in the distal interdigital mesenchyme and peridigital tissues (**A**, arrowheads). (**C**) *Hoxa13* localizes to the distal joint/nail bed in E14.5 limbs (arrowheads). (**B,D**) In homozygous mutants, elevated levels of $Hoxa13^{GFP}$ transcripts were detected throughout the autopod. (**E,F**) Alcian-blue staining of E15.5 mutant limbs reveals defects in distal digit separation (**F**, arrows) and chondrogenesis (arrowheads) as compared to wild-type controls (**E**). **Pi** = pisiform carpal element. (**G,H**) *Bmp7* expression is reduced in the distal interdigital tissues (arrows) of homozygous mutants compared to wild-type controls (arrowheads) at E12.5. (**I,J**) By E13.5 the peridigital expression of *Bmp7* is also reduced in *Hoxa13* mutant limbs (arrows) compared to wild-type (arrowheads). (**K,L**) *Bmp2* expression is also reduced in the interdigital tissues of E12.5 mutant embryos (arrows) when compared wild-type (arrowheads). (**M,N**) *Bmp2* expression is also reduced in the distal joints/nail beds of *Hoxa13* mutants (arrows) as compared to E14.5 controls (arrowheads). (**O-R**) *Msx2,* a target of BMP-signaling, also exhibits reduced interdigital expression in E12.5-13.5 mutant limbs (arrows) as compared to age-matched controls (arrowheads). (**S,U**) BMP7 (arrowhead) and HOXA13-GFP co-localize (yellow cells in panels **U** and **V**) in the interdigital tissues of E12.5 limbs. (**T,V**) Age-matched homozygous mutants exhibit reduced numbers of BMP7 positive cells in the same interdigital regions (arrow), a finding consistent with reduced *Bmp7* transcripts in these same tissues (compare **H and T**). Bar is 50 μm.

Figure 2.1

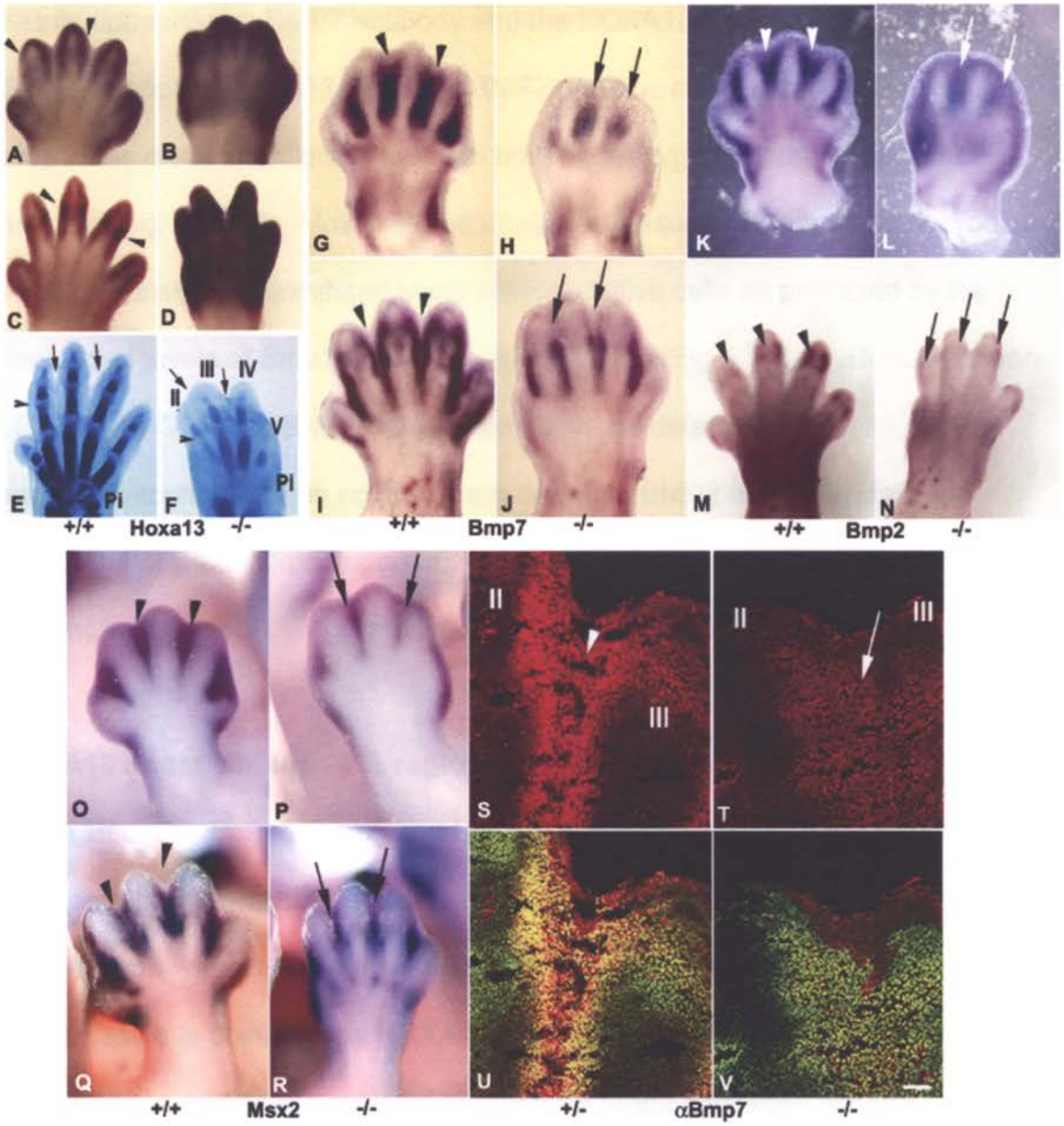
A
B
C
D
E
Pi
F
II
III
IV
V
Pi
+/+
Hoxa13
-/-
G
H
I
J
+/+
Bmp7
-/-
K
L
M
N
+/+
Bmp2
-/-
O
P
Q
R
+/+
Msx2
-/-
II
III
S
II
III
T
U
V
+/-
αBmp7
-/-

To verify that BMP7 and HOXA13 proteins co-localize to the same cells in developing interdigital tissues, we examined BMP7 and HOXA13 protein distributions using a BMP7 antibody and the HOXA13-GFP fusion protein. In E12.5 autopods, HOXA13-GFP and BMP7 proteins co-localized to the same cells in the distal interdigital tissues of both heterozygous and homozygous mutants (Fig 2.1 S-V). However, the interdigital tissues of *Hoxa13* homozygous mutants consistently exhibited fewer BMP7 positive cells as predicted by the decreased levels of *Bmp7* transcripts in this region (Fig 2.1 H,J). Co-localization of HOXA13-GFP and BMP2 proteins could not be determined by immunohistochemistry as commercially available BMP2 antibodies failed to detect BMP2 protein in autopod frozen sections at E12.5 or E13.5 (data not shown).

HOXA13 directly binds DNA regions upstream of *Bmp2* and *Bmp7*

Because *Bmp2*, *Bmp7,* and *Hoxa13* are co-expressed in the developing limb, and their expression is reduced in *Hoxa13* mutants, we hypothesized that HOXA13 may directly regulate *Bmp2* and *Bmp7* expression in the distal autopod. To address this possibility, a HOXA13 DNA-binding domain peptide (A13-DBD) was used to screen DNA regions upstream of *Bmp2* and *Bmp7* for direct HOXA13 binding. Prior to this analysis, it was necessary to confirm that the putative DNA-binding domain present in the carboxyl-terminus of HOXA13 actually folds into a DNA-binding structure and to determine the biophysical conditions that maintain proper folding for subsequent DNA-binding studies.

Characterization of the A13-DBD secondary structure by circular dichroic spectroscopy (CD) revealed the peptide stably folds into an alpha-helical structure, consistent with the predicted helix-turn-helix DNA-binding motif encoded by the A13-DBD peptide (Fig 2.2 A, left panel). The folded A13-DBD peptide also exhibited reasonable thermal stability, maintaining its alpha-helical structure between 4 and 25°C (Fig 2.2 A, right panel). At temperatures greater than 25°C the A13-DBD peptide showed a cooperative transition to a denatured conformation (Fig 2.2A, right panel), confirming the majority of the A13-DBD peptide folds into the detected alpha-helical motif. Based on this analysis we performed our DNA-binding experiments at temperatures between 4 and 25°C in order to maintain A13-DBD secondary structure stability. In contrast, full-length HOXA13 could not be examined for proper folding and function, as the molecule prepared by *in vivo* translation was only soluble in a denatured state, preventing CD analysis as well as its use as a DNA-binding molecule (data not shown).

To identify HOXA13 binding sites upstream of *Bmp2* and *Bmp7*, the A13-DBD peptide was incubated with 200-400 base pair (bp) regions upstream of *Bmp2* and *Bmp7*. In the presence of the A13-DBD peptide, strong DNA binding was detected within 600 bp of the *Bmp2* initiation codon, whereas for *Bmp7*, an A13-DBD binding site was not detected until 3,000 bp upstream of the initiation codon (data not shown). Using self-annealing oligonucleotides, the minimal DNA sequences bound by the A13-DBD peptide were identified (Fig 2.2 B). Within the *Bmp2* upstream region, four A13-DBD binding sites, *Bmp2 C1-C4*, were identified. For the bound *Bmp7* upstream region, a single A13-DBD binding site,

Bmp7C1, was identified (Fig 2.2 B). Competition experiments revealed that the A13-DBD peptide exhibited specificity and differential affinity for each of the bound DNA sequences (Fig 2.2 B,C). For *Bmp2*, the A13-DBD peptide exhibited the highest affinity for regions C1 and C3, which required competitor DNA concentrations between 300 and 750 nM to displace the bound radiolabeled probe. In contrast, the A13-DBD peptide exhibited less affinity for *Bmp2* region C4, where 150 nM concentrations of competitor DNA were sufficient to completely displace the corresponding radiolabeled oligonucleotide (Fig 2.2 B). A fourth *Bmp2* DNA region, *Bmp2*C2, was also bound by the A13-DBD peptide, however 2-4 fold higher concentrations of A13-DBD were required to affect its electrophoretic mobility (Fig 2.2 C).

Figure 2.2 Structural and functional analysis of the HOXA13 DNA-binding domain. The amino acid sequence of the A13-DBD peptide is presented above panel **A**. (**A**, left panel) Structural analysis of the A13-DBD peptide by circular dichroism spectroscopy indicates the peptide folds into a stable alpha-helical DNA-binding motif at 4°C (blue curve). At 60°C the majority of the alpha helical content is lost by thermal denaturation (red curve). (**A**, right panel) Thermal stability measurements of the A13-DBD peptide; the alpha-helical conformation is maintained between 4 and 25°C. At temperatures above 25°C the peptide cooperatively transitions to its denatured conformation. (**B,C,E**) A13-DBD peptide binds DNA regions upstream of *Bmp2* and *Bmp7*. Asterisks = unbound radiolabeled DNA, arrowheads = A13-DBD-DNA complexes. (**B**) Quantitation of the A13-DBD affinity for the bound DNA regions using increasing concentrations (black triangles) of cold competitor DNA (0, 150, 300, and 750 nM). (**C**) The *Bmp2C2* region requires 2-fold greater concentrations of A13-DBD to affect its electrophoretic mobility. (**D**) Radiolabeled control DNA sequences exhibited no change in electrophoretic mobility when incubated with 4-fold (2 μM) higher concentrations of the A13-DBD peptide. (**E**) A13-DBD binding specificity was confirmed using the *Bmp7C1* binding site, which could not be displaced from the A13-DBD peptide using 750 nM concentrations of the unlabeled negative control DNA (cNC), but is completely displaced using 750 nM unlabeled *Bmp7C1* competitor DNA (cBMP7C1). (**F**) Analysis of the DNA sequences bound by the A13-DBD reveal a novel series of Hox binding sites. Core TAAT site is designated in bold type.

Figure 2.2

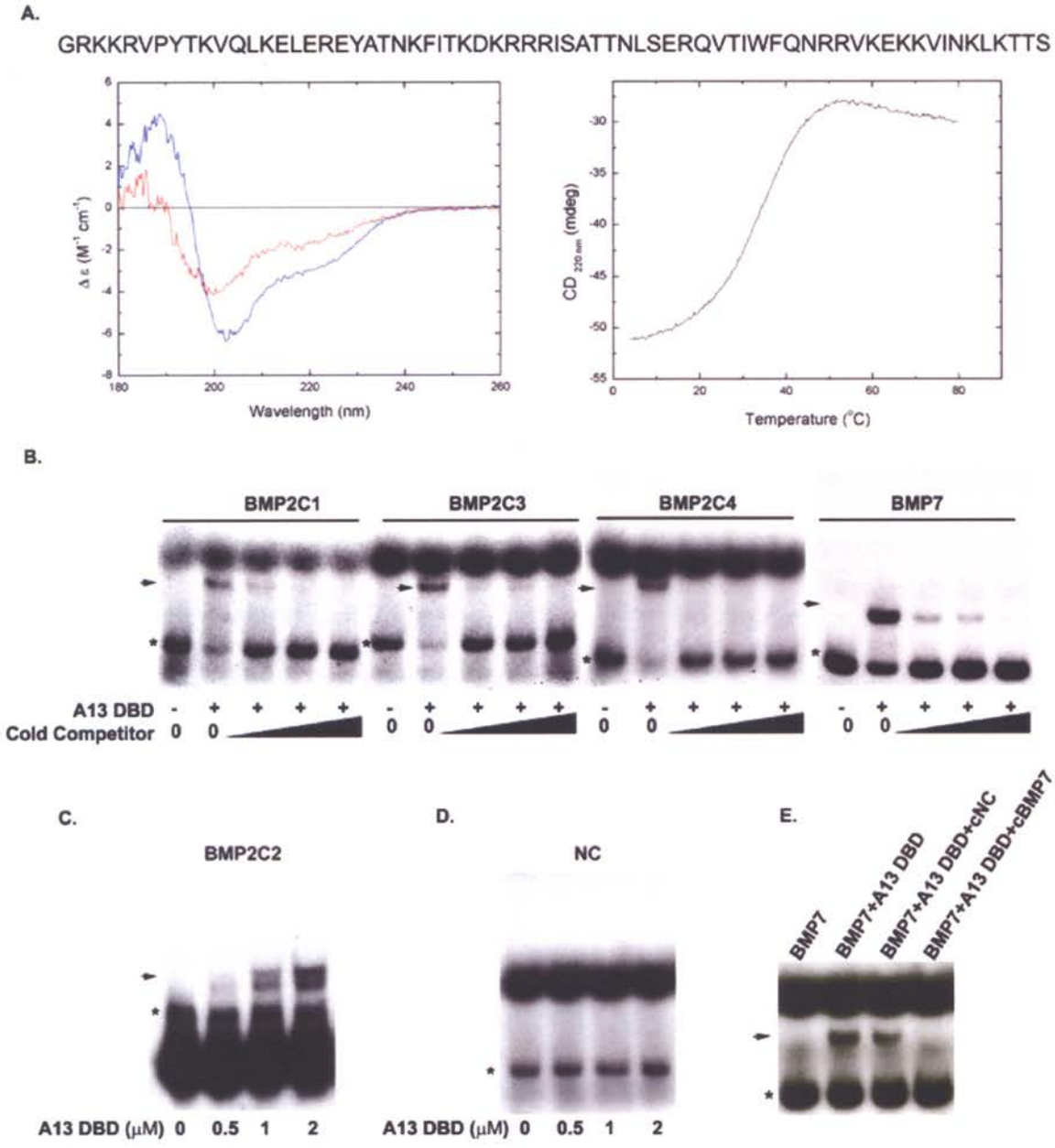

F.

BMP2C1	-598	ATTTAGT**TAAT**TGCAGGTTCAAGAAG
BMP2C2	-469	TAGCAG**TAAT**CTTGAG
BMP2C3	-368	TTGTGTCTGT**TAAT**ATGCACATGAGCGAG
BMP2C4	-225	CTTTT**TAAT**TGGGAGTTAAGAAG
BMP7s1	-3113	TTGACTGAGAGA**TAAT**GGGGTGGAAGGAG
NC		TGCTCCTTCGTCTGTCCTGCATACA
Consensus ≤ 500 nM A13-DBD		**(G/T)(T/A)TAAT(T/A/G)(G/T)**

Analysis of the *Bmp7C1* binding site revealed the highest A13-DBD affinity for any of the A13-DBD bound sequences, requiring competitor DNA concentrations greater than 750 nM to completely displace the radiolabeled *BMP7C1* oligonucleotide (Fig 2.2 B,E). The DNA-binding specificity of the A13-DBD was confirmed using a randomized self-annealing oligonucleotide which exhibited no changes in electrophoretic mobility in the presence of four-fold higher concentrations of A13-DBD peptide (Fig 2.2 D). Similarly, concentrations of control oligonucleotide greater than 750 nM could not displace the A13-DBD-bound *Bmp7C1* oligonucleotide, confirming high affinity and specificity for the *Bmp7C1* binding site (Fig 2.2 E).

Analysis of the DNA sequences bound by the A13-DBD peptide revealed a HOX-specific TAAT nucleotide core sequence (Fig 2.2 F). However the nucleotides flanking the TAAT site varied greatly from sequences bound by other Hox proteins, suggesting that HOXA13 may recognize unique DNA sequences to facilitate its tissue-specific regulation of gene expression (Catron et al., 1993; Pellerin et al., 1994). Interestingly, a second TAAT-containing region (*Bmp7s2*) was identified in the sequences upstream of *Bmp7*, however in the presence of the A13-DBD peptide the *Bmp7s2* sequence did not exhibit any change in electrophoretic mobility (data not shown), suggesting that nucleotides flanking the TAAT core sequence in *Bmp7s1* confer binding specificity.

The *Bmp2* and *Bmp7* sequences bound by A13-DBD function as enhancers of gene expression *in vivo*

A 384 base-pair fragment containing the four *Bmp2* binding sites (BMP2C1-C4) was cloned into a luciferase reporter plasmid and tested for *in vivo* transcriptional regulation by HOXA13. Cells transfected with the *Bmp2* luciferase vector and the *Hoxa13* expression plasmid (pCMV-A13) exhibited a consistent increase in relative luciferase activity (RLA) compared to control transfections lacking pCMV-A13 (Fig 2.3 A). Comparisons of forward and reverse orientations of the 384 base-pair upstream region revealed a 2.5 and 1.8-fold increase in RLA, suggesting that the 384 base-pair *Bmp2* region functions as a HOXA13-regulated enhancer of gene expression (Fig 2.3 A,C). Similarly, a 216 base-pair fragment containing the *Bmp7C1* binding site also caused an increase in luciferase reporter expression, resulting in 1.8 and 2.0-fold increase in RLA for the forward and reverse orientations (Fig 2.3 B,C). Our detection of direct interactions between A13-DBD and these enhancer elements as well as the ability of these enhancer elements to drive reporter expression only in the presence of HOXA13 strongly supports our hypothesis that HOXA13 directly regulates the expression of *Bmp2* and *Bmp7* in the developing autopod.

HOXA13 associates with the *Bmp2* and *Bmp7* enhancer elements in the developing autopod

To verify that HOXA13 also binds the *Bmp2* and *Bmp7* enhancer regions *in vivo*, a *Hoxa13* antibody was developed to immunoprecipitate endogenous

HOXA13-DNA complexes from limb bud chromatin. To identify both wild-type and mutant HOXA13 proteins, the *Hoxa13* antibody (αHoxa13) was raised against the amino terminal region of HOXA13, which is conserved in both wild-type and mutant protein isoforms. Analysis of the proteins recognized by αHoxa13 revealed two predominant bands by Western Blot hybridization whose sizes matched the predicted molecular weights of HOXA13 wild-type (43 kDa) and mutant proteins (64 kDa) (Fig 2.3 D). The ability of αHoxa13 to immunoprecipitate native HOXA13 was confirmed by Western Blot analysis of precipitated cell lysates expressing full length HOXA13 tagged with an HA epitope (Fig 2.3 E). In cultured limb mesenchyme, the *Hoxa13* antibody co-localizes with endogenous HOXA13-GFP, confirming the specificity of the *Hoxa13* antibody (Fig 2.3 F-I).

Figure 2.3 HOXA13 activates transcription from the *Bmp2* and *Bmp7* enhancer regions and associates with these enhancers *in vivo*. Co-transfection of luciferase reporter plasmids containing forward or reverse orientations of the *Bmp2* enhancer sequence (**A,C**) or the *Bmp7* enhancer sequence (**B,C**) and pCMV-A13 resulted in 2.5 and 1.8-fold (*Bmp2*) and 1.8 and 2.0-fold (*Bmp7*) increases in RLA. Bars represent the standard deviation of results derived from four transfection assays. (**D**) Western blot analysis of protein lysates derived from *Hoxa13* wild-type (+/+), heterozygous mutant (+/-) and homozygous mutant (-/-) tissues confirms that the Hoxa13 antibody recognizes the correct molecular weight species for wild-type HOXA13 (43 kDa) and mutant HOXA13-GFP (64 kDa). (**E**) The Hoxa13 antibody immunoprecipitates HA-tagged full-length HOXA13. (**F-I**) Immunostaining of cultured limb mesenchyme from HOXA13-GFP mutant mice with the Hoxa13 antibody reveals strong nuclear co-localization (arrows) between the endogenous HOXA13-GFP protein (panel F) and the Hoxa13 antibody (panels G and H). Nuclei are stained with DAPI (panel **I**). (**J-L**) ChIP using the Hoxa13 antibody confirms that wild-type (+/+) HOXA13 binds the *Bmp2* (**J**) and *Bmp7s1* (**K**) enhancer regions in the developing limb; immunoprecipitates from mutant limbs (-/-) lacking the HOXA13 DNA-binding domain did not contain the *Bmp2* and *Bmp7s1* enhancer regions. (**L**) The absence of *Bmp7s2* sequences in wild-type immunoprecipitates confirms HOXA13 specificity for the sequences in *Bmp2* and *Bmp7s1*. The TAAT sequences present in the *Bmp2, Bmp7s1,* and *Bmp7s2* regions are listed below panels **J,K**, and **L.** NC=negative PCR control, PC= positive PCR control.

Figure 2.3

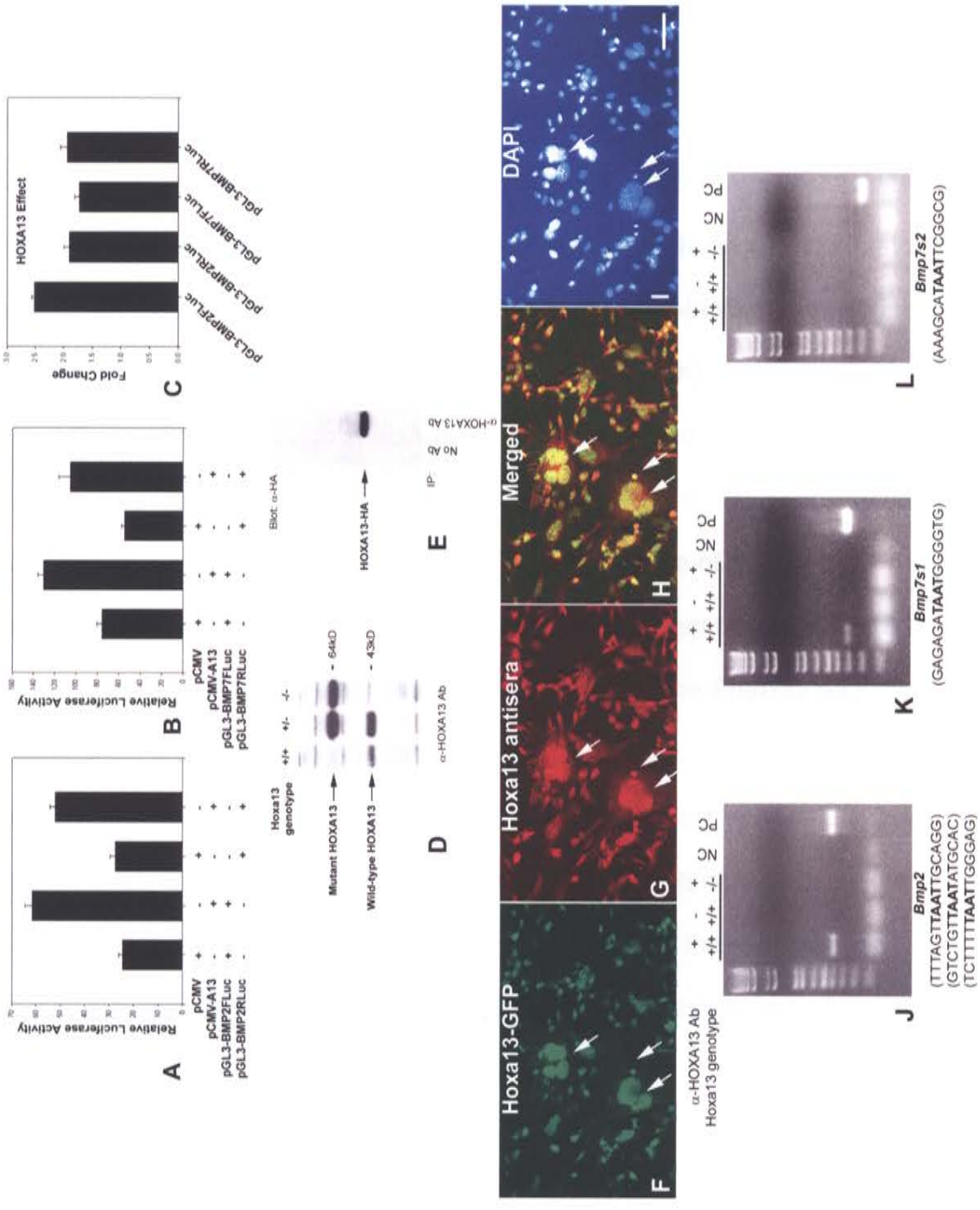
A
Relative Luciferase Activity
pCMV
pCMV-A13
pGL3-BMP2FLuc
pGL3-BMP2RLuc
B
Relative Luciferase Activity
pCMV
pCMV-A13
pGL3-BMP7FLuc
pGL3-BMP7RLuc
C
HOXA13 Effect
Fold Change
pGL3-BMP2FLuc
pGL3-BMP2RLuc
pGL3-BMP7FLuc
pGL3-BMP7RLuc
D
Hoxa13 genotype
+/+ +/- -/-
Mutant HOXA13
64kD
Wild-type HOXA13
43kD
Blot: α-HA
E
α-HOXA13 Ab
IP:
No Ab
α-HOXA13 Ab
F
Hoxa13-GFP
G
Hoxa13 antisera
H
Merged
I
DAPI
α-HOXA13 Ab
Hoxa13 genotype
+/+ +/- -/-
NC
PC
J
Bmp2
(TTTAGTTAATTGCAGG)
(GTCTGTTAATATGCAC)
(TCTTTTTAATTGGGAG)
K
Bmp7s1
(GAGAGATAATGGGGTG)
L
Bmp7s2
(AAAGCATAATTCGGCG)

Next, to verify that endogenous HOXA13 binds the same *Bmp2* and *Bmp7* enhancer elements in the developing limb, αHoxa13 was used to immunoprecipitate chromatin from wild-type and homozygous mutant limbs. In wild-type limbs, chromatin immunoprecipitated with αHoxa13 consistently contained the enhancer elements bearing the *Bmp2C1, C3, C4,* and *Bmp7s1* nucleotide sequences (Fig 2.3 J,K). In contrast, chromatin immunoprecipitations from *Hoxa13* homozygous mutant limbs did not contain these same enhancer regions, which is consistent with the ablation of the DNA-binding domain in the *Hoxa13*^{GFP} mutant allele (Stadler et al., 2001) (Fig 2.3 J,K).

To confirm the *in vivo* specificity of HOXA13 for the TAAT-containing sequences in the *Bmp2* and *Bmp7* enhancers, wild-type αHoxa13 chromatin immunoprecipitates were also examined for the presence of the *Bmp7s2* sequence which contains a TAAT core sequence but is not bound by the A13-DBD peptide (data not shown). In all cases examined, the *Bmp7s2* sequence could not be detected in wild-type chromatin immunoprecipitates, confirming the *in vivo* specificity of HOXA13 for the *Bmp2* and *Bmp7s1* sequences (Fig 2.3 L). These results strongly suggest that endogenous HOXA13 directly binds the *Bmp2* and *Bmp7* enhancer sequences, and that through these interactions HOXA13 controls the expression of *Bmp2* and *Bmp7* in the distal limb.

Reduced *Bmp2* and *Bmp7* expression underlies the loss of IPCD in the *Hoxa13* homozygous mutant limb

Recognizing that HOXA13 can regulate gene expression through the *Bmp2* and *Bmp7* enhancer elements *in vivo* (Fig 2.3 A-C) and associates with these enhancer sites in the developing limb (Fig 2.3 J,K), we hypothesized that the limb phenotypes exhibited by *Hoxa13* homozygous mutants must be due, in part, to insufficient levels of BMP2 and BMP7. Testing this hypothesis, we examined whether increasing the levels of BMP2 or BMP7 in *Hoxa13* mutant autopods could rescue some aspects of the interdigital or interarticular joint phenotypes. For the interarticular malformations, supplementation of the autopod tissues with BMP2 or BMP7-treated beads could not restore the normal formation of the joint regions (Fig 2.1 E,F; data not shown). In contrast, supplementation of the interdigital tissues with either BMP2 or BMP7-treated beads restored distal IPCD in *Hoxa13* homozygous mutants, whereas control experiments using PBS-treated beads did not affect the levels of IPCD in either homozygous mutant or heterozygous control limbs (Fig 2.4A-F). This result suggests that BMP insufficiency may underlie the loss of IPCD in *Hoxa13* mutant limbs.

However, while exogenous BMP2 or BMP7 can reinitiate IPCD in *Hoxa13* mutant limbs, the levels of IPCD were never equivalent to identical treatments in *Hoxa13* heterozygous limbs (compare Fig 2.4 A with D, and B with E). This result suggests that the competency of the interdigital tissues to fully respond to BMP signals may also be affected in *Hoxa13* mutant limbs. To test this

possibility, we examined whether exogenous treatments with BMP2 or BMP7 induced *Msx2* expression to different degrees in wild-type versus mutant limbs. Exogenous applications of BMP2 or BMP7 induced *Msx2* expression in the tissue immediately surrounding the implanted beads in *Hoxa13* mutant and wild-type limbs, whereas treatments with beads soaked in PBS did not induce *Msx2* expression (Fig 2.4 G-L). For both BMP2- and BMP7-treatments, the level of *Msx2* induction was consistently lower in the homozygous mutant limbs (Fig 2.4 H,J), confirming that the interdigital tissues of *Hoxa13* mutants lack the competency to fully transduce BMP signals. This finding suggests that additional components in the BMP-signaling pathway may be affected by loss of HOXA13 function, although no differences in the expression of BMP-receptors *Ia*, *Ib* or *II* were detected between wild-type and *Hoxa13* mutant limbs at E12.5-13.5 (data not shown).

Figure 2.4 Supplementation of *Hoxa13* homozygous mutant limbs with BMP2 or BMP7 partially restores interdigital programmed cell death (IPCD) and *Msx2* expression.

(**A-C**) *Hoxa13* heterozygotes exhibited elevated levels of IPCD when treated with beads soaked in 0.1 mg/ml rhBMP2 or rhBMP7, whereas PBS control beads did not elevate IPCD beyond normal levels in organ cultured limbs. (**D-F**) IPCD is partially restored in *Hoxa13* homozygous mutants in the presence of rhBMP2- or rhBMP7-treated beads, whereas PBS-treated beads did not reinitiate IPCD. Arrows denote sites of IPCD as detected by TUNEL (red signal). (**G-J**) Organ cultures of *Hoxa13* mutant limbs treated with rhBMP2 or rhBMP7 exhibit reduced levels of *Msx2* induction (arrows) compared to age-matched controls. (**K,L**) Control treatments using PBS-beads had no affect on *Msx2* expression (arrows). Roman numerals denote digits II, III, and IV. Bar is 50 μm.

Figure 2.4

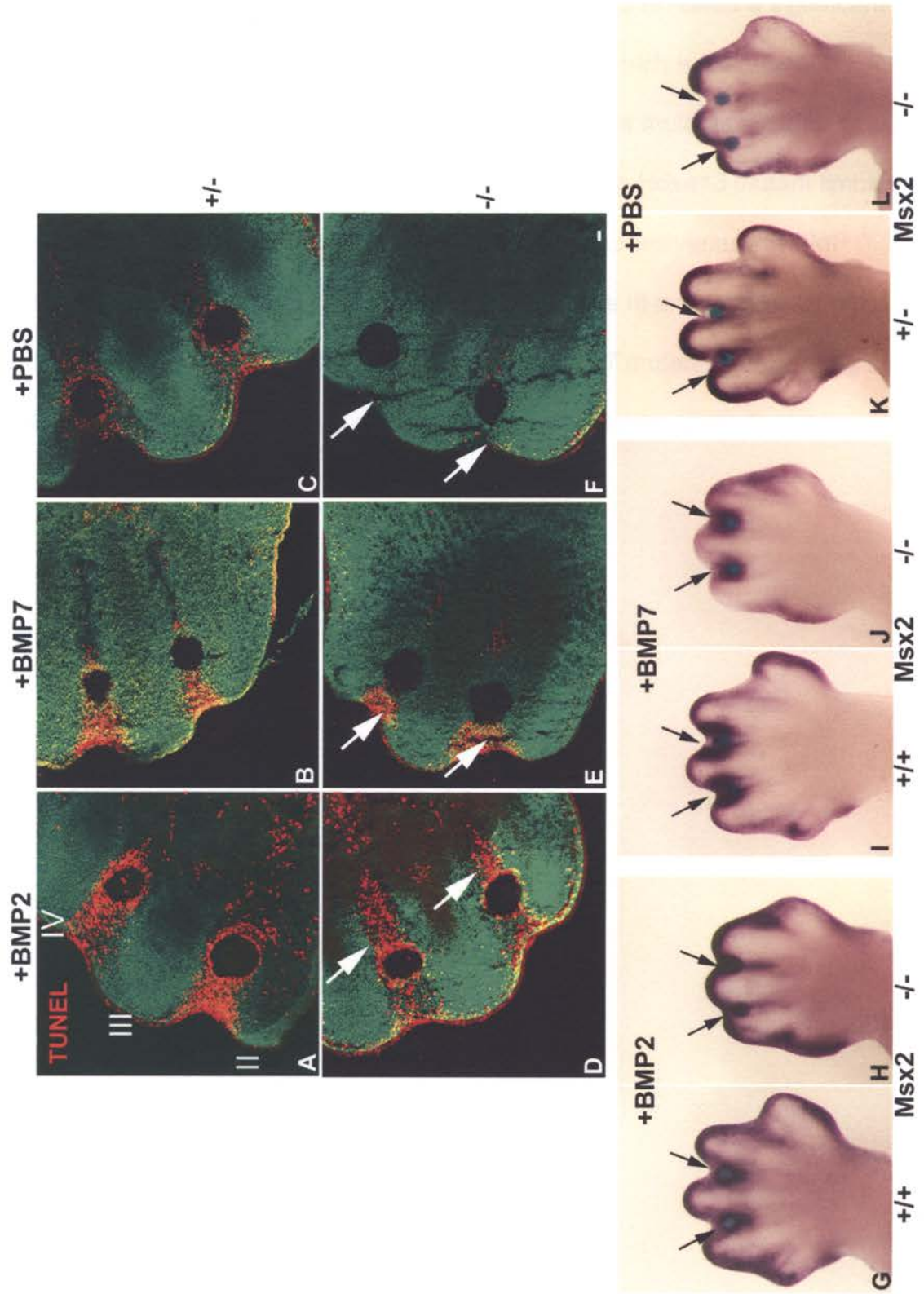
+BMP2
+BMP7
+PBS
+/-
-/-
TUNEL
II
III
IV
A
B
C
D
E
F
+BMP2
+BMP7
+PBS
+/+
Msx2
-/-
G
H
I
J
K
L

IPCD is delayed in *Bmp7* mutant mice

TUNEL analysis of *Bmp7* mutant limbs at E 13.5 revealed a significant delay in IPCD between digits II and III (Fig 2.5 A-D), which is the same interdigital region lacking IPCD in *Hoxa13* homozygous mutants (Stadler et al., 2001). This result suggests that reductions in BMP7 in *Hoxa13* mutant limbs can affect IPCD initiation, particularly in tissues where responsiveness to BMP signals is also reduced. For the region between digits III and IV, TUNEL positive cells were detected at slightly elevated levels in *Bmp7* mutants, suggesting that BMP7 may regulate IPCD in a differential manner between digits II and III versus III and IV.

Figure 2.5 IPCD is delayed in *Bmp7* homozygous mutant limbs. (**A,B**) TUNEL analysis of IPCD in E 13.5 *Bmp7* mutants revealed a delay in IPCD between digits II and III (**B**, arrow) when compared to age-matched heterozygous controls (**A**, arrowhead). (**C,D**) Bright-field analysis of the same *Bmp7* heterozygous and mutant limbs. (**E-G**) Analysis of *Hoxa13* induction by exogenous BMP2 or BMP7. Wild-type limbs treated with 0.1 mg/ml BMP2 (**E**) or BMP7 (**F**) did not exhibit any increase in *Hoxa13* expression when compared to PBS controls (**G**), indicating that in the developing autopod, BMP2 and BMP7 do not regulate *Hoxa13* expression.

Figure 2.5

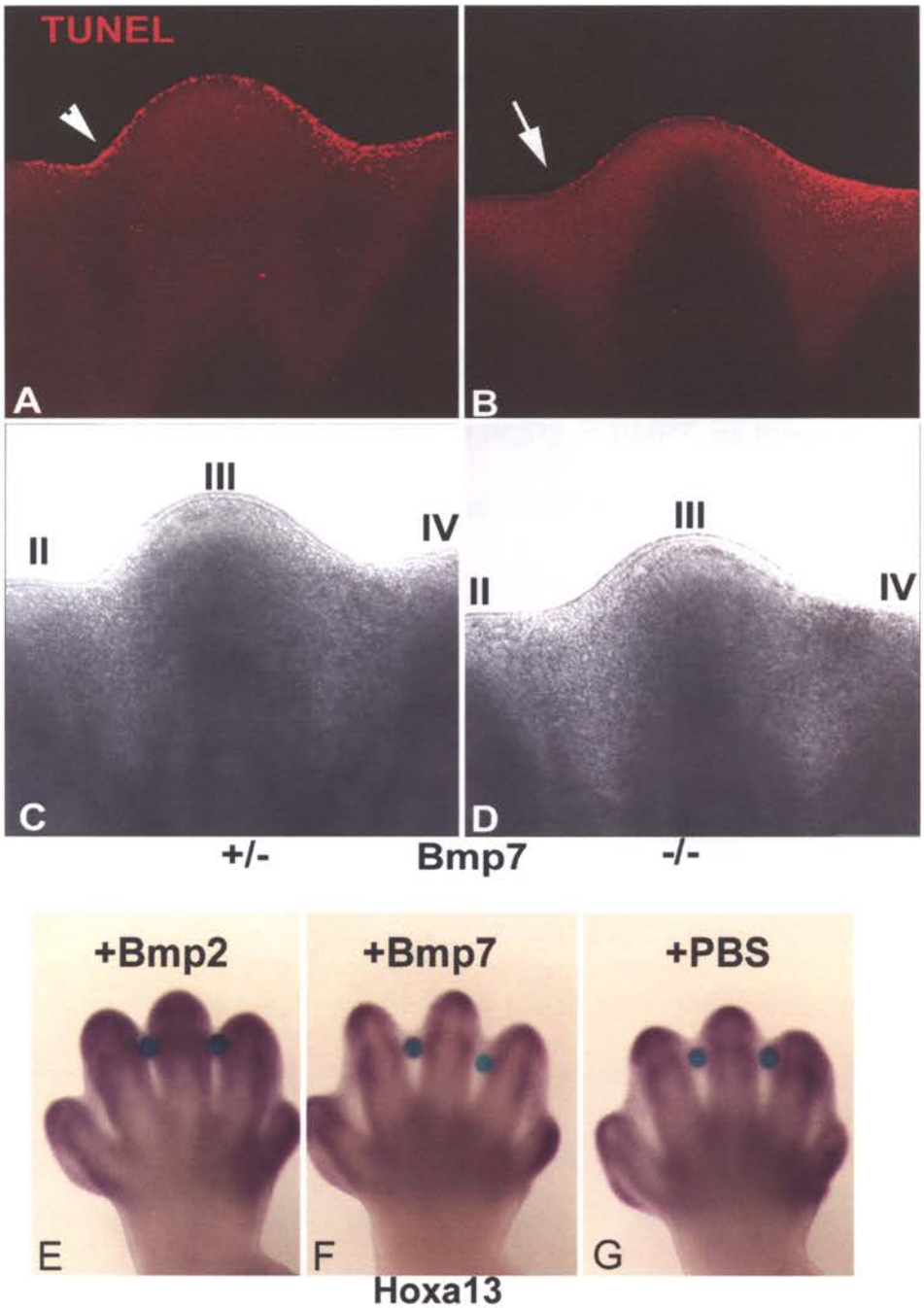

HOXA13 functions upstream of *Bmp2* and *Bmp7* in the developing autopod

Previous investigations of BMP function indicate that BMP2 can induce *Hoxa13* expression to control forelimb muscle patterning (Hashimoto et al., 1999). This result led us to examine whether BMP2 or BMP7 may function in a similar manner in the developing mouse autopod. In all cases examined (4/4), supplementation of the interdigital tissues with BMP2 or BMP7 did not induce *Hoxa13* expression (Fig 2.5 E-G). Furthermore, the elevated levels of *Hoxa13* mRNA in *Hoxa13* mutant autopods (see Fig 2.1 B,D) supports the conclusion that *Hoxa13* expression is independent of BMP2 or BMP7, as these same tissues exhibit reduced levels of *Bmp2* and *Bmp7* expression (see Fig 2.1 H,J,L,N).

IV. Discussion

Hoxa13, *Bmp2*, and *Bmp7* are co-expressed in the developing autopod mesenchyme

The initial finding of this study is that *Hoxa13* is expressed in specific spatio-temporal domains coincident with *Bmp2* and *Bmp7* expression during embryonic limb development. Further characterization of these expression patterns in *Hoxa13* mutant limbs identified a loss of *Bmp2* and *Bmp7* expression in the distal limb mesenchyme, consistent with the severe defects in IPCD and chondrogenesis exhibited by mutant autopods in these same regions. This characterization places *Hoxa13*, *Bmp2* and *Bmp7* in the same tissues at the same time during normal limb development, and identifies *Bmp2* and *Bmp7* as being reduced in the absence of functional HOXA13.

Hoxa13 coordinates BMP signaling during distal limb development

In the present study one of our major conclusions is that HOXA13 directly regulates the expression of both *Bmp2* and *Bmp7* in the distal autopod. In the absence of HOXA13 function, the interdigital tissues also exhibit reduced responsiveness to BMP-induced programmed cell death. Together these results suggest that HOXA13 functions at multiple levels of the BMP-signaling pathway to direct IPCD and distal digit development. The function of Hox proteins to regulate multiple steps in a developmental pathway is well described in *D. melanogaster*, where Ubx function is required to regulate multiple genes during

the specification of wing and haltere structures (Weatherbee et al., 1998). Studies of BMP-receptor function support the conclusion that HOXA13 regulates BMP-signaling to control digit chondrogenesis, as mice lacking BmpR-IB in the distal limb exhibit defects in chondrogenesis remarkably similar to *Hoxa13* mutants (Baur et al., 2000; Stadler et al., 2001; Yokouchi et al., 1995). Similarly, the expression of dominant-negative isoforms of BmpR-IB in chick also affect IPCD as well as the chondrogenic capacity of the distal limb mesenchyme, phenotypes both described in *Hoxa13* mutant limb mesenchyme (Stadler et al., 2001; Zou and Niswander, 1996; Zou et al., 1997b).

In mice, the function of BMP2 during distal limb development is unknown as *Bmp2* homozygous mutants fail to develop to the limb bud stage (Zhang and Bradley, 1996). In *Bmp7* homozygous mutants, the predominant limb phenotype is the addition of an extra anterior digit, whereas the interdigital tissues are completely resolved (Dudley et al., 1995; Hofmann et al., 1996; Luo et al., 1995). The resolution of the interdigital tissues in *Bmp7* mutant mice has been explained by compensatory BMPs co-expressed in these same tissues (Dudley et al., 1995; Dudley and Robertson, 1997; Francis-West et al., 1999b; Francis et al., 1994; Hogan et al., 1994; Kingsley, 1994; Luo et al., 1995; Lyons et al., 1995; Lyons et al., 1989). In the limb, IPCD can be stimulated by BMP2, BMP4, and BMP7 (Gañan et al., 1996; Guha et al., 2002; Merino et al., 1999a; Yokouchi et al., 1996). However, in *Bmp7* mutants, the delay in IPCD at E 13.5 provides strong evidence that compensatory factors such as BMP2 and BMP4 do not utilize the same Bmp-signaling components as BMP7, suggesting that additional factors

like bioavailability, oligomerization, or receptor utilization may also regulate the timing of IPCD (Bosukonda et al., 2000; Capdevila and Johnson, 1998; Groppe et al., 2002; Keller et al., 2004; Lyons et al., 1995; Nohe et al., 2002; Zou and Niswander, 1996; Zou et al., 1997b). Thus, in *Hoxa13* homozygous mutants, two compounding events contribute to the loss of IPCD. First, BMP2 and BMP7 are reduced in the mutant interdigital tissues below a threshold necessary for IPCD initiation. Second, the competency of the interdigital tissues to respond to BMP signals is also affected by loss of *Hoxa13* function.

Surprisingly, mice heterozygous for both *Bmp2* and *Bmp7* (*Bmp2/7*) do not exhibit any defects in limb development (Katagiri et al., 1998). This result is most likely explained by compensatory levels of additional BMPs or the up-regulation of BMP2, BMP7, or their receptors in *Bmp2/7* compound heterozygotes, which to date have not been determined in these mice. Clearly, conditional mutants producing combinatorial losses of redundant BMP proteins will be required to define the functions of these growth factors during distal limb development, particularly in regions where BMPs regulate both digit chondrogenesis and IPCD. Interestingly, the differential utilization of BMPs to direct digit chondrogenesis may also affect IPCD, as apoptosis in limb mesenchyme is directly linked to the level of chondrogenesis (Merino et al., 1999a; Omi et al., 2000). This finding is consistent with the differential IPCD in *Hoxa13* mutant limbs where digits II and III exhibit the least chondrogenesis and IPCD (Fig 2.1 D-F).

Isolation of HOXA13-*Bmp2* and -*Bmp7* enhancer complexes in the developing autopod defines *Bmp2 and Bmp7* as direct targets of HOXA13 regulation

Using a biochemical approach we confirmed the carboxyl-terminal region of HOXA13 folds into a functional DNA-binding motif and binds DNA in a sequence-specific manner. *In vivo*, the A13-DBD peptide facilitated the identification of HOXA13 binding sites upstream of *Bmp2* and *Bmp7*. Quantitation of A13-DBD affinity for these enhancer elements revealed a novel series of nucleotide sequences that are preferentially bound with affinities almost two-fold greater than the DNA regions bound by other homeodomain peptides (Catron et al., 1993).

In vivo, the interactions between HOXA13 and the *Bmp2* and *Bmp7* enhancer regions are conserved as both enhancer elements were present in immunoprecipitated complexes of HOXA13 bound to DNA. The association of HOXA13 with the *Bmp2* and *Bmp7* enhancer regions in the developing limb strongly suggests that HOXA13 directly regulates the expression of these genes during autopod formation. It is important to note that because chromatin immunoprecipitations do not separate protein complexes prior to immunoprecipitation, we cannot exclude the possibility that HOXA13 interacts with the *Bmp2* and *Bmp7* enhancer regions as part of a protein complex. Arguing against this possibility is the absence of the *Bmp2* and *Bmp7* enhancer regions in immunoprecipitations using *Hoxa13* mutant limbs that lack the HOXA13 DNA-binding domain, as well as the utilization of these enhancers by

full-length HOXA13 to direct gene expression *in vivo.* In addition, the specificity of HOXA13 DNA-binding is confirmed by the presence of an additional TAAT-containing sequence upstream of *Bmp7* which is not bound by either the A13-DBD peptide (data not shown) or full length endogenous HOXA13 as determined by chromatin immunoprecipitation from wild-type autopods (Fig 2.3 L). This finding confirms that the nucleotides flanking the core TAAT sequence are critical for HOXA13 binding, supporting our hypothesis that HOXA13 interacts with specific DNA sequences to facilitate its tissue-specific regulation of gene expression (Catron et al., 1993; Pellerin et al., 1994).

Previous investigations of HOXA13 function indicate that *Bmp4* expression may also be regulated by HOXA13 DNA-binding (Suzuki et al., 2003). However, by our analysis, the expression of *Bmp4* appears normal in *Hoxa13* mutant limbs (data not shown), suggesting that the cooperative regulation of *Bmp4* by SP1 may compensate for the loss of HOXA13 DNA-binding function. This finding is consistent with the absence of the *Bmp4* sequence in the wild-type limb chromatin immunoprecipitated with a *Hoxa13* antibody (data not shown). In the N-terminus of HOXA13, protein-protein interactions may also facilitate some aspects of its function, as mutations expanding the number of N-terminal polyalanine residues cause defects in limb and genitourinary development that are similar to those resulting from mutations ablating the HOXA13 DNA-binding domain (Goodman et al., 2000; Mortlock and Innis, 1997).

In this investigation we present the first evidence that during limb development HOXA13 directly interacts with gene-regulatory elements upstream

of *Bmp2* and *Bmp7*. *In vivo,* the loss of HOXA13 DNA-binding function abolishes interactions with these enhancer elements and reduces the expression of *Bmp2* and *Bmp7* in the developing autopod, causing defects that phenocopy malformations associated with perturbations in BMP signaling. Together, these findings strongly suggest that HOXA13 controls the morphogenesis of discrete autopod tissues by regulating *Bmp2* and *Bmp7* expression through direct interactions with *Bmp2* and *Bmp7* enhancer elements, confirming our hypothesis that the phenotypes exhibited by *Hoxa13* mutant mice reflect a loss in the tissue-specific regulation of direct target genes.

V. Materials and Methods

Mouse strains

Hoxa13 homozygous mutant mice were produced by heterozygous mutant intercrosses using the previously described *Hoxa13*^{GFP} mutant allele and genotyping procedures (Stadler et al., 2001). *Bmp7* mutant embryos were produced by intercrosses of heterozygous mutant *Bmp7* mice (Jackson Laboratories). The *Bmp7* mutant allele was originally described by Luo et al., 1995. Embryo genotypes were determined using PCR with primers specific for the PGK-HPRT disruption present in the mutant *Bmp7* allele and DNA derived from the embryo yolk sac. Finally, all care and analysis of *Hoxa13*^{GFP} and *Bmp7* mice was done in accordance with an approved mouse handling protocol.

RNA in situ hybridization and immunohistochemistry

Antisense riboprobes specific for *Bmp2*, *Bmp4*, and *Bmp7* were generated using plasmids kindly provided by B. Hogan (*Bmp2* and *Bmp4*) and R. Beddington (*Bmp7*) whereas *Hoxa13*, *Msx2,* and BMP-receptor *IA, IB,* and *II* riboprobes were produced as described (Morgan et al., 2003). Whole mount *in situ* hybridization, immunohistochemistry, and confocal imaging of limb frozen sections were performed as described (Manley and Capecchi, 1995; Morgan et al., 2003). Antibodies to BMP2/4 (AF355) and BMP7 (AF354) were purchased from R & D systems and used at 0.02 µg/ml on frozen limb sections.

Analysis of programmed cell death

TUNEL analysis was performed as described (Stadler et al., 2001). Limbs from E13.5 *Hoxa13* and *Bmp7* wild-type, heterozygous-, and homozygous-mutant embryos were examined using a Bio-Rad MRC 1024 confocal laser imaging system fitted with a Leica DMRB microscope. Images were produced by compiling z-series scans of the intact limb buds, typically averaging 40-50 sections at 1 μm per section. Kalman Digital Noise reduction was used for all samples.

Limb organ culture and BMP supplementation

Affi-gel blue beads (Bio-Rad) washed 5 times in sterile PBS were incubated at 4°C overnight in solutions containing 0.1 mg/ml of rhBMP2 (R and D Systems) or rhBMP7 (R and D Systems), or sterile PBS. Beads were inserted into the interdigital mesenchyme of E13.5 wild-type, heterozygous- and homozygous-mutant limbs between digits II and III, and III and IV. Limb explants containing the beads were placed on 0.4 μm HTTP Isopore membrane filters (Millipore), coated with gelatin in 60 mm organ culture dishes (Falcon) and grown in BGJb media (Invitrogen), supplemented with 50% rat whole embryo culture serum (Harlan Bioproducts), 50 U/ml penicillin, and 50 μg/ml streptomycin, for 8 hours in an incubator at 37°C, 10% CO_2. The limb explants were examined for induced *Msx2* expression or for changes in programmed cell death using TUNEL analysis of frozen sections as described (Morgan et al., 2003).

Protein synthesis and purification

The sixty-seven amino acid HOXA13 DNA-binding domain (A13-DBD) (GRKKRVPYTKVQLKELEREYATNKFITKDKRRRISATTNLSERQVTIWFQNRRV KEKKVINKLKTTS) was synthesized on an ABI 443A peptide synthesizer (Applied Biosystems, Foster City, CA) using Fmoc-Ser(tBu)-PEG-PS resin (PerSeptive Biosystems 0.16 mmol/g) and Fmoc amino acids (Anaspec). After synthesis, the peptide was purified to greater than 95% purity, using a Gilson Model 321 High Performance Liquid Chromatography (HPLC) system fitted with a semi-preparative reversed-phase peptide column (Grace Vydac, C18, 15 μm, 300 Å, 250 x 25 mm). The mass and purity of the A13-DBD peptide was verified using a Micromass time-of-flight mass spectrometer (Q-tof micro), peptide sequencing, and amino acid analysis.

Circular Dichroism Spectroscopy

The thermal stability and folding of the A13-DBD peptide into a helix-turn-helix DNA-binding motif was verified by circular dichroism (CD). The A13-DBD peptide was reconstituted to a final concentration of 100 μM in 50 mM NaF buffered to pH 7.2 with phosphate buffer. CD spectra were obtained using an Aviv 202 spectropolarimeter and a 0.1 mm path length rectangular cell (Hellma). The wavelength spectra represent at least an average of 10 scans with 0.1 nm wavelength steps. Thermal transitions were recorded at a heating rate of 10°C/hour in a 1 mm cell.

DNA-binding site identification with the HOXA13 DNA-binding domain

The A13-DBD peptide was solubilized to a concentration of 500 nM in PBS and incubated with radioactively labeled *Bmp2* and *Bmp7* upstream regions (200-300 base pair fragments) at 4° C in gel shift buffer (Promega). 5' upstream sequences for *Bmp2* and *Bmp7*, representing nucleotides -600 to +1 for *Bmp2* (Ensembl ref:ENSMUSG00000027358) and -3113 to +1 for *Bmp7* (Ensembl ref: ENSMUSG00000008999) were examined for binding by the A13-DBD peptide using electrophoretic mobility shift assays (EMSA) on a 4% non-denaturing polyacrylamide gel buffered with 0.5X TBE. PCR fragments exhibiting reduced electrophoretic mobility in the presence of the A13-DBD peptide were sub-divided into 30-50 base-pair regions and synthesized as self annealing oligonucleotides (Oligos Etc.) to narrow the regions bound by HOXA13. Double stranded oligonucleotides were prepared by heating 1 μM oligonucleotide stock solutions in 50 mM Tris-HCL pH 7.2, 50 mM NaCl to 95 °C for 5 minutes and allowing them to cool to room temperature. Annealed oligonucleotides (12 nM) were radiolabeled using terminal transferase and α^{32}P-ddATP (5000 Ci/mmol) (Amersham) as described by the manufacturer (Roche). Peptide concentrations and EMSA assay conditions were the same as described with the exception that 6% polyacrylamide 0.5X TBE gels were utilized to resolve the protein-DNA complexes.

Sequences of the self-annealing oligonucleotides:

BMP7C1:TTGACTGAGAGATAATGGGGTGGAAGGAGCCCCTCCTTCCACCC-CATTATCTCTCAGTCAA

BMP2C1:ATTTAGTTAATTGCAGGTTCAAGAAGCCCCTTCTTGAACCTGCAA-TTAACTAAAT

BMP2C3:TTGTGTCTGTTAATATGCACATGAGCGAGCCCCTCGCTCATGTGC-ATATTAACAGACACAA

BMP2C4:CTTTTTAATTGGGAGTTAAGAAGCCCCTTCTTAACTCCCAATTAAA-AAG

Luciferase Plasmid Constructs

DNA regions bound by the A13-DBD peptide were amplified from mouse genomic DNA using PCR and the following primers:

BMP2 5'-ATTTAGTTAATTGCAGGAAGGT-3' and 5'-ACTCCCAATTAAAAAGA-GCATT-3'. ***BMP7s1*** 5'-GGAAGTGCAGAAGCACCC-3' and 5'-ATGGTAATCAC-TCAGACCTAA-3'. PCR conditions used a 2 minute soak at 94°C followed by 35 cycles of 94°C, 54°C, and 72°C for 30 seconds each step. Amplified PCR products were cloned in both orientations into a *Sma*I site of the pGL3 luciferase vector (Promega) to produce the pGL3BMP2FLuc, pGL3BMP2RLuc, pGL3BMP7FLuc, and pGL3BMP7RLuc plasmids. The sequences and orientation of the cloned fragments were verified using di-deoxy terminator fluorescent sequencing.

Hoxa13-HA expression plasmid

The *Hoxa13*-HA expression plasmid (pCMV-A13) used in the luciferase and immunoprecipitation assays was produced using a two-kilobase genomic region containing the murine *Hoxa13* locus. An HA epitope tag was added to the 3' end of the *Hoxa13* coding region using a unique *Spe*I restriction site to add the following annealed oligonucleotides:

5'-CTAGTGGAGGATACCCATACGACGTCCCAGACTACGCTTAAGATATCA-3'

5'-CTAGTGATATCTTAAGCGTAGTCTGGGACGTCGTATGGGTATCCTCCA-3'.

Cell Culture and transfection

NG108-15 cells were grown as recommended by the supplier (ATCC). At 90% confluence the cells were passaged into 12 well dishes (Costar) and grown at 37°C, 10% CO_2 for 24 hours then transfected with 2 µg of pGL3BMP2 or pGL3BMP7, 2 µg of pCMV-A13, or 2 µg of empty pCMV vector, and 0.5 µg of the pRL-CMV Renilla plasmid (Promega) to normalize for transfection efficiency. All transfections used the Superfect reagent as recommended by the manufacturer (Qiagen). Forty-eight hours after transfection, cells were rinsed with PBS, lysed with M-Per lysis reagent (Pierce), and processed to detect luciferase activity using the Dual-Glo Luciferase Assay System (Promega). Luciferase activity was determined as the average of three separate readings of each well (1 second/read) using a Packard Fusion Universal Microplate Analyzer (Perkin Elmer). For each experimental condition four separate transfections were performed. Results were normalized for transfection efficiency using relative

Renilla luciferase expression levels as described by the manufacturer (Promega) and plotted using SigmaPlot 8.0 (SPSS).

Hoxa13 antibody production

A HOXA13 peptide, corresponding to amino acids 1-43 of the murine HOXA13 (MTASVLLHPRWIEPTVMFLYDNGGGLVADELNKNMEGAAAAAA) (Mortlock and Innis, 1997) was used to immunize New Zealand White rabbits. Samples exhibiting high *Hoxa13* antibody titers by ELISA were assessed for specificity to the full-length HOXA13 using western blot and immunohistochemistry of cultured limb mesenchyme derived from mice heterozygous for a temperature sensitive T-antigen (Immorto® mice, Charles River Laboratories) and homozygous for the *Hoxa13-GFP* mutant allele. A Cytological Nuclear Stain Kit (Molecular Probes) was used to label nuclei with DAPI.

Chromatin Immunoprecipitation (ChIP)

ChIP assays were performed using a Chromatin Immunoprecipitation Assay as described (Upstate Biotechnology), with the following modifications: Limb buds from E12.5 $Hoxa13^{GFP}$ wild-type and homozygous mutant embryos were dissected in PBS containing 15 µl/mL protease inhibitor cocktail (PIC) (Sigma). Lysates were sonicated 4 x 10 seconds at 4°C using a Microson (Misonix) sonicator at 15% output. To avoid sample heating, tubes were placed in an ice/EtOH bath for 5 seconds before and after each sonication. Cell lysates were pre-cleared with 80 µl Gammabind (Amersham) containing 40 µg/ml tRNA

(Roche) in 10 mM Tris-HCl pH 8, 1 mM EDTA (GBS). After pre-clearing, all centrifugation steps were performed at 1,000 rpm for 2 minutes. 15 µl of *Hoxa13* antibody or control solution (PBS) were used at the immunoprecipitation step. For collection of *Hoxa13* antibody/HOXA13/DNA complexes, 60 µl of GBS was added to the samples. The Gammabind/ *Hoxa13* antibody/HOXA13/DNA complexes were washed 2 x 5 minutes at 4°C for each wash step. DNA was eluted from the immune complexes by digesting overnight at 45°C in 50 mM Tris-HCl pH 8.4, 1 mM EDTA, 0.5% Tween-20 containing 20 µg/ml Proteinase K (Invitrogen). Eluted DNA from the antibody or no antibody control samples were assessed for the presence of the *Bmp2*, *Bmp7s1, or Bmp7s2* DNA regions using PCR and the primers described above. For *Bmp7s2* the following primers were used to PCR amplify immunoprecipitated chromatin: 5'-GCCTCTGTTCTTGCT-GCGCT-3 and 5'-ACATGAACATGGGCGCCG-3'.

VI. Acknowledgements

The authors wish to thank Dr. Brigid Hogan for the critical reading of this manuscript. This work was supported by research grants from the Shriners Hospital for Children and the National Institutes of Health (HSS) and by an NIH pre-doctoral fellowship (WMK).

CHAPTER 3

Quantitative analysis of HOXA13 function

HOXA13 regulation of *Sostdc1*

HOXA13 suppresses the BMP antagonist Sostdc1 in the limb through a novel high affinity binding

Wendy M. Knosp[2], Chie Saneyoshi[1], Siming Shou[1], Hans Peter Bächinger[1,3], and H. Scott Stadler[1,2]

[1]Shriners Hospital for Children, Research Division, Portland, Oregon 97239, USA

[2]Department of Molecular and Medical Genetics, Oregon Health and Science University, Portland, Oregon 97239 USA

[3]Department of Biochemistry and Molecular Biology, Oregon Health and Science University, Portland, Oregon 97239, USA

As of August 12, 2006, submitted to ***The EMBO Journal***

I. Abstract

Progress towards understanding the developmental functions of HOX proteins has lagged, a result directly linked to our poor understanding of their transcriptional properties. In the limb, mutations in *Hoxa13* cause malformations of the appendicular skeleton including digit loss and syndactyly. To correlate how mutations in *Hoxa13* cause these defects, we characterized its transcriptional function and identified a series of novel gene regulatory sequences bound by *HOXA13* with high affinity. Applying this transcriptional characterization, we identified a limb-specific function for the BMP antagonist, *Sostdc1*, and confirmed that HOXA13 suppresses *Sostdc1* using its high affinity gene regulatory sequences. In the absence of HOXA13, *Sostdc1* is ectopically expressed in the distal limb, causing reduced expression of BMP-activated genes and decreased SMAD phosphorylation. Limb chromatin immunoprecipitation confirmed HOXA13 binding at two conserved *Sostdc1* regulatory sites *in vivo*. *In vitro,* HOXA13 represses gene expression through the *Sostdc1* gene regulatory elements. Together these findings provide a critical advance in our understanding of HOXA13's transcriptional function as well as its role in regulating BMP signaling during limb development.

II. Introduction

Although *Hox* genes represent some of the longest studied developmental genes, progress towards understanding how they regulate the formation of specific structures has slowed, a result directly attributable to their poor transcriptional characterization. Indeed for many HOX proteins, little is known about their preferred DNA binding sites, affinity, or the utilization of these sites to control target gene expression. When the DNA binding properties of HOX proteins have been characterized, significant advances in interpreting their developmental functions have occurred (Lei et al., 2006; Tour et al., 2005; Wang et al., 2006). Key to this functional characterization is the emerging concept that HOX proteins utilize binding sites longer than the canonical "TAAT" motif, a process facilitated both by the intrinsic amino acid composition and structure of the homeodomain as well as extrinsic interactions with members of the PBC and MEIS classes of TALE proteins (Catron et al., 1993; Moens and Selleri, 2006; Pellerin et al., 1994; Salsi and Zappavigna, 2006; Treisman et al., 1989; Williams et al., 2005a; Williams et al., 2005b). Because HOX proteins regulate development through direct interactions with these longer gene-regulatory elements, investigations are currently focused on elucidating their full-length high affinity DNA binding sites. For several homeodomain proteins, the characterization of the full-length binding site confirms that the bases flanking a core sequence motif play an essential role in conferring DNA binding specificity as variations in the flanking nucleotides cause substantial differences in DNA

binding affinity and may critically affect the tissue-specific regulation of a particular target gene (Catron et al., 1993; Pellerin et al., 1994).

HOXA13 is expressed in distinct domains of the developing embryo including the limb, genitourinary tract, and umbilical arteries (Dollé and Duboule, 1989; Fromental-Ramain et al., 1996b; Knosp et al., 2004; Morgan et al., 2003; Stadler et al., 2001; Warot et al., 1997). In the absence of HOXA13 function, distal limb development is compromised, causing pre-axial digit loss, reduced carpal/tarsal chondrogenesis, and a loss of interdigital programmed cell death (Fromental-Ramain et al., 1996b; Knosp et al., 2004; Stadler et al., 2001). Recently, we identified *Bmp2* and *Bmp7* as direct targets of HOXA13 in the interdigital tissues (IDT). This regulation is mediated by HOXA13 DNA binding interactions, yet the definitive sequences bound by HOXA13 in the *Bmp2* and *Bmp7* loci were unclear as multiple AT-rich sequences were identified at the sites of *in vivo* HOXA13 interaction (Knosp et al., 2004).

To determine the high affinity sequences bound by HOXA13, we performed an *in vivo* systematic evolution of ligands (SELEX) screen (Tuerk and Gold, 1990). From this screen three major DNA motifs were identified: "TAAA," "TAAT," and "TAAC," all containing a "TAA" core sequence. Quantitative analysis of the nucleotides flanking this "TAA" core site identified "AAATAAAA" as the highest affinity HOXA13 binding site. Discovery of this DNA binding site facilitated the identification of *Sostdc1* as a novel HOXA13 target gene in the developing limb. Interestingly, while previous characterizations of *Sostdc1* revealed strong expression and function as a BMP antagonist in the developing

tooth cusp and kidney, its role in the developing limb was unreported (Kassai et al., 2005; Laurikkala et al., 2003). This finding, in conjunction with elevated *Sostdc1* expression in *Hoxa13* homozygous mutant limbs, led us to hypothesize that HOXA13 suppresses *Sostdc1* to facilitate BMP signaling during normal limb development. Indeed, while *Bmp4*, *Bmp5*, and *Bmp7* expression were unaffected in the ventral digit I anlagen, multiple genes normally activated by BMP signaling were reduced in the ectopic *Sostdc1* domain, causing a concomitant reduction in SMAD phosphorylation within these same tissues. *In vivo*, HOXA13 binds the *Sostdc1* locus in the limb at two conserved regions. *In vitro*, HOXA13 can utilize these bound sequences to suppress gene expression in a dosage-dependent manner. Together, these findings provide an important resource to identify genes directly regulated by HOXA13 and extend our understanding of HOXA13's role as a key regulator of BMP-signaling during normal limb development.

III. Results

Identification of HOXA13 DNA binding sites

The HOXA13 core binding sequences were identified using a systematic evolution of ligands (SELEX) screen. A library of randomized, double stranded oligonucleotides were incubated with a HOXA13 DNA binding domain peptide (A13-DBD) (Fig 3.1 A) (Knosp et al., 2004). DNA sequences exhibiting reduced electrophoretic mobility due to A13-DBD binding were isolated and subjected to five consecutive rounds of binding and electrophoretic enrichment (Fig 3.1 B). One hundred independent sequences selected by this process were examined using Vector NTI software (InforMax, Inc) which revealed 50% of the A13-DBD bound sequences contained a "TAAA" core sequence (Fig 3.1 C,D). "TAAC" and "TAAT" core sequences were also identified in 30% and 20% of the remaining sequences respectively, suggesting that HOXA13 may utilize three separate core binding sites to regulate target gene expression (Fig 3.1 C,D).

A.

TACGTCGAATTCGTCAGTXXXXXXXXXXXXXXXXGATGGATCCTGATGTAGA

B.

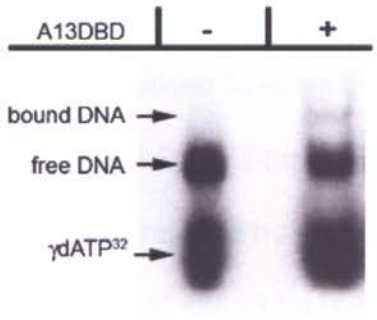

C.

```
1          10          20
------GCGATAAAACTATTGGT-
-----CCGAATAAAACCCGCT---
-------ACATAAAACTGGCTGC-
------CCCATAAAACCGGCCC--
----CCAGTATAAACAACCC----
--CCGGCCTATAATACCC------
----CACCCGTAATATCGCC----
--------CATAACAGGAAGCGCC
-----CCCAATAACAGCGTGT---
-----CCCAATAACAAGTGGT---
```

D.

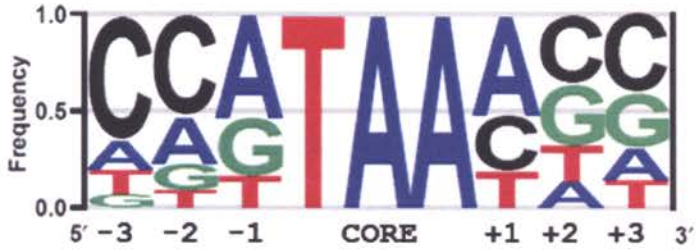

Figure 3.1 Identification of HOXA13 DNA binding sites. (A) The randomized DNA sequence used for DNA binding selection. (B) Electrophoretic mobility shift assay (EMSA) of A13-DBD peptide bound to DNA sequences present in the first round of DNA binding selection. Bound DNA, free DNA, and γdATP32 are labeled (arrows). (C) Alignment of 10 representative DNA sequences bound by A13-DBD after 5 rounds of selection. Core DNA sequence motifs are highlighted. (D) Energy normalized logo (EnoLOGOS) plot of the A13-DBD binding site derived from 100 selected and aligned DNA sequences. Height of each represented base is weighted based on its frequency at a given position within the 100 aligned SELEX sequences.

Affinity analysis of the core binding site and its flanking nucleotide sequences

To identify the full length sites preferred by HOXA13, an affinity analysis series was performed using fluorescence polarization anisotropy to determine which nucleotides flanking the "TAA" core confer the highest A13-DBD binding affinity (Fig 3.2 A). Starting with an initial sequence "CCA**TAA**ACC," the core sequence predicted by the enoLOGOS plot (Fig 3.1 D), the nucleotides flanking the core "TAA" site (3 bp upstream and 3 bp downstream) were altered and assessed for A13-DBD binding affinity. Altering the nucleotide composition at the six positions flanking the core binding site caused substantial changes in A13-DBD binding affinity (Fig 3.2 B-G). Notably, changes at positions -2, -1, and +1 had the greatest affect on A13-DBD binding affinity (Fig 3.2 C-E). For the -2 position, the replacement of the favored "A" nucleotide with a "G" caused nearly a 16-fold decrease in binding affinity (ΔK_d= 5.45 nM to 86.38 nM) (Fig 2C). Similarly, the replacement of the "A" nucleotide with a "C" at the -1 position also altered the A13-DBD affinity, causing a 16-fold reduction (ΔK_d= 9.41 nM to 153.55 nM) (Fig 3.2 D). At the + 1 position, A13-DBD binding affinity varied from the canonical "TAA**T**" sequence reported for other homeodomains (Catron et al., 1993), preferring an "A" in this position which increased A13-DBD affinity 10-fold (Fig 3.2 E).

Figure 3.2 Quantitation of HOXA13 DNA binding affinity. (A) The DNA sequence used for quantitative analysis of A13-DBD binding, X indicates an A, T, C, or G at that position. (B-G) Fluorescence polarization analyses with base substitutions at positions -3 (B), -2 (C), -1 (D), +1 (E), +2 (F), +3 (G) of the DNA sequence in (A). (H) EnoLOGOS plot of the A13-DBD high affinity DNA sequence derived from the K_d's in (B-G). Height of each represented base is weighted using the association constant (K_a) of A13-DBD at each position within the sequence. For anisotropy graphs, the standard deviation of the dissociation constant (K_d) is indicated in parentheses.

Figure 3.2

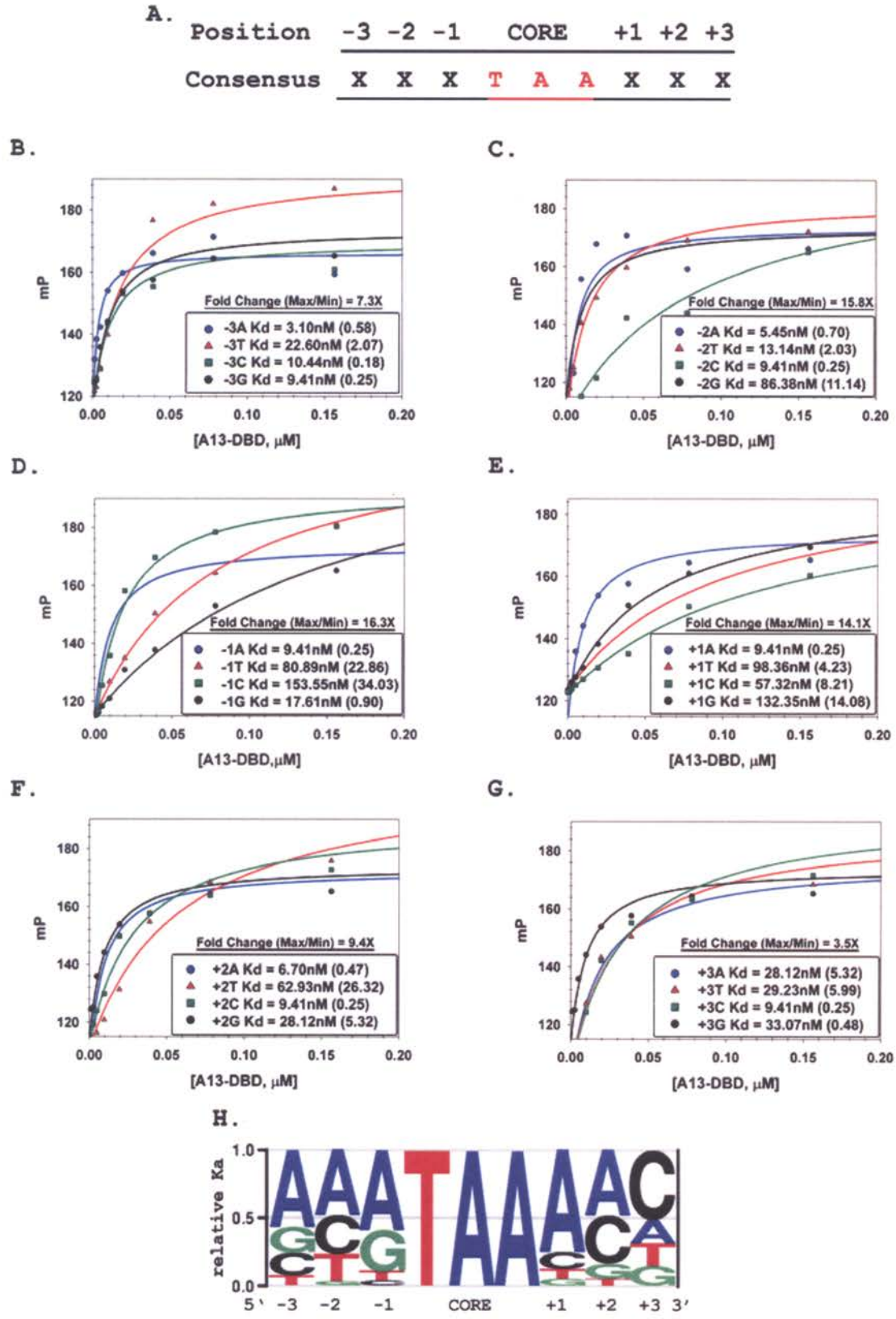
A.
Position -3 -2 -1 CORE +1 +2 +3
Consensus X X X T A A X X X
B.
Fold Change (Max/Min) = 7.3X
-3A Kd = 3.10nM (0.58)
-3T Kd = 22.60nM (2.07)
-3C Kd = 10.44nM (0.18)
-3G Kd = 9.41nM (0.25)
C.
Fold Change (Max/Min) = 15.8X
-2A Kd = 5.45nM (0.70)
-2T Kd = 13.14nM (2.03)
-2C Kd = 9.41nM (0.25)
-2G Kd = 86.38nM (11.14)
D.
Fold Change (Max/Min) = 16.3X
-1A Kd = 9.41nM (0.25)
-1T Kd = 80.89nM (22.86)
-1C Kd = 153.55nM (34.03)
-1G Kd = 17.61nM (0.90)
E.
Fold Change (Max/Min) = 14.1X
+1A Kd = 9.41nM (0.25)
+1T Kd = 98.36nM (4.23)
+1C Kd = 57.32nM (8.21)
+1G Kd = 132.35nM (14.08)
F.
Fold Change (Max/Min) = 9.4X
+2A Kd = 6.70nM (0.47)
+2T Kd = 62.93nM (26.32)
+2C Kd = 9.41nM (0.25)
+2G Kd = 28.12nM (5.32)
G.
Fold Change (Max/Min) = 3.5X
+3A Kd = 28.12nM (5.32)
+3T Kd = 29.23nM (5.99)
+3C Kd = 9.41nM (0.25)
+3G Kd = 33.07nM (0.48)
mP
[A13-DBD, μM]
H.
relative Ka
5' -3 -2 -1 CORE +1 +2 +3 3'

Assessing the affects of all nucleotide substitutions revealed a consensus HOXA13 binding site of "AAATAAAA" (Fig 3.2 H). Examination of A13-DBD affinity for its consensus site revealed strong binding with a K_d of 3.87 nM (Fig 3.3 A,B). Interestingly, HOXD13, the closest paralog of HOXA13, exhibited nearly 15-fold less affinity for this same sequence (K_d= 56.35 nM), suggesting high specificity for HOXA13 binding to this consensus site (Fig 3.3 B). Finally, we confirmed that the full length HOXA13 protein also binds this same sequence with an affinity identical to the A13-DBD peptide (K_d = 3.61 ± 0.30 nM vs. 3.87 ± 0.49 nM), validating the modular function of the HOXA13 DNA binding domain (Fig 3.3 C).

A.

Position	-3	-2	-1	CORE	+1	+2	+3
Consensus	A	A	A	T	A	A	A	A	C

B.

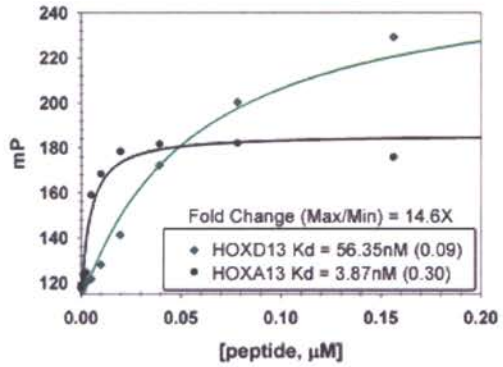

C.

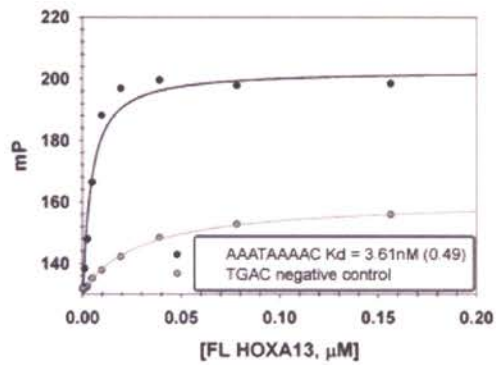

Figure 3.3 Quantitative analysis of the HOXA13 high affinity DNA sequence. (A) The high affinity DNA sequence used for fluorescence anisotropy experiments in B and C. (B) Fluorescence polarization analyses of A13-DBD (black line) and D13-DBD (green line) binding to the high affinity DNA sequence in (A). (C) Full length HOXA13 protein (black line) binding to the high affinity DNA sequence shown in (A) and to a negative control DNA sequence (gray line). For anisotropy graphs, the standard deviation of the dissociation constant (K_d) is indicated in parentheses.

Sostdc1 is ectopically expressed in *Hoxa13* mutant limbs

A major goal of our DNA binding screen was to utilize the HOXA13 DNA binding sites to assist in the identification of genes directly regulated by HOXA13. Using high density microarrays (Affymetrix) the gene expression profiles present in E12.5 *Hoxa13* wild-type and homozygous mutant autopods were compared (data not shown). From this analysis, a 2-fold increase in the expression of the BMP antagonist *Sostdc1* (Ectodin, AB059271) was detected in homozygous mutant limbs. Our detection of *Sostdc1* expression in the autopod was surprising, as previous characterizations of *Sostdc1* expression reported the tooth bud and kidney as the predominant regions of expression (Kassai et al., 2005; Laurikkala et al., 2003; Yanagita et al., 2004).

Analysis of *Hoxa13* and *Sostdc1* expression in wild-type limbs revealed reciprocal domains of expression (Fig 3.4 A-F). At E12.5, *Hoxa13* is expressed in the autopod mesenchyme, whereas *Sostdc1* is expressed in the distal zeugopod, which does not express *Hoxa13* (Fig 3.4 A,D). At E13.5, the transition of *Hoxa13* expression to the digits is coincident with the appearance of *Sostdc1* expression in the interdigital tissues and distal zeugopod (Fig 3.4 B,E). At E14.5, *Hoxa13* is strongly expressed in the ventral autopod, particularly in digit I, the phalangeal joints, and the developing footpads, whereas *Sostdc1* expression is markedly reduced in the same domains (Fig 3.4 C,F). In *Hoxa13* homozygous mutant limbs *Sostdc1* expression is elevated in regions affected by the loss of HOXA13 function, including proximal portions of the autopod (Fig 3.4 D,G), the ventral digit I domain as well as the developing footpads (Fig 3.4 E-F,H-I).

To validate the *in situ* hybridization results, quantitative RT-PCR (QRT-PCR) was performed using RNA isolated from the affected ventral limb domain (Fig 3.4 J,K). A comparison of *Sostdc1* expression in wild-type and homozygous mutant ventral digit I tissues confirmed a consistent 2-fold increase in expression in the mutant limb (n = 3 independent analyses) (Fig 3.4 K). Analysis of the *Bmp* genes expressed in the ectopic *Sostdc1* domain of the ventral digit I tissues revealed *Bmp4*, *Bmp5*, and *Bmp7* to be the predominantly expressed BMP-family members (Fig 3.4 K). *Bmp2* expression was not detected in the E14.5 digit I domain (data not shown). QRT-PCR analysis revealed no differences in *Bmp4*, *Bmp5*, or *Bmp7* expression between wild-type and homozygous mutant limbs (Fig 3.4 K).

Figure 3.4 Ectopic *Sostdc1* in *Hoxa13* mutant autopods correlates with domains of *Hoxa13* expression. (A-C) *Hoxa13* expression in wild-type autopods, proximal expression boundaries are indicated by white arrowheads. (A) *Hoxa13* expression is present throughout the E12.5 ventral autopod. (B) At E13.5, *Hoxa13* expression is localized to the peridigital (white arrows) and developing footpad (white asterisks). (C) By E14.5, *Hoxa13* expression is in the developing digits, joints (white arrows) and footpad tissues (white asterisks). (D) At E12.5, *Sostdc1* expression is restricted to the zeugopod. (E) By E13.5, *Sostdc1* is expressed in the interdigital tissues between digits II & III, III & IV, and IV & V (white arrows) as well as in the proximal autopod (white arrowheads), but not in the developing footpads (white asterisks). (F) *Sostdc1* expression at E14.5 is in discrete bands within digits I-V (white arrows) and the proximal autopod (white arrowheads), but not in the developing footpads (white asterisks). (G-I) *Sostdc1* expression in *Hoxa13* homozygous mutant autopods. (G) At E12.5, *Sostdc1* expression has expanded into the autopod (white arrowheads) and overlaps with the proximal expression domain of *Hoxa13* (compare white brackets in A, D, and G). (H) In E13.5 autopods there is ectopic *Sostdc1* expression in the proximal autopod (white arrowheads), developing footpads and ventral digit I tissues (white asterisks). *Sostdc1* expression is also increased in the interdigital tissues (compare white arrows in E and H). (I) At E14.5 *Sostdc1* expression is present in the footpads and digit I (white asterisks) as well as in the proximal autopod (white arrowheads). *Sostdc1* expression persists in the interdigital tissues between digits II & III, III & IV, and IV & V and is expanded in

Figure 3.4 *continued*

the digits as compared to wild-type (compare white arrows in F and I). (J) *Sostdc1 in situ* of an E14.5 wild-type ventral limb, white bars indicate the digit I and footpad region microdissected for QRT-PCR in (K). (K) QRT-PCR using E14.5 mRNA isolated from *Hoxa13*$^{+/+}$ and *Hoxa13*$^{-/-}$ digit I tissues, calculated as the fold change in expression of mutant divided by wild-type.

Figure 3.4

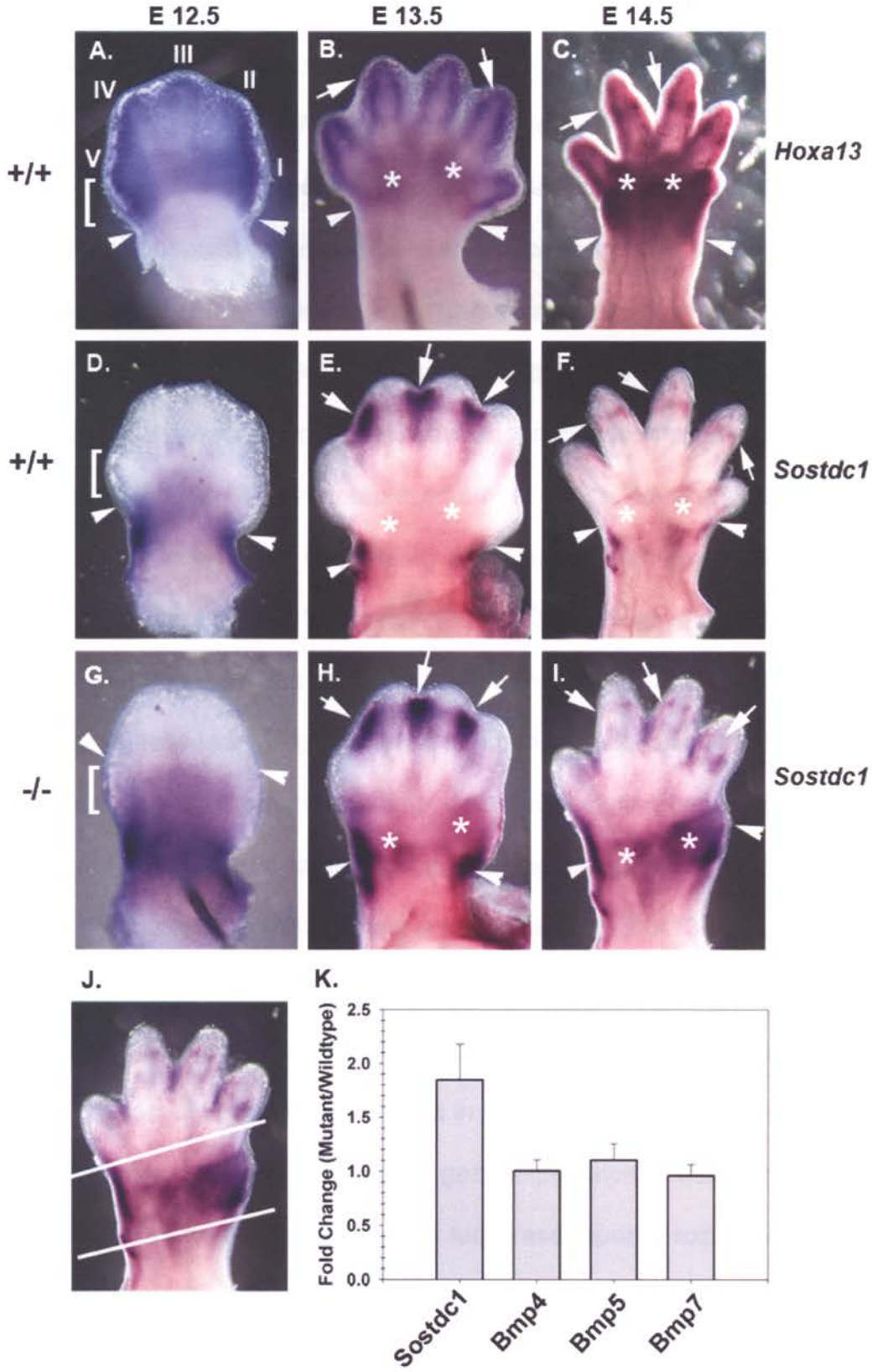
E 12.5
E 13.5
E 14.5
A.
B.
C.
III
IV
II
V
I
+/+
Hoxa13
D.
E.
F.
+/+
Sostdc1
G.
H.
I.
-/-
Sostdc1
J.
K.
Fold Change (Mutant/Wildtype)
2.5
2.0
1.5
1.0
0.5
0.0
Sostdc1
Bmp4
Bmp5
Bmp7

HOXA13 binds to conserved DNA sequences within *Sostdc1* in the developing autopod and functions to repress gene expression

VISTA plot analysis (Frazer et al., 2004) of the murine *Sostdc1* locus identified two regions, Sost5'FL and Sost3'FL, containing multiple high affinity HOXA13 binding sites (Fig 3.5 A,B,D). Sequence analysis of these regions revealed high conservation among several vertebrate species including: mouse (*M. musculus*), rat (*R. norvegicus*), dog (*C. familiaris*) and human (*H. sapien*) (Fig. 3.5 B) (Mayor et al., 2000). To assess whether HOXA13 binds the Sost5'FL and Sost3'FL sites *in vivo*, a chromatin immunoprecipitation assay (ChIP) was used to identify HOXA13-DNA complexes present in the developing limb. The Hoxa13 antibody used in the ChIP assay is capable of immunoprecipitating both wild-type and mutant HOXA13 proteins (Fig 2.3 D,E; Knosp et al., 2004). ChIP analysis of wild-type limb bud chromatin confirmed that HOXA13 associates with both *Sostdc1* sites *in vivo* (Fig 3.5 C). In contrast, parallel assays using homozygous mutant chromatin could not detect association between the mutant HOXA13 protein and these same sites, confirming that the DNA binding domain deleted in the mutant HOXA13 protein is essential for HOXA13-DNA association (Fig 3.5 C) (Stadler et al., 2001).

Based on the conservation of the Sost5'FL and Sost3'FL sequences and HOXA13's association with these regions *in vivo*, we hypothesized that these sites are bound by HOXA13 to suppress gene expression. Testing this hypothesis *in vivo*, we examined whether luciferase reporter expression directed by the Sost5'FL or Sost3'FL gene regulatory elements could be suppressed by

HOXA13. Indeed, transfections with increasing amounts of a HOXA13 expression plasmid (125 ng, 250 ng and 500 ng) suppressed pGL4Sost5'FL luciferase expression in a dose-dependent manner, resulting in a 2.5-fold reduction in reporter expression compared to the control (Fig 3.5 E). Removing three of the five HOXA13 binding sites in the Sost5'FL element (Sost5'Δ1) reduced HOXA13's capacity to suppress luciferase expression regardless of the dosage of the HOXA13 plasmid (Fig 3.5 F). Luciferase reporter constructs containing the 3' *Sostdc1* regulatory element, pGL4Sost3'FL, also responded to increasing dosages of HOXA13, suppressing luciferase expression 4-fold compared to controls (Fig 3.5 G). Removal of six of the ten HOXA13 binding sites in the Sost3'FL element (Sost3'Δ1) caused a similar reduction in HOXA13's capacity to suppress luciferase expression (Fig 3.5 H). The removal of all ten HOXA13 binding sites in the Sost3'FL element (Sost3'Δ2) completely negated HOXA13's capacity to suppress reporter expression, confirming that HOXA13 utilizes these high affinity binding sites to suppress gene expression *in vivo* (Fig 3.5 I).

Figure 3.5 HOXA13 binds DNA sequences in *Sostdc1* to repress gene expression. (A) VISTA plot of *Sostdc1* sequence conservation between human and mouse. Gene information is color-coded as labeled: pink = conserved non-coding sequence (CNS), light blue = untranslated region (UTR), blue = conserved exon. Black boxes indicate conserved genomic regions containing HOXA13 DNA binding sites. (B) Detailed view of Sost5'FL (left) and Sost3'FL (right) DNA sequence conservation between mouse, rat, human and dog. (C) ChIP assay of HOXA13 bound to high affinity DNA sequences within Sost5'FL (top) and Sost3'FL (bottom) genomic regions in E12.5 forelimb autopod tissues. *Hoxa13* +/+ (left lanes) and *Hoxa13* -/- (right lanes) ChIP samples are labeled (input, +Hoxa13 antibody, IgG control, water control). (D) Alignment of HOXA13 high affinity binding sites present in Sost5'FL and Sost3'FL. Sequence positions relative to the start codon of *Sostdc1* are indicated for each binding site (#1-15), binding sites present in the ChIP fragments are underlined. (E-I) Luciferase assays using a deletion series of Sost5' and Sost3' genomic regions. Relative luciferase units (RLU) are indicated on the Y axis, and the quantity of transfected pCAGGS-HOXA13 is labeled on the X axis (the 0 ng lane is transfected with 500 ng empty pCAGGS plasmid as a control). (E) Co-transfection of HOXA13 and Sost5'FL represses luciferase expression 2.5-fold when compared to control pCAGGS transfections. (F) The truncated Sost5'FLΔ1 is only repressed 1.4-fold. (G) Co-transfection of Sost3'FL and HOXA13 represses luciferase expression 4-fold. (H) The Sost3'Δ1 truncation is repressed 2-fold while the Sost3'Δ2 truncation relieves the HOXA13 repression (I).

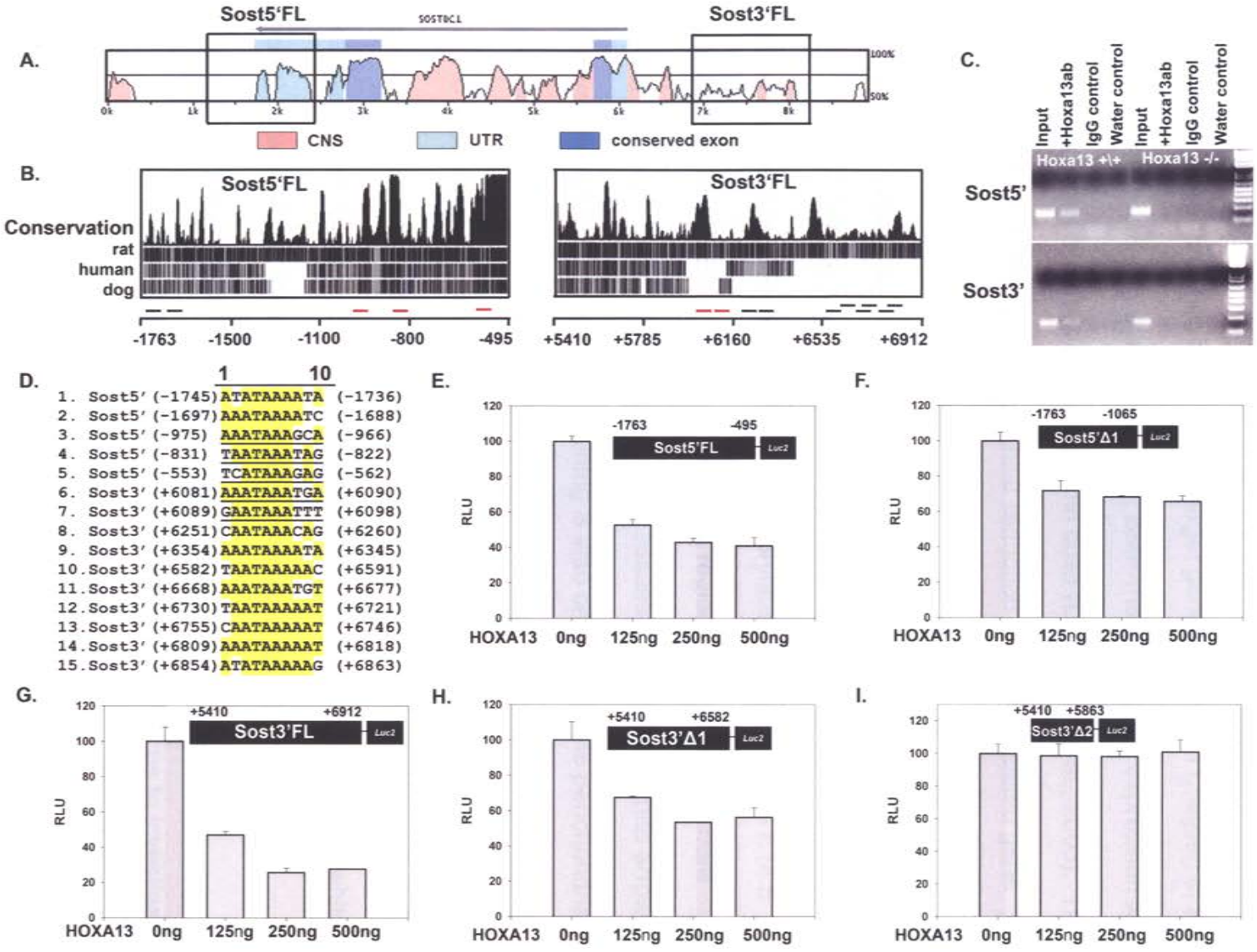
A.
Sost5'FL
SOST5CL
Sost3'FL
100%
50%
0k
1k
2k
3k
4k
5k
6k
7k
8k
CNS
UTR
conserved exon
B.
Sost5'FL
Sost3'FL
Conservation
rat
human
dog
-1763
-1500
-1100
-800
-495
+5410
+5785
+6160
+6535
+6912
C.
Input
+Hoxa13ab
IgG control
Water control
Input
+Hoxa13ab
IgG control
Water control
Hoxa13 +\+
Hoxa13 -/-
Sost5'
Sost3'
D.
1 10
1. Sost5' (-1745) ATATAAAATA (-1736)
2. Sost5' (-1697) AAATAAAATC (-1688)
3. Sost5' (-975) AAATAAAGCA (-966)
4. Sost5' (-831) TAATAAATAG (-822)
5. Sost5' (-553) TCATAAAGAG (-562)
6. Sost3' (+6081) AAATAAATGA (+6090)
7. Sost3' (+6089) GAATAAATTT (+6098)
8. Sost3' (+6251) CAATAAACAG (+6260)
9. Sost3' (+6354) AAATAAAATA (+6345)
10. Sost3' (+6582) TAATAAAAAC (+6591)
11. Sost3' (+6668) AAATAAATGT (+6677)
12. Sost3' (+6730) TAATAAAAAT (+6721)
13. Sost3' (+6755) CAATAAAAAT (+6746)
14. Sost3' (+6809) AAATAAAAAT (+6818)
15. Sost3' (+6854) ATATAAAAAG (+6863)
E.
-1763
-495
Sost5'FL
Luc2
RLU
HOXA13 0ng 125ng 250ng 500ng
F.
-1763
-1065
Sost5'Δ1
Luc2
RLU
HOXA13 0ng 125ng 250ng 500ng
G.
+5410
+6912
Sost3'FL
Luc2
RLU
HOXA13 0ng 125ng 250ng 500ng
H.
+5410
+6582
Sost3'Δ1
Luc2
RLU
HOXA13 0ng 125ng 250ng 500ng
I.
+5410
+5863
Sost3'Δ2
Luc2
RLU
HOXA13 0ng 125ng 250ng 500ng

Figure 3.5

BMP signaling is reduced in the ventral autopod and correlates with ectopic *Sostdc1* expression

The transduction of BMP signaling is facilitated by receptor-mediated SMAD1/5/8 phosphorylation and induced target gene expression (Zwijsen et al., 2003). In the presence of ectopic *Sostdc1*, BMP-mediated gene expression was strongly antagonized in the developing tooth cusp (Laurikkala et al., 2003). This finding led us to hypothesize that a similar reduction in BMP-mediated gene expression and SMAD phosphorylation would be present in the mutant limb regions over-expressing *Sostdc1*.

Immunohistochemistry using a phosphorylation-specific SMAD 1/5/8 antibody revealed strong SMAD 1/5/8 phosphorylation in the wild-type E14.5 autopod (Fig 3.6 A,C-E). In the dorsal digit I-II region, phospho-Smad1/5/8 staining is present primarily in the interdigital tissues (Fig 3.6 C,D, white arrows). In the ventral autopod, Smad1/5/8 staining is also detected in the perichondrial region of digit I (Fig 3.6 E, white arrowhead) as well as the developing footpad (Fig 3.6 E, white asterisks). In contrast, age-matched *Hoxa13* homozygous mutants exhibited reduced levels of SMAD 1/5/8 phosphorylation in the domains over-expressing *Sostdc1*, including the interdigital tissues (Fig 3.6 B,F,G, white arrows) as well as the ventral digit I/footpad domain (Fig 3.6 F-H, white arrowheads/white asterisks).

This reduction in SMAD 1/5/8 phosphorylation prompted us to investigate whether BMP-regulated target genes were also misexpressed in the ectopic *Sostdc1* domain. QRT-PCR analysis using RNA isolated from the *Sostdc1*

domain confirmed that BMP target genes were down-regulated in *Hoxa13* homozygous mutants, including: *Msx1* (-3 fold), *Collagen type II* (-3 fold), *Collagen type X* (-2.5 fold), *Sox9* (-3.5 fold) and *Ihh* (-1.7 fold) (Fig 3.6 I). Interestingly, some putative BMP target genes did not exhibit reduced expression, including: *Msx2*, *Id2*, *Mfh1*, *Bambi*, and *Runx2*, suggesting that BMP-independent processes may also be used to maintain their expression (Fig 3.6 I).

Figure 3.6 Reduced BMP signaling correlates with ectopic *Sostdc1* in the *Hoxa13* mutant autopod. (A and B) *Sostdc1 in situ* of E14.5 *Hoxa13*$^{+/+}$ (A) and *Hoxa13*$^{-/-}$ (B) ventral forelimbs. The white boxes indicate the digit I tissues analyzed in (C-H), arrows point to the interdigital tissues (IDT) between digits I and II. (C-H) A dorsal to ventral series of frontal frozen sections through *Hoxa13* +/- (C-E) and -/- (F-H) digit I and footpad (FP), immunostained with α-PSMAD1/5/8 (red signal) and endogenous HOXA13-GFP (green signal). Digits I & II and the IDT are labeled in white. (C) PSMAD1/5/8 staining is present in the IDT between digits I & II (white arrow). (D) PSMAD1/5/8 staining in the IDT has expanded within digit I (white arrows). (E) Within the FP there are multiple domains of PSMAD1/5/8 staining (white asterisks). (F) Within *Hoxa13 -/-* digit I there is reduced PSMAD1/5/8 staining in the IDT (white arrow). (G) PSMAD1/5/8 staining is reduced within *Hoxa13 -/-* digit I tissues (compare white arrows and arrowheads in D,G). (H) PSMAD1/5/8 staining is not visible within the *Hoxa13*$^{-/-}$ FP (compare asterisks in E,H). (I) QRT-PCR using E14.5 mRNA isolated from the *Hoxa13*$^{+/+}$ and *Hoxa13*$^{-/-}$ digit I and FP, calculated as the fold change in mutant divided by wild-type expression.

Figure 3.6

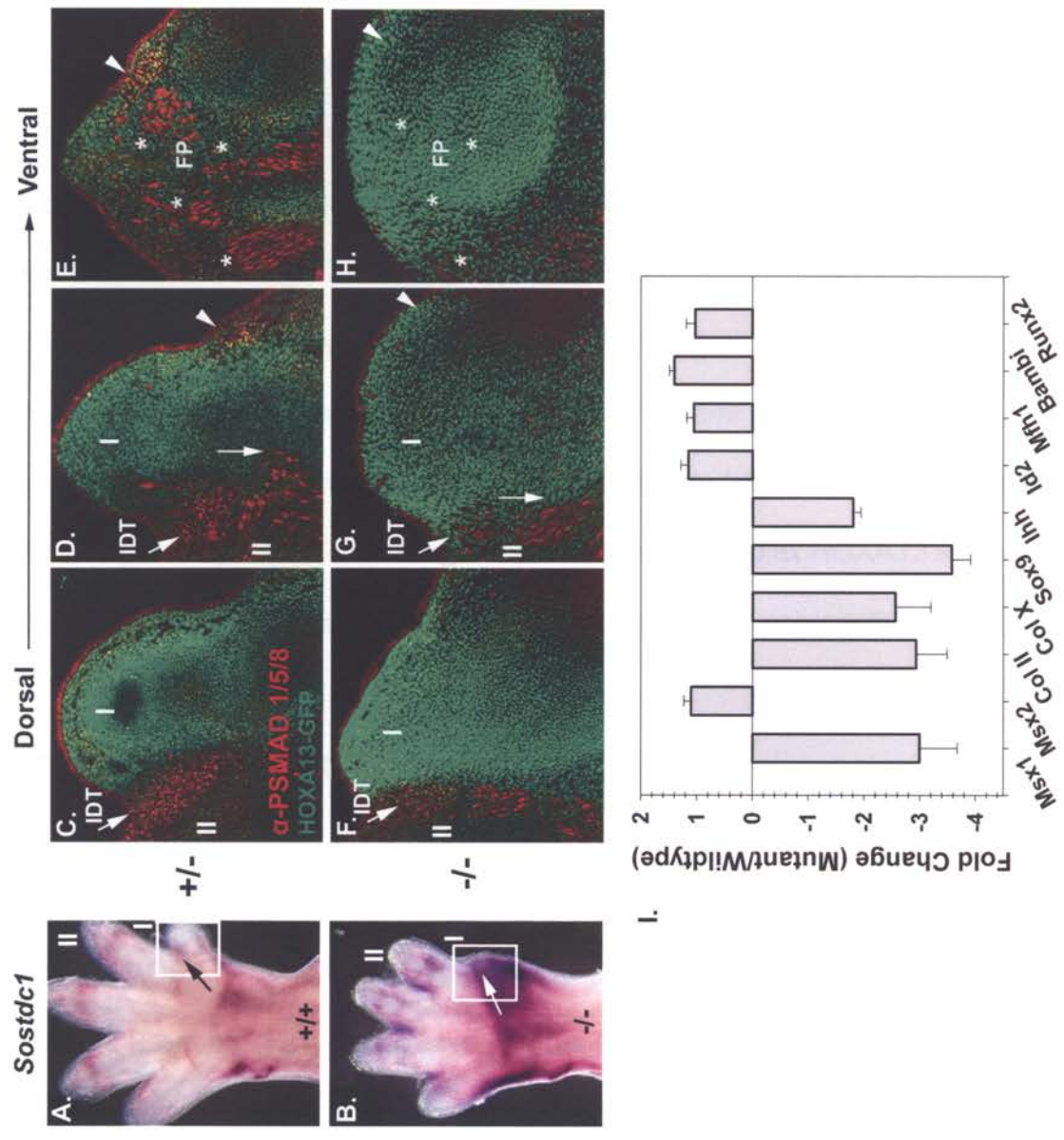
Sostdc1
A.
B.
+/+
-/-
II
I
Dorsal
Ventral
+/-
-/-
C.
D.
E.
F.
G.
H.
IDT
FP
α-PSMAD 1/5/8
HOXA13-GFP
I.
Fold Change (Mutant/Wildtype)
2
1
0
-1
-2
-3
-4
Msx1
Msx2
Col II
Col X
Sox9
Ihh
Id2
Mfh1
Bambi
Runx2

IV. Discussion

HOXA13 function is essential for the normal development of the distal limb and genitourinary tract. Prior to this investigation, mutational studies of HOXA13 have focused on the cellular mechanisms affected by its loss of function such as defects in cell adhesion, reduced proliferation, and a decrease in programmed cell death (Knosp et al., 2004; Morgan et al., 2003; Stadler et al., 2001). In the present study, we sought to extend what was known about HOXA13's developmental function by characterizing its biochemical properties as a transcription factor. From this analysis, we identified the DNA sequences preferred by HOXA13 as well as their utilization to regulate the expression of the BMP antagonist *Sostdc1*, providing a mechanism to interpret HOXA13's developmental function from a quantitative transcriptional perspective.

HOXA13 binds a novel gene-regulatory sequence

The HOXA13 core ("TAAA") and full length ("AAATAAAA") binding sites are unique when compared to sequences bound by other Abd-B proteins, including: HOXA10, HOXC13, and HOXD13 which appear to bind a "TTA(G/C)" core motif (Benson et al., 1995; Jave-Suárez et al., 2002; Salsi and Zappavigna, 2006; Shen et al., 1997). Interestingly, while HOXA10, HOXC13, and HOXD13 appear to bind the same core sequence, the bases flanking this motif vary for each protein, suggesting that the disparate phenotypes exhibited by HOXA10, HOXC13, and HOXD13 knockout mice can be explained, in part, by the capacity

of these proteins to bind discrete gene-regulatory elements (Davis and Capecchi, 1996; Favier et al., 1996; Fromental-Ramain et al., 1996b; Godwin et al., 1998).

Trans-acting factors are also likely to participate in the tissue-specific regulation of HOXA13 target genes. Notably, proteins such as MEIS1B and SMAD5 appear to be involved in modulating HOXA13 function, although HOXA13 and MEIS1B do not appear to co-localize in the distal limb (Williams et al., 2005a; Williams et al., 2005b). This finding, in conjunction with the capacity of full length HOXA13 and A13-DBD to bind specific sequences with high affinity without additional accessory proteins, strongly suggests that properties inherent to the HOXA13 homeodomain may be sufficient to regulate specific target genes. This conclusion is supported by the substantial difference in affinity for the "AAATAAAA" sequence between the HOXA13 and HOXD13 homeodomains, which share greater than 90% amino acid identity. The functional specificity of HOXA13 is also supported by domain swap experiments where the replacement of the HOXA11 homeodomain by the HOXA13 homeodomain revealed a lack of redundancy in the limb and female reproductive tract, supporting the conclusion that HOXA13 possesses independent function during limb development (Zhao and Potter, 2001).

HOXA13 modulates the feedback between growth factor and antagonist to facilitate BMP signaling throughput

BMP signaling plays an important role in the patterning of the digits, the footpads, and removal of the interdigital tissues (Dudley et al., 1995; Hogan, 1996; Jena et al., 1997; Katagiri et al., 1998; Knosp et al., 2004; Merino et al., 1998; Zuzarte-Luis and Hurlé, 2002). Coincident with BMP function is the expression of BMP antagonists such as Gremlin, Bambi, Noggin, Chordin, and Sostdc1, which are often induced by BMPs to target the BMP signal to a discrete region (Grotewold et al., 2001; Kameda et al., 1999; Khokha et al., 2003; Laurikkala et al., 2003; Pereira et al., 2000; Stottmann et al., 2001). This feedback loop provides a mechanism to modulate BMP signaling in order to control tissue patterning. Based on the present findings we conclude that HOXA13 suppresses the antagonist component of the BMP-SOSTDC1 feedback loop to facilitate the levels of BMP signaling necessary for the proper development of the distal autopod (Fig 3.7).

Figure 3.7 HOXA13 regulation of BMP signaling in the developing autopod. (A) Depiction of HOXA13 function in a wild-type E14.5 autopod. HOXA13 up-regulates the expression of *Bmp2* and *Bmp7* in the peridigital tissues and represses *Sostdc1* expression in the developing digit and footpad tissues, resulting in proper footpad development, digit formation and separation. (B) In the absence of functional HOXA13, *Sostdc1* is ectopically expressed in digit I, footpads, and interdigital tissues (shaded). SOSTDC1 inhibits BMP function, resulting in reduced BMP target gene expression, reduced chondrogenesis, interdigital webbing and a loss of digit I and footpad development.. (C) Within a *Hoxa13*$^{+/+}$ cell, HOXA13 binds DNA sequences 5' and 3' of the *Sostdc1* gene to suppress transcription. BMPs are expressed and transduce a signal resulting in the phosphorylation of Smads1/5/8, binding to Smad4, translocation to the nucleus and binding of the protein complex at gene regulatory regions of BMP target genes to mediate transcription. (D) In a *Hoxa13*$^{-/-}$ cell, the HOXA13-GFP chimeric protein lacks the DNA binding homeodomain and is unable to bind DNA. *Sostdc1* repression is lost and *Sostdc1* is ectopically expressed and antagonizes BMPs, resulting in perturbations in BMP target gene expression.

Figure 3.7

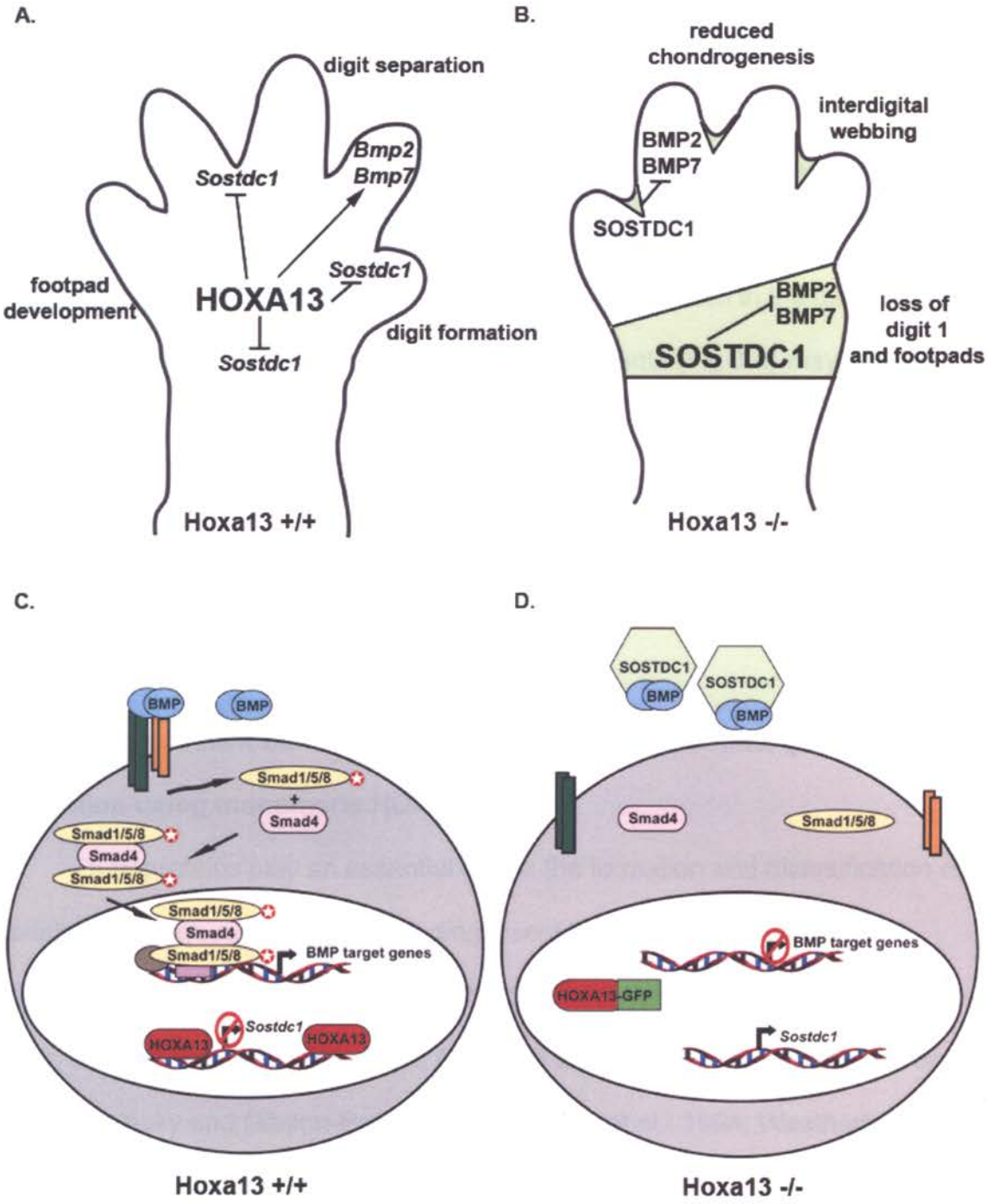
A.
digit separation
Bmp2
Bmp7
Sostdc1
footpad
development
HOXA13
Sostdc1
Sostdc1
digit formation
Hoxa13 +/+
B.
reduced
chondrogenesis
interdigital
webbing
BMP2
BMP7
SOSTDC1
BMP2
BMP7
SOSTDC1
loss of
digit 1
and footpads
Hoxa13 -/-
C.
BMP
BMP
Smad1/5/8
+
Smad4
Smad1/5/8
Smad4
Smad1/5/8
Smad1/5/8
Smad4
Smad1/5/8
BMP target genes
Sostdc1
HOXA13
HOXA13
Hoxa13 +/+
D.
SOSTDC1
BMP
SOSTDC1
BMP
Smad4
Smad1/5/8
BMP target genes
HOXA13-GFP
Sostdc1
Hoxa13 -/-

In the absence of HOXA13's suppressive function *Sostdc1* is expressed, effectively antagonizing BMP-induced target gene expression (Fig 3.7). Previous characterizations of SOSTDC1 in the tooth bud confirm a high affinity for multiple BMPs including BMP2, BMP4, BMP6, and BMP7. When SOSTDC1 was ectopically applied to mouse preosteoblastic MC3T3-E1 cells, it clearly antagonized BMP-mediated osteoblast differentiation (Laurikkala et al., 2003). Interestingly, our identification of ectopic *Sostdc1* expression in the distal limb and interdigital tissues of *Hoxa13* homozygous mutants (Fig 3.4) may also help to explain why *Hoxa13* heterozygous mutant limbs respond more robustly to exogenous BMP2 or BMP7 treatments than their homozygous mutant counterparts, as ectopic levels of SOSTDC1 would limit the therapeutic effect afforded by the BMP treatment (Knosp et al., 2004).

Multiplexing of HOX binding sites: a mechanism to facilitate gene regulation using monomeric HOXA13

HOX proteins play an essential role in the formation and diversification of serially homologous structures including insect body segments and flight appendages, as well as the vertebrate hindbrain, axial skeleton and limb (Burke et al., 1995; Cohn and Tickle, 1999; Galant et al., 2002; Lewis, 1978; Mohit et al., 2006; Ruvinsky and Gibson-Brown, 2000; Warren et al., 1994; Weatherbee et al., 1998). A mechanism common to the HOX-mediated diversification of these structures is the use of multiple binding sites to modulate target gene expression (Capovilla et al., 1994; Capovilla et al., 2001; Galant et al., 2002; Weatherbee et

al., 1998). In *Sostdc1*, the removal of the clustered HOXA13 binding sites negated HOXA13's capacity to suppress gene expression, a finding consistent with studies in Drosophila where multiple Ubx binding sites are required to suppress spalt expression in the developing haltere (Galant et al., 2002). Multiple binding site usage may provide a unique gene regulatory code to explain how tissues expressing two HOX proteins parse the gene regulatory signals necessary for tissue development. In the limb, *Hoxa13* and *Hoxd13* are co-expressed in multiple tissue domains, yet their loss of function phenotypes are distinct (Fromental-Ramain et al., 1996b; Morgan et al., 2003; Stadler et al., 2001; Warot et al., 1997). Here the use of clustered binding sites in conjunction with the differential affinity of HOXA13 and HOXD13 for these sites provides a mechanism to explain not only their unique loss of function phenotypes, but also how HOX proteins may function to activate or suppress target genes independent of PBC or MEIS accessory protein function.

Previous reports have identified several genes that are up-regulated by HOXA13 (Knosp et al., 2004; Williams et al., 2005c); however, in this body of work we have identified and characterized a gene, *Sostdc1*, that is down-regulated by HOXA13. It is interesting to speculate how HOXA13 may mediate these opposite transcriptional effects through the use of different types of DNA binding sites. Future work to dissect out the roles of different types of HOXA13 binding sites in transcriptional regulation will provide further insight into the function of this transcription factor in embryonic development and disease.

V. Materials and Methods

Selection of the HOXA13 binding site from Random DNA Sequences

The A13-DBD peptide used for DNA binding assays was generated as previously described (Chapter 2, Knosp et al., 2004). For the systematic evolution of ligands by exponential enrichment (SELEX) screen, a library of 52 bp double stranded random sequence oligonucleotides were generated by PCR with the "Random 16" oligonucleotide 5'-TACGTCGAATTCGTCAGTN_{16}GATGGATCC-TGATGTAGA-3' as the template, (where *N* indicates that either G, A, T, or C was randomly inserted at that position) and oligonucleotides R16F 5'-TACGTCGA-ATTCGTCAGT-3' and R16R 5'-TCTACATCAGGATCCATC-3' were used as primers to generate a pool of primary double stranded "Random 16" DNA. Amplified double stranded "Random 16" DNA was radiolabeled by T4 polynucleotide kinase in the presence of (γ-^{32}P) dATP (4500 Ci/mmol, MPBio). ^{32}P-labeled "Random 16" DNA sequences were then incubated with 5 µM A13-DBD peptide and EMSA was performed as previously described (Knosp et al., 2004). The A13-DBD-bound DNA fragments were excised from the gel and eluted by 2 hour incubation at 65°C in DNA buffer (50 mM Tris-HCl pH 8.4, 1 mM EDTA, 0.5% Tween-20). Eluted DNA was purified using a sephadex G-25 column, amplified using R16F and R16R primers, and used for the next cycle of selection. After a total of 5 rounds of selection and amplification, the eluted DNA was cloned into the pt3t7 vector, transformed into TOP10 *E. coli* (Invitrogen), the plasmids were recovered, and the cloned regions were sequenced and analyzed

using VectorNTI software (InforMax, Inc.). Energy normalized LOGOS were generated using the EnoLOGOS web tool (Workman et al., 2005), the height of each represented base is weighted based on its frequency at a given position within the 100 aligned SELEX sequences.

Fluorescence Anisotropy

The 63 amino acid HOXD13 homeodomain peptide (D13-DBD) (GRKKRVPYTKLQLKELENEYAINKFINKDKRRRISAATNLSERQVTIWFQNRRV KDKKIVSKC) was synthesized and purified as previously described (Chapter 2, Knosp et al., 2004). Fluorescence anisotropy measurements were performed on a Pan Vera Beacon 2000 fluorescence anisometer (InVitrogen). Self-annealing oligonucleotides were chemically synthesized carrying a fluorescein via a hexyl linker (6-FAM) at the 5' end and purified by high pressure liquid chromatography (Integrated DNA Technologies) (Table 1). Oligonucleotides were resuspended as a 100 µM stock in TE (10 mM Tris pH 8, 1 mM EDTA), diluted to 100 nM in Annealing Buffer (1 M NaCl, 10 mM Tris-HCl, 0.1 mM EDTA, pH 8), denatured at 95°C for 10 min and annealed by cooling to room temperature for 30 min. Increasing amounts of A13-DBD peptide (0-200 nM) were added to a solution containing 2 nM fluorescein-labeled DNA in 20 mM Tris pH 7.5, 80 mM KCl, 10 mM MgCl2, 0.2 mM EDTA, 1 mM DTT and incubated at 15°C for 1 hour. Measurements were collected at 15°C with a 10 sec delay, each experiment was repeated 3 times and values averaged in order to determine the dissociation

constant and standard deviation. A non-linear least squares fit was used to calculate the association constant (K_a) of the protein-DNA interactions:

$$A = \frac{1 + K[P] + K[DNA] - \sqrt{(1 + K[P] + K[DNA])^2 - 4[P][DNA]K^2}}{2\,K[DNA]} (A_m - A_0) + A_0$$

A = anisotropy value, A_m = maximum anisotropy value detected, A_0 = minimum anisotropy value detected (anisotropy without protein), K = K_a, [P] = protein concentration, and [DNA] = DNA concentration fixed at 1nM. The dissociation constants were calculated using the formula $K_d = 1/K_a$.

Table 1. Fluorescein-conjugated oligonucleotides

Primer Name	Fluorescein-conjugated Oligonucleotide Sequences
A13site	5'- 6-FAM-CCCATAAACCCCCCCGGTTTATGGG-3'
A13-3G	5'-6-FAM-CGCATAAACCCCCCCGGTTTATGCG-3'
A13-3T	5'-6-FAM-CTCATAAACCCCCCCGGTTTATGAG-3'
A13-3A	5'-6-FAM-CACATAAACCCCCCCGGTTTATGTG-3'
A13-2G	5'-6-FAM-CCGATAAACC CCCCC GGTTTATCGG-3'
A13-2T	5'-6-FAM-CCTATAAACCCCCCCGGTTTATAGG-3'
A13-2A	5'-6-FAM-CCAATAAACCCCCCCGGTTTATTGG-3'
A13-1G	5'-6-FAM-CCCGTAAACCCCCCCGGTTTACGGG-3'
A13-1T	5'-6-FAM-CCCTTAAACCCCCCCGGTTTAAGGG-3'
A13-1C	5'-6-FAM-CCCCTAAACCCCCCCGGTTTAGGGG-3'
A13+3G	5'-6-FAM-CCCATAAGCCCCCCCGGCTTATGGG-3'
A13+3T	5'-6-FAM-CCCATAATCCCCCCCGGATTATGGG-3'
A13+3C	5'-6-FAM-CCCATAACCCCCCCCGGGTTATGGG-3'
A13+4G	5'-6-FAM-CCCATAAAGCCCCCCGCTTTATGGG-3'
A13+4T	5'-6-FAM-CCCATAAATCCCCCCGATTTATGGG-3'
A13+4A	5'-6-FAM-CCCATAAAACCCCCCGTTTTATGGG-3'
A13+5G	5'-6-FAM-CCCATAAACGCCCCCCGTTTATGGG-3'
A13+5T	5'-6-FAM-CCCATAAACTCCCCCAGTTTATGGG-3'
A13+5A	5'-6-FAM-CCCATAAACACCCCCTGTTTATGGG-3'
TGAC	5'-6-FAM-TGACTGACTGACTGCCCCCCAGTCAGTCAGTCA-3'

Full length HOXA13 expression and purification

The *Hoxa13* cDNA was cloned into the pET16b expression plasmid with an in frame N-terminal His tag and transformed into Rosetta2 E. coli (Novagen). HOXA13 expression was induced with the addition of 100 mM IPTG for 1 hour, cells were collected by centrifugation at 4,500 rpm, lysed in B-Per (Pierce), and the cell pellet solubilized in 6 M Guanidine HCl, 300 mM NaCl, 50 mM sodium phosphate pH 7. The AthenaES Protein Folding Buffer #6 (50 mM MES pH 6, 240 mM NaCl, 10 mM KCl, 1 mM EDTA, 0.5 M Arginine, 0.4 M Sucrose, 0.5% TritonX-100, 0.5% PEG 3550, 1 mM GSH, 0.1 mM GSSH) was identified using the AthenaES Protein Refolding Kit to screen for buffers compatible with refolding the denatured His-HOXA13. His-HOXA13 was then purified using TALON beads (Clontech) according to the manufacturer's protocol with the following modification: purified protein was eluted in Folding Buffer #6 containing 250 mM imidazole. Purified protein was dialyzed into Folding Buffer #6 to remove imidazole and quantitated by amino acid analysis. Fluorescence anisotropy measurements were obtained as described above.

In situ Hybridization

The antisense riboprobe specific for *Hoxa13* was produced as previously described (Morgan et al., 2003). The 450 bp Sostdc1 riboprobe was generated using the primers SostF 5'-AACAGCACCCTGAATCAAGC-3' and SostR 5'-TCTCTTCCG-CTCTCTGTGGT-3' and amplified by PCR from E12.5 embryonic cDNA. The rabbit anti-phosphorylated Smad1/5/8 antibody (a gift from Dr. E.

Laufer, Columbia University) was used at a 1:1000 dilution. Whole mount *in situ* hybridization, immunohistochemistry and confocal imaging of limb frozen sections were performed as previously described (Manley and Capecchi, 1995; Morgan et al., 2003).

Quantitative RT-PCR

Hoxa13 wild type and homozygous mutant E14.5 forelimb digit I and footpad tissues were microdissected in DEPC-treated PBS and snap frozen on dry ice. Six microdissected tissues were pooled for total RNA isolation using RNA STAT-60 as per protocol (Tel-Test). First strand cDNA was synthesized using 2.5 µg total RNA according to the manufacturer's protocol (ImPromII Reverse Transcription System, Promega). Three independent samples of each genotype (*Hoxa13* wild-type or homozygous mutant) were used for QRT-PCR analyses with the SYBR Green PCR Master Mix (Applied Biosystems) on an Applied Biosystems Model 7700 Sequence Detector thermal cycler and normalized to either Actin or Gapdh expression. The oligonucleotide sequences of the primers used are found in Table 2.

Table 2. Quantitative RT-PCR primer sequences

Gene name	Forward primer	Reverse Primer
Actin	5'-ACTGGGACGACATGGAGAAG-3'	5'-GGGGTGTTGAAGGTCTCAAA-3'
Gapdh	5'-CACTGCCACCCAGAAGACTGT-3'	5'-GGAAGGCCATGCCAGTGA-3'
Sostdc1	5'-CGGTGTGTCAACGACAAGAC-3'	5'-AAGTTGTGGCTGGACTCGTT-3'
Bmp4	5'-CAGGGCTTCCACCGTATAAA-3'	5'-CAGGGCTCACATCGAAAGTT-3'
Bmp5	5'-TTCAAGGCAAGCGAGGTACT-3'	5'-TGCAGGCTTGTTTTTGTTCA-3'
Bmp7	5'-GGAAGCATGTAAGGGTTCCA-3'	5'-TTCCTGGCAGACATTTTTCC-3'
Msx1	5'-AAGTTCCGCCAGAAGCAGTA-3'	5'-CCTGCAGTCTCTTGGCCTTA -3'
Msx2	5'-AAGGGCTAAGGCGAAAAGAC-3'	5'-GATAGGGAAGGGCAGACTGA-3'
Col II	5'-TGGTGACAAGGGAGAAAAGG-3'	5'-ATACCCTCCAGCCATCTGAG-3'
Col X	5'-CCTGGTTCATGGGATGTTTT-3'	5'-GACCAGGAATGCCTTGTTCT-3'
Sox9	-AGGAAGCTGGCAGACCAGTA-3'	5'-TGTAATCGGGGTGGTCTTTC-3'
Ihh	5'-GAGCTCACCCCCAACTACAA-3'	5'-GTCACCCGCAGTTTCACAC-3
Id2	5'-ATCCCCCAGAACAAGAAGGT-3'	5'-TGTCCAGGTCTCTGGTGATG-3'
Mfh1	5'-GCGCTTCAAGAAGAAGGATG-3'	5'-CCTCGCTCTTAACCACGACT-3'
Bambi	5'-TTTGGAATGCTGTCACGAAG-3'	5'-GAGGAAGTCAGCTCCTGCAT-3'
Runx2	5'-AGACTGCAAGAAGGCTCTGG-3'	5'-ACGCCATAGTCCCTCCTTTT-3'

Chromatin Immunoprecipitation

Chromatin immunoprecipitation assays (ChIP) were performed using an anti-HOXA13 antibody as previously described (Upstate Biotechnology) (Chapter 2, Knosp et al., 2004), with the following modifications: cross-linked tissues were lysed in 100 µl cell lysis buffer (5 mM PIPES pH 8.0 , 85 mM KCl , 0.5 % NP40) containing 15 µl/ml protease inhibitor cocktail (PIC, Sigma), and incubated on ice for 10 min. Lysates were centrifuged at 500 x **g** for 5 min at 4°C to pellet the nuclei. Nuclei were resuspended in 50 µl nuclei lysis buffer (50 mM Tris-HCl pH 8.1, 10 mM EDTA, 1 % SDS) including 15 µl/ml PIC and incubated on ice for 10 min. Lysates were sonicated for 10 cycles of 30 sec "on" and 1 min "off" at 4°C using a Bioruptor (Cosmo Bio) to an average length of 200 bp to 1,000 bp. The chromatin was pre-cleared with 40 µl of Salmon Sperm DNA/ Protein A Agarose (Upstate Biotechnology) for 1 hour at 4°C and then centrifuged at 100 x ***g*** for 1 min. The Protein A Agarose/antibody/HOXA13/chromatin complexes were washed five times with 500 µl of wash buffers (Upstate Biotechnology). After elution and reversing crosslinks, chromatin was precipitated with 2.5 volumes of ethanol and incubated at -20°C for 1 hour and the pellet dissolved in 100 µl of TE. Chromatin was then treated with 25 µl of 5X PK buffer (50 mM Tris-HCl ph 7.5, 25 mM EDTA, 1.25 % SDS) and 2 µl proteinase K (20 mg/ml) per sample and incubated at 55°C for 1 hour. Chromatin was purified using the Qiaquick PCR cleanup kit (Qiagen). Eluted DNA from the antibody, control IgG and no antibody ChIP samples and from the input chromatin, were assessed for the presence of the Sost5' and Sost3' DNA regions using PCR and the following

primers: Sost5'F 5'-CCAGACGGTGACAGCACTTA-3'; Sost5'R 5'-GCATTCTG-CATGTCTCTTGC-3'; Sost3'F 5'-CAGGGCCTACATAGTAGGTA-3'; Sost3'R 5'–CAATTAGTATAGTTAGCAATTAAC-3'.

Luciferase Reporter Constructs

The 5' and 3' regions from the *Sostdc1* locus (NCBI M35 mouse assembly; ENSMUSG00000036169) were identified as conserved regions containing multiple high affinity HOXA13 binding sites. The 5' region containing five high affinity HOXA13 binding sites, Sost5'FL, is located between nucleotides -1763 and -495 upstream of the of the *Sostdc1* initiation codon (Fig 3.5 B and D). This region was amplified from mouse genomic DNA using PCR with the following primers: Sost5'F1 5'-TCCCGACACCATC-TTGTTTT-3'; Sost5'R1 5'-GTGTAG-GGCTTCGGAGTGAA-3' followed by restriction digest with Bgl II. The 3' *Sostdc1* region containing ten HOXA13 binding sites, Sost3'FL, was amplified using the primers: Sost3'F1 5'-CAGTTGGAAGGGTCTGTGGT-3'; Sost3'R1 5'-GGCTTCCCACGGTAGAGATT-3'. The Sost3'FL region is located downstream of the initiation codon (+1) between base positions +5410 to +6912 (Fig. 3.5 B and D). The PCR-amplified Sost5'FL and Sost3'FL products were cloned into the EcoR V site of the pGL4.10 luciferase vector (Promega) to produce the pGL4Sost5'FL and pGL4Sost3'FL reporter plasmids. Deletion constructs removing the high affinity HOXA13 binding sites were produced by restriction digests of the pGL4Sost5'FL and pGL4Sost3'FL reporter plasmids. The Sost5'Δ1 construct was produced by a Hind III restriction digest, which removed

bases -1066 to -495 and ablated three of the five high affinity HOXA13 binding sites in the Sost5'FL element. Sost3'Δ1 was subcloned from the pGL4Sost3'FL plasmid by sequential restriction digests with PpuM I and Bgl II, which removed bases +6583-6912 and six of the ten high affinity HOXA13 binding sites. The Sost3'Δ2 deletion was produced by sequential restriction digests with Nde I and Bgl II, which removed bases +5864-6912 ablating all ten high affinity HOXA13 binding sites. The sequences and orientation of all cloned fragments were verified using di-deoxy terminator fluorescent sequencing (Applied Biosystems).

Cell Culture and Luciferase Assays

NG108-15 cells (mouse neuroblastoma and rat glioma somatic cell hybrid, ATCC#HB-12317) were maintained and transfected as previously described (Knosp et al., 2004). Transfections were performed in 12 well plates (Costar) using 2 µg pGL4 plasmid, 0.25 µg pRL-CMV Renilla, and 0.125 µg - 0.5 µg pCAGGS-HOXA13 or empty pCAGGS control plasmid per well. Cell lysates were processed to detect luciferase activity using the Dual-Glo Luciferase Assay System (Promega) in OptiPlate-96F black plates (Packard) as described (Promega) (Knosp et al., 2004). Luciferase activity was detected using a Packard Fusion Universal Microplate Analyzer (Perkin Elmer); wells were read 3 times for 1 sec each and averaged. Two replicates of each transfection were performed and each transfection assay was repeated 3 times. Results were normalized for Renilla and control transfections were set to a RLU value of 100 and plotted using SigmaPlot 9.0 (Systat).

VI. Acknowledgements

We thank Dr. Ed Laufer for kindly providing the anti-phospho-Smad1/5/8 antibody. This work is supported by grants from the Shriners Hospital for Children (HSS) (HPB), the National Institutes of Health (5R01DK066539-01) (HSS) as well as an NIH pre-doctoral training grant (NIH-5T32GM008617-09) (WMK) and an N.L. Tartar Research Fellowship (WMK). Biostatical and Affymetrix microarray support was provided in part by the Biostatistics Shared Resource of the OHSU Cancer Institute (P30 CA69533).

CHAPTER 4

Conclusions and Future Directions

Conclusions

The complex processes that regulate embryonic growth and development are critical for the formation of a healthy functioning organism. The timing and location of gene expression is integral for the patterning of complex tissues, such as those that comprise the limb. In this dissertation, I have addressed the molecular function of the transcription factor HOXA13 and its role in mediating target gene transcription to pattern the developing limb by addressing the following questions:

1. What is the status of BMP expression and function in Hoxa13 homozygous mutant autopods?

Analysis of *Bmp* expression in the developing limb revealed reduced expression of *Bmp2* and *Bmp7*, and increased expression of the BMP antagonist *Sostdc1* in *Hoxa13* homozygous mutant autopods (Fig 2.1 and 3.4). These initial findings correlate with the *Hoxa13* mutant phenotype of reduced chondrogenesis and IPCD in these same tissues that exhibit changes in the expression of genes involved in BMP signaling.

In addition, analysis of BMP target gene expression and Smad phosphorylation within the affected digit I domain revealed reduced BMP signaling in these tissues (Fig 2.1 and 3.6). This finding is consistent with limb organ culture experiments where supplementation of *Hoxa13* mutant limbs was sufficient to initiate IPCD but did not fully induce *Msx2* expression (Fig 2.4),

suggesting the competency to respond to BMP signals is affected by loss of HOXA13 function.

In this work we have made the novel discovery that a BMP antagonist, *Sostdc1*, is expressed in the limb (Fig 3.4). Although *Sostdc1* expression and function as a BMP antagonist have been demonstrated in the developing tooth bud and kidney, an expression domain in the limb has not previously been described. We find that *Sostdc1* has a dynamic expression pattern throughout limb development, which negatively correlates with domains of HOXA13 function. In addition, the loss of HOXA13 function leads to ectopic expression of this antagonist and correlates with the reduced capacity of *Hoxa13* mutant tissues to respond to BMP signals.

2. Identify DNA sequences bound by the HOXA13 homeodomain and quantitate these interactions.

To identify DNA sequences bound by the HOXA13 transcription factor I screened a pool of randomized DNA sequences using a purified and folded HOXA13 homeodomain peptide. Sequencing analysis of the selected DNA sequences revealed a core "TAAA" sequence present in 50% of the aligned sequences (Fig 3.1). Quantitation of HOXA13 DNA binding revealed that alterations of the bases flanking the core "TAAA" sequence could dramatically affect HOXA13 DNA binding affinity (Fig 3.2). A systematic analysis of HOXA13 DNA binding affinity for each possible nucleotide (A, T, C or G) at each position revealed a high affinity "AAATAAAA" HOXA13 binding site.

To confirm these findings I developed a method for expression, purification and folding of full length HOXA13 protein. To my knowledge this has not been successfully achieved for any HOX protein, as they are notoriously insoluble and difficult to work with. The full length purified and folded HOXA13 protein was found to bind the "AAATAAAA" sequence with the same affinity as the HOXA13 homeodomain peptide, confirming our DNA binding analyses. In addition, studies with a HOXD13 homeodomain peptide revealed a 15-fold difference in binding affinity, supporting our hypothesis that the HOXA13 homeodomain has inherent specificity (Fig 3.3B).

3. Identify novel HOXA13 target genes misexpressed in Hoxa13 homozygous mutant autopods.

The approach that I took to identify novel HOXA13 target genes was two-fold: initially we examined the expression patterns of genes known to be involved in the processes affected by loss of functional HOXA13 (i.e. chondrogenesis and IPCD); secondly, after ascertaining HOXA13 DNA binding sites and performing autopod microarrays, we identified HOXA13 binding sites in genes misexpressed in *Hoxa13* homozygous mutant autopods.

Using these approaches I identified *Bmp2*, *Bmp7*, and *Sostdc1* as novel HOXA13 target genes in the developing autopod. ChIP analysis of DNA sequences flanking these genes identified genomic regions bound by HOXA13 *in vivo*, and luciferase analysis of these genomic regions confirmed HOXA13 transcriptional regulation in the presence of HOXA13 DNA binding sites.

Future Directions

Together, these findings provide a framework for understanding how HOXA13 functions to pattern the developing limb. Interestingly, HOXA13 can both activate *Bmp2* and *Bmp7* expression and repress *Sostdc1* expression in the developing autopod. How HOXA13 functions as both a transcriptional activator and repressor is currently unknown. One possibility is the use of different HOXA13 binding sites in specific spatial combinations within the genome. The use of different arrangements of binding sites could confer a "code" for either activation or repression of target genes. Now that the DNA sequences preferred by HOXA13 have been identified, it will be possible to begin to analyze how different DNA binding sites function to effect transcription *in vivo*. A complete analysis of *in vivo* HOXA13 binding sites and transcriptional effects will be a useful component to understanding not only how HOXA13 functions, but also provide a framework for understanding how HOX proteins and other transcription factors may mediate transcriptional regulation.

Now that a method for expressing, purifying and folding full length HOXA13 protein has been elucidated, the next step will be to purify large quantities of HOXA13 protein for additional biochemical analyses of the DNA binding interaction. The protein-DNA interactions that I have characterized and quantitated can now be analyzed at the molecular level by producing HOXA13-DNA crystal structures. Further work to optimize a buffer compatible with HOXA13 folding and crystallization will allow for these studies to proceed.

Additionally, the use of CD spectroscopy analysis of the full length HOXA13 protein will lend insight into the secondary structure of the HOXA13 protein. The N-terminal domain of HOXA13 is unique compared to other HOX proteins, and structural studies of the full length HOXA13 protein will provide new information about how HOXA13 interacts with DNA.

Another level of complexity is the potential role of interacting proteins affecting HOXA13 function. Although a few potential HOXA13 interacting proteins have been identified, their role in regulating target gene expression in affected tissues has not been characterized. Additional studies to identify HOXA13 interacting proteins in the tissues affected by loss of HOXA13 function should provide further insight into how this protein is functioning *in vivo* to pattern the developing embryo.

A further direction for this research is the study of the role of HOXA13 in cancer. A translocation involving *Hoxa13* has been identified in acute myeloid leukemia, resulting in the overexpression of a chimeric protein containing the HOXA13 homeodomain (Fujino et al., 2002; Taketani et al., 2002). The identification of small molecules that affect the ability of HOXA13 to bind DNA could prove useful as therapeutic agents that would perturb HOXA13-DNA interactions and target gene expression in tumorigenic tissues overexpressing HOXA13. The pursuit of this is quite tenable as we have a method for directly quantitating effects on HOXA13-DNA binding *in vitro* and testing transcriptional regulation *in vivo*.

In conclusion, I have characterized the DNA sequences bound by HOXA13 and identified three novel HOXA13 target genes within the developing autopod: *Bmp2*, *Bmp7* and *Sostdc1*. These analyses provide the first assessment of HOXA13 DNA binding site affinities and the *in vivo* use of these DNA sequences by HOXA13 to mediate gene transcription. As a result of these findings, I have identified the BMP signaling pathway as a component of HOXA13 transcriptional regulation in the developing autopod. These studies offer novel insight into the molecular mechanisms underlying defects in limb development and patterning.

REFERENCES

Akarsu, A. N., Stoilov, I., Yilmaz, E., Sayli, B. S. and Sarfarazi, M. *(1996). Genomic structure of HOXD13 gene: a nine polyalanine duplication causes synpolydactyly in two unrelated families. Hum Mol Genet* ***5****, 945-52.*

Akiyama, H., Chaboissier, M. C., Martin, J. F., Schedl, A. and de Crombrugghe, B. *(2002). The transcription factor Sox9 has essential roles in successive steps of the chondrocyte differentiation pathway and is required for expression of Sox5 and Sox6. Genes Dev* ***16****, 2813-28.*

Allera, A., Herbst, M. A., Griffin, J. E., Wilson, J. D., Schweikert, H. U. and McPhaul, M. J. *(1995). Mutations of the androgen receptor coding sequence are infrequent in patients with isolated hypospadias. J Clin Endocrinol Metab* ***80****, 2697-9.*

Avsian-Kretchmer, O. and Hsueh, A. J. *(2004). Comparative genomic analysis of the eight-membered ring cystine knot-containing bone morphogenetic protein antagonists. Mol Endocrinol* ***18****, 1-12.*

Balemans, W. and Van Hul, W. *(2002). Extracellular regulation of BMP signaling in vertebrates: a cocktail of modulators. Dev Biol* ***250****, 231-50.*

Baskin, L. S., Erol, A., Jegatheesan, P., Li, Y., Liu, W. and Cunha, G. R. *(2001). Urethral seam formation and hypospadias. Cell Tissue Res* ***305****, 379-87.*

Baskin, L. S., Erol, A., Li, Y. W. and Cunha, G. R. *(1998). Anatomical studies of hypospadias. J Urol* ***160****, 1108-15; discussion 1137.*

Baur, S. T., Mai, J. J. and Dymecki, S. M. *(2000). Combinatorial signaling through BMP receptor IB and GDF5: shaping of the distal mouse limb and the genetics of distal limb diversity. Development* ***127****, 605-19.*

Benson, G. V., Nguyen, T. H. and Maas, R. L. *(1995). The expression pattern of the murine Hoxa-10 gene and the sequence recognition of its homeodomain reveal specific properties of Abdominal B-like genes. Mol Cell Biol* ***15****, 1591-601.*

Bi, W., Deng, J. M., Zhang, Z., Behringer, R. R. and de Crombrugghe, B. *(1999). Sox9 is required for cartilage formation. Nat Genet* ***22****, 85-9.*

Bi, W., Huang, W., Whitworth, D. J., Deng, J. M., Zhang, Z., Behringer, R. R. and de Crombrugghe, B. *(2001). Haploinsufficiency of Sox9 results in defective cartilage primordia and premature skeletal mineralization. Proc Natl Acad Sci U S A* ***98****, 6698-703.*

Bosnakovski, D., Mizuno, M., Kim, G., Takagi, S., Okumur, M. and Fujinag, T. *(2006). Gene expression profile of bovine bone marrow mesenchymal stem cell during spontaneous chondrogenic differentiation in pellet culture system. Jpn J Vet Res* ***53****, 127-39.*

Bosukonda, D., Shih, M. S., Sampath, K. T. and Vukicevic, S. *(2000). Characterization of receptors for osteogenic protein-1/bone morphogenetic protein-7 (OP-1/BMP-7) in rat kidneys. Kidney Int* ***58****, 1902-11.*

Boulet, A. M. and Capecchi, M. R. *(2004). Multiple roles of Hoxa11 and Hoxd11 in the formation of the mammalian forelimb zeugopod. Development* ***131****, 299-309.*

Bridges, C. B. *(1921). Current Maps of the Location of the Mutant Genes of Drosophila Melanogaster. Proc Natl Acad Sci U S A* ***7****, 127-32.*

Bridges, C. B. *(1935). Salivary chromosome maps with a key to the banding of the chomosomes of Drosophila melanogaster. J. Hered.* ***26****, 60-64.*

Bridges, C. B. and Morgan, T. H. *(1923). The Third-Chromosome Group of Mutant Characters of Drosophila Melanogaster. Washington, D.C.: The Carnegie Institution.*

Burke, A. C., Nelson, C. E., Morgan, B. A. and Tabin, C. *(1995). Hox genes and the evolution of vertebrate axial morphology. Development* ***121****, 333-46.*

Capdevila, J. and Izpisua Belmonte, J. C. *(2001). Patterning mechanisms controlling vertebrate limb development. Annu Rev Cell Dev Biol* ***17****, 87-132.*

Capdevila, J. and Johnson, R. L. *(1998). Endogenous and ectopic expression of noggin suggests a conserved mechanism for regulation of BMP function during limb and somite patterning. Dev Biol* ***197****, 205-17.*

Capovilla, M., Brandt, M. and Botas, J. *(1994). Direct regulation of decapentaplegic by Ultrabithorax and its role in Drosophila midgut morphogenesis. Cell* ***76****, 461-75.*

Capovilla, M., Kambris, Z. and Botas, J. *(2001). Direct regulation of the muscle-identity gene apterous by a Hox protein in the somatic mesoderm. Development* ***128****, 1221-30.*

Caronia, G., Goodman, F. R., McKeown, C. M., Scambler, P. J. and Zappavigna, V. *(2003). An I47L substitution in the HOXD13 homeodomain causes a novel human limb malformation by producing a selective loss of function. Development* ***130****, 1701-12.*

Catron, K. M., Iler, N. and Abate, C. *(1993). Nucleotides flanking a conserved TAAT core dictate the DNA binding specificity of three murine homeodomain proteins. Mol Cell Biol* ***13****, 2354-65.*

Chen, M. and O'Connor, K. L. *(2005). Integrin alpha6beta4 promotes expression of autotaxin/ENPP2 autocrine motility factor in breast carcinoma cells. Oncogene* ***24****, 5125-30.*

Chiang, C., Litingtung, Y., Lee, E., Young, K. E., Corden, J. L., Westphal, H. and Beachy, P. A. *(1996). Cyclopia and defective axial patterning in mice lacking Sonic hedgehog gene function. Nature* ***383****, 407-13.*

Cohn, M. J. and Tickle, C. *(1999). Developmental basis of limblessness and axial patterning in snakes. Nature* ***399****, 474-9.*

Crossley, P. H., Minowada, G., MacArthur, C. A. and Martin, G. R. *(1996). Roles for FGF8 in the induction, initiation, and maintenance of chick limb development. Cell* ***84****, 127-36.*

Davis, A. P. and Capecchi, M. R. *(1994). Axial homeosis and appendicular skeleton defects in mice with a targeted disruption of hoxd-11. Development* ***120****, 2187-98.*

Davis, A. P. and Capecchi, M. R. *(1996). A mutational analysis of the 5' HoxD genes: dissection of genetic interactions during limb development in the mouse. Development* ***122****, 1175-85.*

Davis, A. P., Witte, D. P., Hsieh-Li, H. M., Potter, S. S. and Capecchi, M. R. *(1995). Absence of radius and ulna in mice lacking hoxa-11 and hoxd-11. Nature* ***375****, 791-5.*

Dealy, C. N., Roth, A., Ferrari, D., Brown, A. M. and Kosher, R. A. *(1993). Wnt-5a and Wnt-7a are expressed in the developing chick limb bud in a manner suggesting roles in pattern formation along the proximodistal and dorsoventral axes. Mech Dev* ***43****, 175-86.*

Debeer, P., Bacchelli, C., Scambler, P. J., De Smet, L., Fryns, J. P. and Goodman, F. R. *(2002). Severe digital abnormalities in a patient heterozygous for both a novel missense mutation in HOXD13 and a polyalanine tract expansion in HOXA13. J Med Genet* ***39****, 852-6.*

Dollé, P. and Duboule, D. *(1989). Two gene members of the murine HOX-5 complex show regional and cell-type specific expression in developing limbs and gonads. Embo J* ***8****, 1507-15.*

Dollé, P., Izpisua-Belmonte, J. C., Falkenstein, H., Renucci, A. and Duboule, D. *(1989). Coordinate expression of the murine Hox-5 complex homoeobox-containing genes during limb pattern formation. Nature* ***342****, 767-72.*

Dudley, A. T., Lyons, K. M. and Robertson, E. J. *(1995). A requirement for bone morphogenetic protein-7 during development of the mammalian kidney and eye. Genes Dev* ***9****, 2795-807.*

Dudley, A. T. and Robertson, E. J. *(1997). Overlapping expression domains of bone morphogenetic protein family members potentially account for limited tissue defects in BMP7 deficient embryos. Dev Dyn* ***208****, 349-62.*

Duncan, I. and Montgomery, G. *(2002). E. B. Lewis and the bithorax complex: part I. Genetics* ***160****, 1265-72.*

Duprez, D., Bell, E. J., Richardson, M. K., Archer, C. W., Wolpert, L., Brickell, P. M. and Francis-West, P. H. *(1996). Overexpression of BMP-2 and BMP-4 alters the size and shape of developing skeletal elements in the chick limb. Mech Dev* ***57****, 145-57.*

Favier, B., Rijli, F. M., Fromental-Ramain, C., Fraulob, V., Chambon, P. and Dolle, P. *(1996). Functional cooperation between the non-paralogous genes Hoxa-10 and Hoxd-11 in the developing forelimb and axial skeleton. Development* ***122****, 449-60.*

Francis-West, P. H., Abdelfattah, A., Chen, P., Allen, C., Parish, J., Ladher, R., Allen, S., MacPherson, S., Luyten, F. P. and Archer, C. W. *(1999a). Mechanisms of GDF-5 action during skeletal development. Development* ***126****, 1305-15.*

Francis-West, P. H., Parish, J., Lee, K. and Archer, C. W. *(1999b). BMP/GDF-signalling interactions during synovial joint development. Cell Tissue Res* ***296****, 111-9.*

Francis, P. H., Richardson, M. K., Brickell, P. M. and Tickle, C. *(1994). Bone morphogenetic proteins and a signalling pathway that controls patterning in the developing chick limb. Development* ***120****, 209-18.*

Frazer, K. A., Pachter, L., Poliakov, A., Rubin, E. M. and Dubchak, I. *(2004). VISTA: computational tools for comparative genomics. Nucleic Acids Res* ***32****, W273-9.*

Fromental-Ramain, C., Warot, X., Lakkaraju, S., Favier, B., Haack, H., Birling, C., Dierich, A., Doll e, P. and Chambon, P. *(1996a). Specific and redundant functions of the paralogous Hoxa-9 and Hoxd-9 genes in forelimb and axial skeleton patterning. Development* ***122****, 461-72.*

Fromental-Ramain, C., Warot, X., Messadecq, N., LeMeur, M., Dolle, P. and Chambon, P. *(1996b). Hoxa-13 and Hoxd-13 play a crucial role in the patterning of the limb autopod. Development* ***122****, 2997-3011.*

Fujino, T., Suzuki, A., Ito, Y., Ohyashiki, K., Hatano, Y., Miura, I. and Nakamura, T. *(2002). Single-translocation and double-chimeric transcripts: detection of NUP98-HOXA9 in myeloid leukemias with HOXA11 or HOXA13 breaks of the chromosomal translocation t(7;11)(p15;p15). Blood* ***99****, 1428-33.*

Galant, R., Walsh, C. M. and Carroll, S. B. *(2002). Hox repression of a target gene: extradenticle-independent, additive action through multiple monomer binding sites. Development* ***129****, 3115-26.*

Gallentine, M. L., Morey, A. F. and Thompson, I. M., Jr. *(2001). Hypospadias: a contemporary epidemiologic assessment. Urology* ***57****, 788-90.*

Gañan, Y., Macias, D., Duterque-Coquillaud, M., Ros, M. A. and Hurlé, J. M. *(1996). Role of TGF beta s and BMPs as signals controlling the position of the digits and the areas of interdigital cell death in the developing chick limb autopod. Development* ***122****, 2349-57.*

Godwin, A. R., Stadler, H. S., Nakamura, K. and Capecchi, M. R. *(1998). Detection of targeted GFP-Hox gene fusions during mouse embryogenesis. Proc Natl Acad Sci U S A* ***95****, 13042-7.*

Goodman, F., Giovannucci-Uzielli, M. L., Hall, C., Reardon, W., Winter, R. and Scambler, P. *(1998). Deletions in HOXD13 segregate with an identical, novel foot malformation in two unrelated families. Am J Hum Genet* ***63****, 992-1000.*

Goodman, F. R., Bacchelli, C., Brady, A. F., Brueton, L. A., Fryns, J. P., Mortlock, D. P., Innis, J. W., Holmes, L. B., Donnenfeld, A. E., Feingold, M. et al. *(2000). Novel HOXA13 mutations and the phenotypic spectrum of hand-foot-genital syndrome. Am J Hum Genet* ***67****, 197-202.*

Grenier, J. K. and Carroll, S. B. *(2000). Functional evolution of the Ultrabithorax protein. Proc Natl Acad Sci U S A* ***97****, 704-9.*

Groppe, J., Greenwald, J., Wiater, E., Rodriguez-Leon, J., Economides, A. N., Kwiatkowski, W., Affolter, M., Vale, W. W., Belmonte, J. C. and Choe, S. *(2002). Structural basis of BMP signalling inhibition by the cystine knot protein Noggin. Nature* ***420****, 636-42.*

Grotewold, L., Plum, M., Dildrop, R., Peters, T. and Ruther, U. *(2001). Bambi is coexpressed with Bmp-4 during mouse embryogenesis. Mech Dev* ***100****, 327-30.*

Guha, U., Gomes, W. A., Kobayashi, T., Pestell, R. G. and Kessler, J. A. *(2002). In vivo evidence that BMP signaling is necessary for apoptosis in the mouse limb. Dev Biol* ***249****, 108-20.*

Gurrieri, F., Kjaer, K. W., Sangiorgi, E. and Neri, G. *(2002). Limb anomalies: Developmental and evolutionary aspects. Am J Med Genet* ***115****, 231-44.*

Haack, H. and Gruss, P. *(1993). The establishment of murine Hox-1 expression domains during patterning of the limb. Dev Biol* ***157****, 410-22.*

Hasegawa, T., Kozlowski, K., Nishimura, G., Hara, H., Hasegawa, Y., Aso, T., Koto, S., Nagai, T. and Tsuchiya, Y. *(1994). Japanese type of spondylo-metaphyseal dysplasia. Pediatr Radiol* ***24****, 194-7.*

Hill, R. E., Jones, P. F., Rees, A. R., Sime, C. M., Justice, M. J., Copeland, N. G., Jenkins, N. A., Graham, E. and Davidson, D. R. *(1989). A new family of mouse homeo box-containing genes: molecular structure, chromosomal location, and developmental expression of Hox-7.1. Genes Dev* ***3****, 26-37.*

Hofmann, C., Luo, G., Balling, R. and Karsenty, G. *(1996). Analysis of limb patterning in BMP-7-deficient mice. Dev Genet* ***19****, 43-50.*

Hogan, B. L. *(1996). Bone morphogenetic proteins: multifunctional regulators of vertebrate development. Genes Dev* ***10****, 1580-94.*

Hogan, B. L., Blessing, M., Winnier, G. E., Suzuki, N. and Jones, C. M. *(1994). Growth factors in development: the role of TGF-beta related polypeptide signalling molecules in embryogenesis. Dev Suppl, 53-60.*

Hollnagel, A., Oehlmann, V., Heymer, J., Ruther, U. and Nordheim, A. *(1999). Id genes are direct targets of bone morphogenetic protein induction in embryonic stem cells. J Biol Chem* ***274****, 19838-45.*

Hombria, J. C. and Lovegrove, B. *(2003). Beyond homeosis--HOX function in morphogenesis and organogenesis. Differentiation* ***71****, 461-76.*

Hsu, D. R., Economides, A. N., Wang, X., Eimon, P. M. and Harland, R. M. *(1998). The Xenopus dorsalizing factor Gremlin identifies a novel family of secreted proteins that antagonize BMP activities. Mol Cell* ***1****, 673-83.*

Innis, J. W., Goodman, F. R., Bacchelli, C., Williams, T. M., Mortlock, D. P., Sateesh, P., Scambler, P. J., McKinnon, W. and Guttmacher, A. E. *(2002). A HOXA13 allele with a missense mutation in the homeobox and a dinucleotide deletion in the promoter underlies Guttmacher syndrome. Hum Mutat* ***19****, 573-4.*

Iwasaki, M., Le, A. X. and Helms, J. A. *(1997). Expression of indian hedgehog, bone morphogenetic protein 6 and gli during skeletal morphogenesis. Mech Dev* ***69****, 197-202.*

Janatpour, M. J., McMaster, M. T., Genbacev, O., Zhou, Y., Dong, J., Cross, J. C., Israel, M. A. and Fisher, S. J. *(2000). Id-2 regulates critical aspects of human cytotrophoblast differentiation, invasion and migration. Development* ***127****, 549-58.*

Jave-Suárez, L. F., Winter, H., Langbein, L., Rogers, M. A. and Schweizer, J. *(2002). HOXC13 is involved in the regulation of human hair keratin gene expression. J Biol Chem* ***277****, 3718-26.*

Jen, Y., Weintraub, H. and Benezra, R. *(1992). Overexpression of Id protein inhibits the muscle differentiation program: in vivo association of Id with E2A proteins. Genes Dev* ***6****, 1466-79.*

Jena, N., Martin-Seisdedos, C., McCue, P. and Croce, C. M. *(1997). BMP7 null mutation in mice: developmental defects in skeleton, kidney, and eye. Exp Cell Res* ***230****, 28-37.*

Johnson, D., Kan, S. H., Oldridge, M., Trembath, R. C., Roche, P., Esnouf, R. M., Giele, H. and Wilkie, A. O. *(2003). Missense mutations in the homeodomain of HOXD13 are associated with brachydactyly types D and E. Am J Hum Genet* ***72****, 984-97.*

Kameda, T., Koike, C., Saitoh, K., Kuroiwa, A. and Iba, H. *(1999). Developmental patterning in chondrocytic cultures by morphogenic gradients: BMP induces expression of indian hedgehog and noggin. Genes Cells* ***4****, 175-84.*

Karaulanov, E., Knochel, W. and Niehrs, C. *(2004). Transcriptional regulation of BMP4 synexpression in transgenic Xenopus. Embo J* ***23****, 844-56.*

Karsenty, G. *(2003). The complexities of skeletal biology. Nature* ***423****, 316-8.*

Kassai, Y., Munne, P., Hotta, Y., Penttila, E., Kavanagh, K., Ohbayashi, N., Takada, S., Thesleff, I., Jernvall, J. and Itoh, N. *(2005). Regulation of mammalian tooth cusp patterning by ectodin. Science* ***309****, 2067-70.*

Katagiri, T., Boorla, S., Frendo, J. L., Hogan, B. L. and Karsenty, G. *(1998). Skeletal abnormalities in doubly heterozygous Bmp4 and Bmp7 mice. Dev Genet* ***22****, 340-8.*

Kaufman, M. and Bard, J. *(1999). The Limbs. In The Anatomical Basis of Mouse Development, pp. 93-97. San Diego, CA: Academic Press.*

Keller, S., Nickel, J., Zhang, J. L., Sebald, W. and Mueller, T. D. *(2004). Molecular recognition of BMP-2 and BMP receptor IA. Nat Struct Mol Biol* ***11****, 481-8.*

Khokha, M. K., Hsu, D., Brunet, L. J., Dionne, M. S. and Harland, R. M. *(2003). Gremlin is the BMP antagonist required for maintenance of Shh and Fgf signals during limb patterning. Nat Genet* ***34****, 303-7.*

Kingsley, D. M. *(1994). What do BMPs do in mammals? Clues from the mouse short-ear mutation. Trends Genet* ***10****, 16-21.*

Kmita, M., Fraudeau, N., Herault, Y. and Duboule, D. *(2002). Serial deletions and duplications suggest a mechanism for the collinearity of Hoxd genes in limbs. Nature* ***420****, 145-50.*

Knoepfler, P. S. and Kamps, M. P. *(1995). The pentapeptide motif of Hox proteins is required for cooperative DNA binding with Pbx1, physically contacts Pbx1, and enhances DNA binding by Pbx1. Mol Cell Biol* ***15****, 5811-9.*

Knosp, W. M., Scott, V., Bachinger, H. P. and Stadler, H. S. *(2004). HOXA13 regulates the expression of bone morphogenetic proteins 2 and 7 to control distal limb morphogenesis. Development* ***131****, 4581-92.*

Koike, S., Keino-Masu, K., Ohto, T. and Masu, M. *(2006). The N-terminal hydrophobic sequence of autotaxin (ENPP2) functions as a signal peptide. Genes Cells* ***11****, 133-42.*

Kurabayashi, M., Dutta, S. and Kedes, L. *(1994). Serum-inducible factors binding to an activating transcription factor motif regulate transcription of the Id2A promoter during myogenic differentiation. J Biol Chem* ***269****, 31162-70.*

Lallemand, Y., Nicola, M. A., Ramos, C., Bach, A., Clement, C. S. and Robert, B. *(2005). Analysis of Msx1; Msx2 double mutants reveals multiple roles for Msx genes in limb development. Development* ***132****, 3003-14.*

Laurikkala, J., Kassai, Y., Pakkasjarvi, L., Thesleff, I. and Itoh, N. *(2003). Identification of a secreted BMP antagonist, ectodin, integrating BMP, FGF, and SHH signals from the tooth enamel knot. Dev Biol* ***264****, 91-105.*

Lee, B., Vissing, H., Ramirez, F., Rogers, D. and Rimoin, D. *(1989). Identification of the molecular defect in a family with spondyloepiphyseal dysplasia. Science* ***244****, 978-80.*

Lengner, C. J., Lepper, C., van Wijnen, A. J., Stein, J. L., Stein, G. S. and Lian, J. B. *(2004). Primary mouse embryonic fibroblasts: a model of mesenchymal cartilage formation. J Cell Physiol* ***200****, 327-33.*

Lei, H., Juan, A. H., Kim, M. S., and Ruddle, F. H. *(2006). Identification of a Hoxc8-regulated transcriptional network in mouse embryo fibroblast cells. Proc Natl Acad Sci U S A.*

Lewandoski, M., Sun, X. and Martin, G. R. *(2000). Fgf8 signalling from the AER is essential for normal limb development. Nat Genet* ***26****, 460-3.*

Lewis, E. B. *(1951). Pseudoallelism and gene evolution. Cold Spring Harb Symp Quant Biol* ***16****, 159-74.*

Lewis, E. B. *(1978). A gene complex controlling segmentation in Drosophila. Nature* ***276****, 565-70.*

Lewis, E. B. *(1994). Homeosis: the first 100 years. Trends Genet* ***10****, 341-3.*

Lewis, E. B. *(1998). The bithorax complex: the first fifty years. Int J Dev Biol* ***42****, 403-15.*

Lipshitz, H. D. *(2005). From fruit flies to fallout: Ed Lewis and his science. Dev Dyn* ***232****, 529-46.*

Logan, C., Hornbruch, A., Campbell, I. and Lumsden, A. *(1997). The role of Engrailed in establishing the dorsoventral axis of the chick limb. Development* ***124****, 2317-24.*

Logan, M. *(2003). Finger or toe: the molecular basis of limb identity. Development* ***130****, 6401-10.*

Long, F., Chung, U. I., Ohba, S., McMahon, J., Kronenberg, H. M. and McMahon, A. P. *(2004). Ihh signaling is directly required for the osteoblast lineage in the endochondral skeleton. Development* ***131****, 1309-18.*

Loomis, C. A., Harris, E., Michaud, J., Wurst, W., Hanks, M. and Joyner, A. L. *(1996). The mouse Engrailed-1 gene and ventral limb patterning. Nature* ***382****, 360-3.*

Loomis, C. A., Kimmel, R. A., Tong, C. X., Michaud, J. and Joyner, A. L. *(1998). Analysis of the genetic pathway leading to formation of ectopic apical ectodermal ridges in mouse Engrailed-1 mutant limbs. Development* ***125****, 1137-48.*

Luo, G., Hofmann, C., Bronckers, A. L., Sohocki, M., Bradley, A. and Karsenty, G. *(1995). BMP-7 is an inducer of nephrogenesis, and is also required for eye development and skeletal patterning. Genes Dev* ***9****, 2808-20.*

Lyons, K. M., Hogan, B. L. and Robertson, E. J. *(1995). Colocalization of BMP 7 and BMP 2 RNAs suggests that these factors cooperatively mediate tissue interactions during murine development. Mech Dev* ***50****, 71-83.*

Lyons, K. M., Pelton, R. W. and Hogan, B. L. *(1989). Patterns of expression of murine Vgr-1 and BMP-2a RNA suggest that transforming growth factor-beta-like genes coordinately regulate aspects of embryonic development. Genes Dev* ***3****, 1657-68.*

Macias, D., Gañan, Y., Sampath, T. K., Piedra, M. E., Ros, M. A. and Hurlé, J. M. *(1997). Role of BMP-2 and OP-1 (BMP-7) in programmed cell death and skeletogenesis during chick limb development. Development* ***124****, 1109-17.*

Manley, N. R. and Capecchi, M. R. *(1995). The role of Hoxa-3 in mouse thymus and thyroid development. Development* ***121****, 1989-2003.*

Mariani, F. V. and Martin, G. R. *(2003). Deciphering skeletal patterning: clues from the limb. Nature* ***423****, 319-25.*

Martin, G. R. *(1998). The roles of FGFs in the early development of vertebrate limbs. Genes Dev* ***12****, 1571-86.*

Mayor, C., Brudno, M., Schwartz, J. R., Poliakov, A., Rubin, E. M., Frazer, K. A., Pachter, L. S. and Dubchak, I. *(2000). VISTA: visualizing global DNA sequence alignments of arbitrary length. Bioinformatics* ***16****, 1046-7.*

McCabe, C. D. and Innis, J. W. *(2005). A genomic approach to the identification and characterization of HOXA13 functional binding elements. Nucleic Acids Res* ***33****, 6782-94.*

McGinnis, W., Garber, R. L., Wirz, J., Kuroiwa, A. and Gehring, W. J. *(1984a). A homologous protein-coding sequence in Drosophila homeotic genes and its conservation in other metazoans. Cell* ***37****, 403-8.*

McGinnis, W., Hart, C. P., Gehring, W. J. and Ruddle, F. H. *(1984b). Molecular cloning and chromosome mapping of a mouse DNA sequence homologous to homeotic genes of Drosophila. Cell* ***38****, 675-80.*

McGinnis, W., Levine, M. S., Hafen, E., Kuroiwa, A. and Gehring, W. J. *(1984c). A conserved DNA sequence in homoeotic genes of the Drosophila Antennapedia and bithorax complexes. Nature* ***308****, 428-33.*

Merino, R., Gañan, Y., Macias, D., Economides, A. N., Sampath, K. T. and Hurlé, J. M. *(1998). Morphogenesis of digits in the avian limb is controlled by FGFs, TGFbetas, and noggin through BMP signaling. Dev Biol* ***200****, 35-45.*

Merino, R., Gañan, Y., Macias, D., Rodriguez-Leon, J. and Hurlé, J. M. *(1999a). Bone morphogenetic proteins regulate interdigital cell death in the avian embryo. Ann N Y Acad Sci* ***887****, 120-32.*

Merino, R., Macias, D., Gañan, Y., Rodriguez-Leon, J., Economides, A. N., Rodriguez-Esteban, C., Izpisua-Belmonte, J. C. and Hurlé, J. M. *(1999b). Control of digit formation by activin signalling. Development* ***126****, 2161-70.*

Merino, R., Rodriguez-Leon, J., Macias, D., Gañan, Y., Economides, A. N. and Hurlé, J. M. *(1999c). The BMP antagonist Gremlin regulates outgrowth, chondrogenesis and programmed cell death in the developing limb. Development* ***126****, 5515-22.*

Min, H., Danilenko, D. M., Scully, S. A., Bolon, B., Ring, B. D., Tarpley, J. E., DeRose, M. and Simonet, W. S. *(1998). Fgf-10 is required for both limb and lung development and exhibits striking functional similarity to Drosophila branchless. Genes Dev* ***12****, 3156-61.*

Miyazono, K., Maeda, S. and Imamura, T. *(2005). BMP receptor signaling: transcriptional targets, regulation of signals, and signaling cross-talk. Cytokine Growth Factor Rev* ***16****, 251-63.*

Moens, C. B. and Selleri, L. *(2006). Hox cofactors in vertebrate development. Dev Biol* ***291****, 193-206.*

Mohit, P., Makhijani, K., Madhavi, M. B., Bharathi, V., Lal, A., Sirdesai, G., Reddy, V. R., Ramesh, P., Kannan, R., Dhawan, J. et al. *(2006). Modulation of AP and DV signaling pathways by the homeotic gene Ultrabithorax during haltere development in Drosophila. Dev Biol* ***291****, 356-67.*

Moon, A. M. and Capecchi, M. R. *(2000). Fgf8 is required for outgrowth and patterning of the limbs. Nat Genet* ***26****, 455-9.*

Morgan, E. A., Nguyen, S. B., Scott, V. and Stadler, H. S. *(2003). Loss of Bmp7 and Fgf8 signaling in Hoxa13-mutant mice causes hypospadia. Development* ***130****, 3095-109.*

Mortlock, D. P. and Innis, J. W. *(1997). Mutation of HOXA13 in hand-foot-genital syndrome. Nat Genet* ***15****, 179-80.*

Muragaki, Y., Mundlos, S., Upton, J. and Olsen, B. R. *(1996). Altered growth and branching patterns in synpolydactyly caused by mutations in HOXD13. Science* ***272****, 548-51.*

Nifuji, A., Miura, N., Kato, N., Kellermann, O. and Noda, M. *(2001). Bone morphogenetic protein regulation of forkhead/winged helix transcription factor Foxc2 (Mfh1) in a murine mesodermal cell line C1 and in skeletal precursor cells. J Bone Miner Res* ***16****, 1765-71.*

Niswander, L. *(2003). Pattern formation: old models out on a limb. Nat Rev Genet* ***4****, 133-43.*

Nohe, A., Hassel, S., Ehrlich, M., Neubauer, F., Sebald, W., Henis, Y. I. and Knaus, P. *(2002). The mode of bone morphogenetic protein (BMP) receptor oligomerization determines different BMP-2 signaling pathways. J Biol Chem* ***277****, 5330-8.*

Norton, J. D., Deed, R. W., Craggs, G. and Sablitzky, F. *(1998). Id helix-loop-helix proteins in cell growth and differentiation. Trends Cell Biol* ***8****, 58-65.*

Ogata, T., Wozney, J. M., Benezra, R. and Noda, M. *(1993). Bone morphogenetic protein 2 transiently enhances expression of a gene, Id (inhibitor of differentiation), encoding a helix-loop-helix molecule in osteoblast-like cells. Proc Natl Acad Sci U S A* ***90****, 9219-22.*

Ohuchi, H., Nakagawa, T., Yamamoto, A., Araga, A., Ohata, T., Ishimaru, Y., Yoshioka, H., Kuwana, T., Nohno, T., Yamasaki, M. et al. *(1997). The mesenchymal factor, FGF10, initiates and maintains the outgrowth of the chick limb bud through interaction with FGF8, an apical ectodermal factor. Development* ***124****, 2235-44.*

Omi, M., Sato-Maeda, M. and Ide, H. *(2000). Role of chondrogenic tissue in programmed cell death and BMP expression in chick limb buds. Int J Dev Biol* ***44****, 381-8.*

Park, Y., Sugimoto, M., Watrin, A., Chiquet, M. and Hunziker, E. B. *(2005). BMP-2 induces the expression of chondrocyte-specific genes in bovine synovium-derived progenitor cells cultured in three-dimensional alginate hydrogel. Osteoarthritis Cartilage* ***13****, 527-36.*

Parr, B. A. and McMahon, A. P. *(1994). Wnt genes and vertebrate development. Curr Opin Genet Dev* ***4****, 523-8.*

Passner, J. M., Ryoo, H. D., Shen, L., Mann, R. S. and Aggarwal, A. K. *(1999). Structure of a DNA-bound Ultrabithorax-Extradenticle homeodomain complex. Nature* ***397****, 714-9.*

Paulozzi, L. J., Erickson, J. D. and Jackson, R. J. *(1997). Hypospadias trends in two US surveillance systems. Pediatrics* ***100****, 831-4.*

Pellerin, I., Schnabel, C., Catron, K. M. and Abate, C. *(1994). Hox proteins have different affinities for a consensus DNA site that correlate with the positions of their genes on the hox cluster. Mol Cell Biol* ***14****, 4532-45.*

Pereira, R. C., Economides, A. N. and Canalis, E. *(2000). Bone morphogenetic proteins induce gremlin, a protein that limits their activity in osteoblasts. Endocrinology* ***141****, 4558-63.*

Phelan, M. L., Rambaldi, I. and Featherstone, M. S. *(1995). Cooperative interactions between HOX and PBX proteins mediated by a conserved peptide motif. Mol Cell Biol* ***15****, 3989-97.*

Piccolo, S., Sasai, Y., Lu, B. and De Robertis, E. M. *(1996). Dorsoventral patterning in Xenopus: inhibition of ventral signals by direct binding of chordin to BMP-4. Cell* ***86****, 589-98.*

Piper, D. E., Batchelor, A. H., Chang, C. P., Cleary, M. L. and Wolberger, C. *(1999). Structure of a HoxB1-Pbx1 heterodimer bound to DNA: role of the hexapeptide and a fourth homeodomain helix in complex formation. Cell* ***96****, 587-97.*

Pizette, S. and Niswander, L. *(2000). BMPs are required at two steps of limb chondrogenesis: formation of prechondrogenic condensations and their differentiation into chondrocytes. Dev Biol* ***219****, 237-49.*

Postlethwait, J. H. and Schneiderman, H. A. *(1971). Pattern formation and determination in the antenna of the homoeotic mutant Antennapedia of Drosophila melanogaster. Dev Biol* ***25****, 606-40.*

Riddle, R. D., Johnson, R. L., Laufer, E. and Tabin, C. *(1993). Sonic hedgehog mediates the polarizing activity of the ZPA. Cell* ***75****, 1401-16.*

Robert, B., Sassoon, D., Jacq, B., Gehring, W. and Buckingham, M. *(1989). Hox-7, a mouse homeobox gene with a novel pattern of expression during embryogenesis. Embo J* ***8****, 91-100.*

Roch, F. and Akam, M. *(2000). Ultrabithorax and the control of cell morphology in Drosophila halteres. Development* ***127****, 97-107.*

Ruvinsky, I. and Gibson-Brown, J. J. *(2000). Genetic and developmental bases of serial homology in vertebrate limb evolution. Development* ***127****, 5233-44.*

Salsi, V. and Zappavigna, V. *(2006). Hoxd13 and Hoxa13 directly control the expression of the EphA7 Ephrin tyrosine kinase receptor in developing limbs. J Biol Chem* ***281****, 1992-9.*

Sampath, T. K. and Reddi, A. H. *(1981). Dissociative extraction and reconstitution of extracellular matrix components involved in local bone differentiation. Proc Natl Acad Sci U S A* ***78****, 7599-603.*

Sekine, K., Ohuchi, H., Fujiwara, M., Yamasaki, M., Yoshizawa, T., Sato, T., Yagishita, N., Matsui, D., Koga, Y., Itoh, N. et al. *(1999). Fgf10 is essential for limb and lung formation. Nat Genet* ***21****, 138-41.*

Shen, W. F., Montgomery, J. C., Rozenfeld, S., Moskow, J. J., Lawrence, H. J., Buchberg, A. M. and Largman, C. *(1997). AbdB-like Hox proteins stabilize DNA binding by the Meis1 homeodomain proteins. Mol Cell Biol* ***17****, 6448-58.*

Solursh, M., Reiter, R. S., Jensen, K. L., Kato, M. and Bernfield, M. *(1990). Transient expression of a cell surface heparan sulfate proteoglycan (syndecan) during limb development. Dev Biol* ***140****, 83-92.*

Spitz, F., Gonzalez, F. and Duboule, D. *(2003). A global control region defines a chromosomal regulatory landscape containing the HoxD cluster. Cell* ***113****, 405-17.*

Stadler, H. S., Higgins, K. M. and Capecchi, M. R. *(2001). Loss of Eph-receptor expression correlates with loss of cell adhesion and chondrogenic capacity in Hoxa13 mutant limbs. Development* ***128****, 4177-88.*

Stottmann, R. W., Anderson, R. M. and Klingensmith, J. *(2001). The BMP antagonists Chordin and Noggin have essential but redundant roles in mouse mandibular outgrowth. Dev Biol* ***240****, 457-73.*

Sutherland, R. W., Wiener, J. S., Hicks, J. P., Marcelli, M., Gonzales, E. T., Jr., Roth, D. R. and Lamb, D. J. *(1996). Androgen receptor gene mutations are rarely associated with isolated penile hypospadias. J Urol* ***156****, 828-31.*

Suzuki, M., Ueno, N. and Kuroiwa, A. *(2003). Hox proteins functionally cooperate with the GC box-binding protein system through distinct domains. J Biol Chem* ***278****, 30148-56.*

Taketani, T., Taki, T., Ono, R., Kobayashi, Y., Ida, K. and Hayashi, Y. *(2002). The chromosome translocation t(7;11)(p15;p15) in acute myeloid leukemia results in fusion of the NUP98 gene with a HOXA cluster gene, HOXA13, but not HOXA9. Genes Chromosomes Cancer* ***34****, 437-43.*

Tickle, C. *(2003). Patterning systems--from one end of the limb to the other. Dev Cell* ***4****, 449-58.*

Tickle, C., Shellswell, G., Crawley, A. and Wolpert, L. *(1976). Positional signalling by mouse limb polarising region in the chick wing bud. Nature* ***259****, 396-7.*

Tischfield, M. A., Bosley, T. M., Salih, M. A., Alorainy, I. A., Sener, E. C., Nester, M. J., Oystreck, D. T., Chan, W. M., Andrews, C., Erickson, R. P. et al. *(2005). Homozygous HOXA1 mutations disrupt human brainstem, inner ear, cardiovascular and cognitive development. Nat Genet* ***37****, 1035-7.*

Tour, E., Hittinger, C. T., and McGinnis, W. *(2005). Evolutionarily conserved domains required for activation and repression functions of the Drosophila Hox protein Ultrabithorax. Development* ***132****, 5271-5281.*

Treisman, J., Gonczy, P., Vashishtha, M., Harris, E. and Desplan, C. *(1989). A single amino acid can determine the DNA binding specificity of homeodomain proteins. Cell* ***59****, 553-62.*

Tuerk, C. and Gold, L. *(1990). Systematic evolution of ligands by exponential enrichment: RNA ligands to bacteriophage T4 DNA polymerase. Science* ***249****, 505-10.*

Urist, M. R., Mikulski, A. and Lietze, A. *(1979). Solubilized and insolubilized bone morphogenetic protein. Proc Natl Acad Sci U S A* ***76****, 1828-32.*

Utsch, B., Becker, K., Brock, D., Lentze, M. J., Bidlingmaier, F. and Ludwig, M. *(2002). A novel stable polyalanine [poly(A)] expansion in the HOXA13 gene associated with hand-foot-genital syndrome: proper function of poly(A)-harbouring transcription factors depends on a critical repeat length? Hum Genet* ***110****, 488-94.*

Vissing, H., D'Alessio, M., Lee, B., Ramirez, F., Godfrey, M. and Hollister, D. W. *(1989). Glycine to serine substitution in the triple helical domain of pro-alpha 1 (II) collagen results in a lethal perinatal form of short-limbed dwarfism. J Biol Chem* ***264****, 18265-7.*

Wang, N., Kim, H. G., Cotta, C. V., Wan, M., Tang, Y., Klug, C. A., and Cao, X. *(2006). TGFbeta/BMP inhibits the bone marrow transformation capability of Hoxa9 by repressing its DNA-binding ability. Embo J* ***25****, 1469-1480.*

Warman, M. L., Abbott, M., Apte, S. S., Hefferon, T., McIntosh, I., Cohn, D. H., Hecht, J. T., Olsen, B. R. and Francomano, C. A. *(1993). A type X collagen mutation causes Schmid metaphyseal chondrodysplasia. Nat Genet* ***5****, 79-82.*

Warot, X., Fromental-Ramain, C., Fraulob, V., Chambon, P. and Dolle, P. *(1997). Gene dosage-dependent effects of the Hoxa-13 and Hoxd-13 mutations on morphogenesis of the terminal parts of the digestive and urogenital tracts. Development* ***124****, 4781-91.*

Warren, R. W., Nagy, L., Selegue, J., Gates, J. and Carroll, S. *(1994). Evolution of homeotic gene regulation and function in flies and butterflies. Nature* ***372****, 458-61.*

Weatherbee, S. D., Halder, G., Kim, J., Hudson, A. and Carroll, S. *(1998). Ultrabithorax regulates genes at several levels of the wing-patterning hierarchy to shape the development of the Drosophila haltere. Genes Dev* ***12****, 1474-82.*

Wellik, D. M. and Capecchi, M. R. *(2003). Hox10 and Hox11 genes are required to globally pattern the mammalian skeleton. Science* ***301****, 363-7.*

Williams, T. M., Williams, M. E., Heaton, J. H., Gelehrter, T. D. and Innis, J. W. *(2005a). Group 13 HOX proteins interact with the MH2 domain of R-Smads and modulate Smad transcriptional activation functions independent of HOX DNA-binding capability. Nucleic Acids Res* ***33****, 4475-84.*

Williams, T. M., Williams, M. E. and Innis, J. W. *(2005b). Range of HOX/TALE superclass associations and protein domain requirements for HOXA13:MEIS interaction. Dev Biol* ***277****, 457-71.*

Williams, T. M., Williams, M. E., Kuick, R., Misek, D., McDonagh, K., Hanash, S. and Innis, J. W. *(2005c). Candidate downstream regulated genes of HOX group 13 transcription factors with and without monomeric DNA binding capability. Dev Biol* ***279****, 462-80.*

Workman, C. T., Yin, Y., Corcoran, D. L., Ideker, T., Stormo, G. D. and Benos, P. V. *(2005). enoLOGOS: a versatile web tool for energy normalized sequence logos. Nucleic Acids Res* ***33****, W389-92.*

Yanagita, M., Oka, M., Watabe, T., Iguchi, H., Niida, A., Takahashi, S., Akiyama, T., Miyazono, K., Yanagisawa, M. and Sakurai, T. *(2004). USAG-1: a bone morphogenetic protein antagonist abundantly expressed in the kidney. Biochem Biophys Res Commun* ***316****, 490-500.*

Yi, S. E., Daluiski, A., Pederson, R., Rosen, V. and Lyons, K. M. *(2000). The type I BMP receptor BMPRIB is required for chondrogenesis in the mouse limb. Development* ***127****, 621-30.*

Yokouchi, Y., Nakazato, S., Yamamoto, M., Goto, Y., Kameda, T., Iba, H. and Kuroiwa, A. *(1995). Misexpression of Hoxa-13 induces cartilage homeotic transformation and changes cell adhesiveness in chick limb buds. Genes Dev* ***9****, 2509-22.*

Yokouchi, Y., Sakiyama, J., Kameda, T., Iba, H., Suzuki, A., Ueno, N. and Kuroiwa, A. *(1996). BMP-2/-4 mediate programmed cell death in chicken limb buds. Development* ***122****, 3725-34.*

Zeng, L., Kempf, H., Murtaugh, L. C., Sato, M. E. and Lassar, A. B. *(2002). Shh establishes an Nkx3.2/Sox9 autoregulatory loop that is maintained by BMP signals to induce somitic chondrogenesis. Genes Dev* ***16****, 1990-2005.*

Zhang, D., Schwarz, E. M., Rosier, R. N., Zuscik, M. J., Puzas, J. E. and O'Keefe, R. J. *(2003). ALK2 functions as a BMP type I receptor and induces Indian hedgehog in chondrocytes during skeletal development. J Bone Miner Res* ***18****, 1593-604.*

Zhang, H. and Bradley, A. *(1996). Mice deficient for BMP2 are nonviable and have defects in amnion/chorion and cardiac development. Development* ***122****, 2977-86.*

Zhang, Y. W., Yasui, N., Ito, K., Huang, G., Fujii, M., Hanai, J., Nogami, H., Ochi, T., Miyazono, K. and Ito, Y. *(2000). A RUNX2/PEBP2alpha A/CBFA1 mutation displaying impaired transactivation and Smad interaction in cleidocranial dysplasia. Proc Natl Acad Sci U S A* ***97****, 10549-54.*

Zhao, Y. and Potter, S. S. *(2001). Functional specificity of the Hoxa13 homeobox. Development* ***128****, 3197-207.*

Zou, H., Choe, K. M., Lu, Y., Massague, J. and Niswander, L. *(1997a). BMP signaling and vertebrate limb development. Cold Spring Harb Symp Quant Biol* ***62****, 269-72.*

Zou, H. and Niswander, L. *(1996). Requirement for BMP signaling in interdigital apoptosis and scale formation. Science* ***272****, 738-41.*

Zou, H., Wieser, R., Massague, J. and Niswander, L. *(1997b). Distinct roles of type I bone morphogenetic protein receptors in the formation and differentiation of cartilage. Genes Dev* ***11****, 2191-203.*

Zuzarte-Luis, V. and Hurlé, J. M. *(2002). Programmed cell death in the developing limb. Int J Dev Biol* ***46****, 871-6.*

Zuzarte-Luis, V. and Hurlé, J. M. *(2005). Programmed cell death in the embryonic vertebrate limb. Semin Cell Dev Biol* ***16****, 261-9.*

Zuzarte-Luis, V., Montero, J. A., Rodriguez-Leon, J., Merino, R., Rodriguez-Rey, J. C. and Hurlé, J. M. *(2004). A new role for BMP5 during limb development acting through the synergic activation of Smad and MAPK pathways. Dev Biol* ***272****, 39-52.*

Zwijsen, A., Verschueren, K. and Huylebroeck, D. *(2003). New intracellular components of bone morphogenetic protein/Smad signaling cascades. FEBS Lett* ***546****, 133-9.*